EMERGENT PHENOMENA IN SUPERCONDUCTORS IN PRESENCE OF INTRABAND AND CROSS-BAND PAIRING

ALFREDO ANDRES VARGAS PAREDES

Università di Camerino

Signatures and consequences of crosspairing in superconductors.

Proof to obtain the degree of doctor in
Physics
Università di Camerino and
University of Antwerp

Supervisors:

Andrea Perali
and
Milorad Milošević

Kachkaniraqmi means I'm still the same.
To my mother, brother and sisters, when we met again I would say:
Kachkaniraqmi!

To my beloved wife whose support was essential for this thesis.

ABSTRACT

In this thesis we investigate the emergence of new phenomena in multigap superconductors and multicomponent Ginzburg-Landau theories in the presence of intraband and cross-band pairing. The first part contains a review of emergent phenomena in superconductors with only intraband pairing, in particular the mechanism behind gap resonances which are accompanied by Higgs and Leggett modes. Then we study the gap resonances induced by two-dimensional quantum confinement and describe its spatial profile using the Bogoliubov-de Gennes equations. In the second part we describe the conditions where the cross-band pair formation is feasible. Using the formalism of Green functions we obtain the equations governing the interplay between intraband and cross-band pairing. Also, we derived the Ginzburg-Landau equations considering both intraband and cross-band pairing. Finally, we describe the crossover between the intraband-dominated and crossband-dominated regimes. These two are delimited by a tendency towards a gapless state. When a magnetic field is applied close to the gapless state, we found new arrangements of vortices like square lattices, stripes, labyrinths or of vortex clusters. The experimental signatures and consequences of crosspairing are discussed for MgB_2 and $Ba_{0.6}K_{0.4}Fe_2As_2$.

ABSTRACT

In deze thesis onderzoeken we het ontstaan van nieuwe fenomenen in multigap supergeleiders en multicomponent Ginzburg-Landau theorieën in de nabijheid van intraband en cross-band koppelingen. Het eerste deel bevat een samenvatting van opkomende fenomenen in supergeleiders met enkel intraband koppeling. Meer specifiek hebben we het over het mechanisme achter gapresonanties die vergezeld zijn van Higgs en Leggett modes. Daarna bestuderen we de gap resonanties die opgewekt worden door quantum confinement in twee dimensies. Dan beschrijven we het profiel in een tweedimensionale ruimte met behulp van de Bogoliubov-de Gennes vergelijkingen. In het tweede deel worden de voorwaarden waaronder cross-band paarvorming mogelijk is beschreven. Gebruikmakend van het Gor'kov Green functieformalisme verkrijgen we de vergelijkingen die de wisselwerking tussen intraband koppeling en crosspairing beheersen. Ook leiden we de Ginzburg-Landau vergelijkingen af wanneer crosspairing aanwezig is. Uiteindelijk beschrijven we de overgang tussen intraband-gedomineerde en cross-band gedomineerde regimes. Deze regimes zijn afgebakend door een gaploze toestand in het homogene

geval of door de nabijheid van langwerpige kettingen van vortices wanneer een magnetisch veld wordt toegepast. De experimentele tekenen en gevolgen van crosspairing worden besproken voor MgB_2 en $Ba_{0.6}K_{0.4}Fe_2As_2$.

PUBLICATIONS

The first three publications include only intraband pairing and the last one include both intraband and cross-band pairing.

1. M. Cariglia, **A. A. Vargas-Paredes**, M. M. Doria, A. Bianconi, M. V. Milošević and A. Perali (2016). *Shape-resonant superconductivity in nanofilms: from weak to strong coupling*. Journal of Superconductivity and Novel Magnetism, 29(12):3081-3086.

2. E. I. B. Rodrigues, **A. A. Vargas-Paredes**, M. M. Doria, and M. Cariglia (2017). *Zero helicity states in the $LaAlO_3$-$SrTiO_3$ interface*. Journal of Superconductivity and Novel Magnetism, 30(5):1327-1334.

3. E. I. B. Rodrigues, M. M. Doria, **A. A. Vargas-Paredes**, M. Cariglia and A. Perali (2017). Zero helicity states in the $LaAlO_3$-$SrTiO_3$ interface: The origin of the mass anisotropy. Journal of Superconductivity and Novel Magnetism, 30(1):145-150.

4. **A. A. Vargas-Paredes**, A. A. Shanenko, A. Vagov, M. V. Milošević, and A. Perali. *Cross-band pairing in two-band superconductors: signatures and consequences.* Submitted to Physical Review B (Rapid Communication).

ACKNOWLEDGMENTS

First, I would like to thank Mauro M. Doria for helpful discussions regarding the review of this thesis. I am thankful to my supervisors Andrea Perali and Milorad Milošević for the opportunity to work in such a nice project about crosspairing in superconductors. Many thanks to my colleagues and friends who were always available for meaningful discussions. Personally, I would like to thank Nikolas Garofil for the Dutch translation of the Abstract, Slaviša Milovanović for the reviewing of Chapter 2 (Introduction) and tips for the usage of the Vlaams Supercomputer Centrum (VSC), Miša Anđelković for the reviewing of Chapter 3 (Multigap and Multicomponent Superconductivity) and discussion of the solutions obtained in this thesis, Željko Jelić for the long discussions regarding the Ginzburg-Landau theory and its code implementation and my family whose supports is always essential for me.

CONTENTS

1 INTRODUCTION 1

I SUPERCONDUCTIVITY WITH ONLY INTRABAND PAIRING

2 INTRODUCTION TO SUPERCONDUCTIVITY 7
- 2.1 Discovery of superconductivity 7
- 2.2 Microscopic theory of superconductivity 8
  - 2.2.1 Bardeen-Cooper-Schrieffer theory 9
  - 2.2.2 Gor'kov Green function formalism of superconductors 11
- 2.3 Phenomenological theory of superconductivity 16
  - 2.3.1 London model 16
  - 2.3.2 Ginzburg-Landau theory 18
  - 2.3.3 Gor'kov derivation of the Ginzburg-Landau theory 23
  - 2.3.4 The vortex state 29

3 MULTIGAP AND MULTICOMPONENT SUPERCONDUCTIVITY 33
- 3.1 Multigap superconductors 33
  - 3.1.1 Two-gaps at zero temperature 36
  - 3.1.2 Two-gaps at finite temperature 38
  - 3.1.3 Shape-Resonant Superconductivity in Nanofilms 39
- 3.2 Multicomponent Ginzburg-Landau theories 47
  - 3.2.1 Multicomponent Ginzburg-Landau equation 48
  - 3.2.2 Reconstruction of the order parameter 51

II SUPERCONDUCTIVITY WITH INTRABAND AND CROSSBAND PAIRING

4 MICROSCOPIC THEORY OF CROSSPAIRING 57
- 4.1 Conditions for cross-band pairing formation 58
- 4.2 N-band Hamiltonian with crosspairing 59
- 4.3 Analytic solutions 61
  - 4.3.1 Analytic solution for $\theta = 0$ 62
  - 4.3.2 Analytic solution for $\theta = \pi$ 63
- 4.4 Numerical solutions 63
  - 4.4.1 Zero Josephson-like coupling 64
  - 4.4.2 Finite Josephson-like coupling 67
  - 4.4.3 The Gapless state 72
- 4.5 Signatures of Crosspairing in Magnesium Diboride and Iron Arsenide 76

5 GINZBURG LANDAU THEORY WITH CROSSPAIRING 83
- 5.1 Derivation of the Ginzburg-Landau equations 84
- 5.2 Reconstruction of the Ginzburg-Landau order parameter 88

5.3 Interface Energy 92
5.4 Vortex Lattice 95
6 CONCLUSIONS AND PERSPECTIVES 103

III APPENDIX

A ANOMALOUS AND NORMAL GREEN FUNCTIONS 109
A.1 Nambu-Gorkov Approach for N-Multiband Hamiltonian with Crosspairing 109
A.2 Derivation of the normal Green function 112
B GINZBURG-LANDAU IN PRESENCE OF CROSSPAIRING 117
C NUMERICAL METHODS 121
C.1 Numerical method to solve the pair amplitude equations 121
C.2 Numerical method to solve the Ginzburg-Landau equations 122

BIBLIOGRAPHY 125

LIST OF FIGURES

Figure 2.1 Discovery of superconductivity 8
Figure 2.2 Phonon exchange between two electrons 10
Figure 2.3 Meissner effect 17
Figure 2.4 Spontaneous Symmetry Breaking 21
Figure 2.5 Ginzburg-Landau characteristic lengths 22
Figure 2.6 Lattice of Abrikosov vortices. 30
Figure 3.1 $s^{+-} \leftrightarrow s^{++}$ transition 36
Figure 3.2 Induced Higgs and Leggett modes 37
Figure 3.3 The role of the Josephson-like coupling 38
Figure 3.4 BCS-ratio in two gap superconductors 39
Figure 3.5 Gap resonance 44
Figure 3.6 Width of the resonance 45
Figure 3.7 Chemical potential in nanofilms 46
Figure 3.8 Spatial Gap profile perpendicular to the film 47
Figure 4.1 Feasibility of crosspairing by band proximity 58
Figure 4.2 Crosspairing for a decoupled system at $T = 0K$ 65
Figure 4.3 Gapless state as predicted in superfluidity 66
Figure 4.4 Crosspairing for a decoupled system at finite temperature 67
Figure 4.5 Crosspairing with weak Josephson-like coupling 68
Figure 4.6 Crosspairing with strong Josephson-like coupling 69
Figure 4.7 Crosspairing with induced repulsion 71
Figure 4.8 Phase change induced by temperature 72
Figure 4.9 DOS across the gapless state 75
Figure 4.10 Fermi Surface of MgB_2 76
Figure 4.11 MgB_2-σ bands at the Γ-point 77
Figure 4.12 MgB_2 in presence of crosspairing 79
Figure 4.13 Fermi surfaces of $Ba_{0.6}K_{0.4}Fe_2As_2$ 80
Figure 4.14 Phase transition driven by temperature in $(BaK)Fe_2As_2$ 81
Figure 5.1 Transition induced by disorder 91
Figure 5.2 Critical temperature and London penetration depth vs. disorder 92
Figure 5.3 Normal-superconducting interface 93
Figure 5.4 Superconducting type dichotomy in presence of crosspairing 95
Figure 5.5 Competitive vortex configuration 97
Figure 5.6 Evolution of the vortex configuration with increasing crosspairing. 98

Figure 5.7 First order melting transition of an Abrikosov melting lattice. 99
Figure 5.8 Labyrinth patterns of the vortex configuration in MgB_2 crystals. 100
Figure C.1 Two dimensional grid 123

LIST OF TABLES

Table 3.1 BCS-ratio from weak to strong coupling 39
Table 3.2 Amplification factors in the resonance 44

ACRONYMS

2D	two dimensional
3D	three dimensional
BEC	Bose-Einstein condensate
BCS	Bardeen-Cooper-Schrieffer
QFT	Quantum Field Theory
GL	Ginzburg-Landau
OP	order parameter
FeSCs	iron-based superconductors
CPT	charge, parity and time
STM	scanning tunneling microscopy
ARPES	angle-resolved photoemission spectroscopy
DFT	density functional theory
QED	quantum electrodynamics
QCD	quantum cromodynamics
DOS	density of states

IBP intraband pairing

CBP cross-band pairing

IPS intraband pairing solution

CPS cross-band pairing solution

IDR intraband-dominated regime

CDR cross-band-dominated regime

1 INTRODUCTION

The study of superconductivity together with competitive orders is crucial to determine the best conditions in which we can obtain high temperature superconductors. In this context, the possible competitive orders can be external or internal to the superconducting phase. As external competitive orders we can mention the magnetic order, charge density waves or spin density waves. On the other hand the internal competitive orders are given within the superconducting phase with itself. In this thesis, we describe one particular competition which has been neglected in most works to date: Cooper pair formation between two electrons belonging to the same band versus Cooper pair formation between two electrons belonging to different bands. In this thesis these two types of pairing will be named as intraband pairing (IBP) for the former and cross-band pairing (CBP) for the latter. The competition between IBP and CBP arises in two-band superconductors when the bands are close or hybridized in the vicinity of the Fermi level. Physically, this competition is caused by the finite density of electrons around the Fermi level and the induced attraction between two electrons which now can form exclusively an intraband or a cross-band Cooper pair.

Systems with band hybridization or partially overlapped bands close to the Fermi level are present in several multigap and multicomponent superconducting materials. These materials are characterized by gap openings in different Fermi surfaces that can be tuned by quantum confinenment, layering stacking, surface effects and electrical gating which allow to find the best configuration with minimal decoherence of the order parameter and therefore with the highest critical temperature T_c. Interestingly, as we will see in this thesis the presence of CBP together with IBP will introduce naturally a phase dependence in the energy spectra of the electronic excitations, the gap opening in the density of states and in the London penetration depth, fact that was never reported and that we will exploit to look again the problem of phase decoherence of the superconducting state. By decoherence of the superconducting phase we mean the vanishing of the superconductivity order parameter together with its phase spread.

Probably, the biggest and common challenge of all quantum applications it is to overcome the problem of quantum decoherence. Thermodinamically, this challenge arises because the system interacts with its surroundings in a non reversible way as dictated by the second law of thermodynamics. Decoherence is present in the energy dissipation of nuclear fusion processes, disentanglement of quantum

qubits in quantum computers and in the phase spread of the superconducting order parameter (OP). In particular the phase decoherence of the superconducting OP can be caused by competition with different orders like magnetism, spin density waves, charge density waves or Coulomb repulsion. Generally this competition is detrimental for superconductivity. Nonetheless, these competitive orders can promote new symmetries in the superconducting OP, allowing superconductivity to endure at the expense of losing *some* phase coherence. For example, within the iron-based superconductors (FeSCs) the s^{+-} symmetry of the order parameter can have its origin as π-phase difference between electron-like and hole-like pair amplitudes [84] or an orbital anti-phase with a π-phase difference between bands of the same type (electron-like or hole-like) [77, 138, 141].

The purpose of this thesis is to study the signatures and consequences of the inclusion cross-band Cooper pairs in superconductors which were mostly described with only intraband Cooper pairs with and without an applied magnetic field. This thesis contains six Chapters and is organized as follows:

- **Chapter 1** is the general introduction and overview of the present thesis.

- **Chapter 2** gives a general introduction to superconductivity in a non historical or chronological order but rather pedagogical. Therefore, we present first its microscopic formulation given the Bardeen-Cooper-Schrieffer (BCS) theory and its remaining problems that would be later elegantly solved with the Gor'kov Green function formalism. Then we introduce the phenomenological theory of superconductivity, starting with the London model, the Ginzburg-Landau theory, its microscopic derivation by Gor'kov and the vortex state when a magnetic field is applied. The Gor'kov Green function formalism and the microscopic derivation of the Ginzburg-Landau theory constitute the theoretical framework of the present thesis.

- **Chapter 3** considers systems with no crosspairing and describes the emergent phenomena characteristic of the interplay of multiple gaps in a superconductor. In particular we present the gap resonances which are accompanied by Higgs and Legget modes in the vicinity of the weak interband coupling (scattering of electrons between different bands). Then we review the microscopic derivation of a multicomponent Ginzburg-Landau (GL) theory from a general multigap superconductor and discuss its regime of validity consistent with the Gor'kov expansion. At the end, we review the reconstructive procedure of the order parameter in multicomponent GL theories with only IBP which can be described by a single-component Ginzburg-Landau equation.

- **Chapter 4** starts by establishing the general conditions for cross-band pair formation. Then using the Gor'kov formalism we formulate the minimal extension of the BCS Hamiltonian that includes crosspairing. Consecutively, we present analytical solutions for the degenerated case at zero temperature and numerical solutions for more general cases at zero and finite temperature. Furthermore we study the gapless state as the most pronounced feature that signals the presence of crosspairing which categorize our system in two pairing regimes: intraband-dominated regime (IDR) and cross-band-dominated regime (CDR). We discuss the signatures and consequences of our findings in MgB_2 and $Ba_{0.6}K_{0.4}Fe_2As_2$.

- **Chapter 5** presents the microscopic derivation of the Ginzburg-Landau theory in the presence of crosspairing with and without reconstruction of the OP. Furthermore, we analyze the normal-superconductive interface in presence of crosspairing and the vortex configuration when the applied magnetic field is constant. We discuss the failure of the reconstructive procedure of the order parameter in presence of crosspairing and emphasize its multicomponent nature within the original microscopic Gor'kov derivation which is only possible due to the presence of both IBP and CBP.

- **Chapter 6** finally summarizes the conclusions of this thesis and propose several perspectives like the role of crosspairing in presence of a spin-flip scattering in $Mg_{1-x}Mn_xB_2$, the competitive signatures of crosspairing with the Majorana states near the gapless state which presents quasi zero-energy bound states and the classification of the vortex configuration at the intermediate state between the IDR and CDR.

Part I

SUPERCONDUCTIVITY WITH ONLY INTRABAND PAIRING

2

INTRODUCTION TO SUPERCONDUCTIVITY

"...And when one works in superconductivity, I warn you before you start, one comes up finally to a terrible shock; one discovers that he is too stupid to solve the problem." (Richard Feynman at the Low Temperature Physics Conference in Seattle, 1956.)

The understanding of man over the laws of nature can be estimated by how the applications of those laws have transformed society. Although several progress has been made towards the understanding of the basic principles needed for superconductivity to developed, we can state that high temperature superconductivity has remain elusive due to its long-promised but limited applicability . The main difficulty to obtain a superconductor is the need to reach temperatures below -200 degrees Celsius which is ten times colder than the freezer inside our homes. This makes the use of superconductivity expensive and technologically difficult to obtain. Nonetheless, several applications are already directly or indirectly in our lives: For example, magnetic levitated transport can be achieved thanks to the quantum locking and magnetic repulsion of superconductors; efficient electrical power transmission due to the zero electrical resistance of superconductors;[1] production of large magnetic fields which are used in particle accelerators; magnetic resonance imaging in hospitals as non-invasive technique for diagnosis; superconducting quantum interference devices (SQUIDs) that can measure 10^{-5} Tesla which is 10^{14} times weaker than a refrigerator magnet; and more recently in the design and construction of lighter and more compact windmills. Any breakthrough in the quest for room temperature superconductivity will lead naturally to further applications which will have a strong impact in our society.

We can state that the understanding of high-temperature superconductivity has remain elusive due to its long-promised but limited applicability

2.1 DISCOVERY OF SUPERCONDUCTIVITY

From the theoretical and experimental point of view, the discovery of superconductivity was fortuitous because no one expected this new phase of matter to emerge. At the end of the nineteenth century, a dutch physicist with very skillful technicians created a laboratory under his name: The Kamerlingh Onnes's laboratory. Later at the beginning of the twentieth century, Kamerlingh Onnes's was on a race to liquify helium with Sir James Dewar from the University

1 The first long superconducting cable was built in the German city of Essen. There, a one kilometer long cable connects two transformer stations inside the city center. The superconducting cable supports up to 10^4 volts instead of the regular 10^5 volts cable.

of Cambridge. At that time, liquid helium was long discovered in the spectra analysis of the sun but was recently obtained in Earth through monazite sand. It was in 1908 that the Kamerlingh Onnes' laboratory successfully manufactured liquid helium and thanks to it its physicists would get every day a cryostat with helium to play with. Theoretically, there was in particular an important question to be solved. Classical thermodynamics predicts that by lowering the temperature any motion should ultimately stop and therefore also the electrical current. However, preliminary measurements to the liquefaction of helium were showing a steady decrease in the resistance until in 1911 Gilles Holst discovered superconductivity [80] by observing a sharp drop in the resistivity of mercury, see Fig. 2.1. The credit of this discovery was not given to Gilles Holst but to Kamerlingh Onnes because he was the founder of the laboratory and the person who won the race of liquifying helium, which later made technologically possible the discovery of superconductivity.

Superconductivity was experimentally discovered by Gilles Holst.

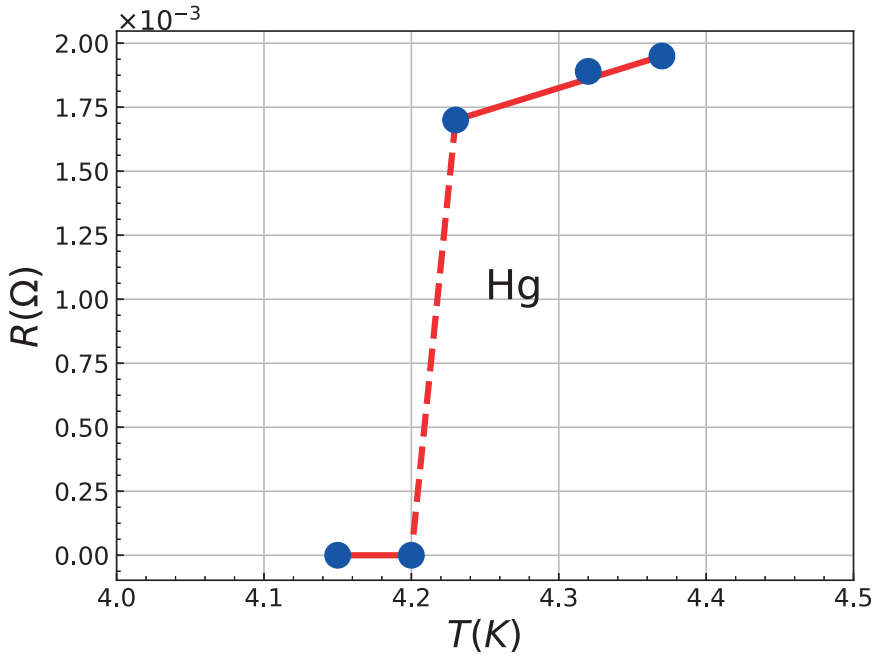

Figure 2.1: Resistance of mercury versus temperature reported by Kamerlingh Onnes. Below the transition temperature of 4.2 K, the resistance was no larger than 10^{-5} Ohms. Data extracted from [28].

2.2 MICROSCOPIC THEORY OF SUPERCONDUCTIVITY

It took almost 40 years after the discovery of superconductivity to understand the microscopic mechanism behind this phenomenon. There are two reasons for this. First, the beginning of World War I in 1914, limited the supply of monazite sand coming from North Carolina

to the Dutch port impacting the further experimental research. Second, quantum mechanics was at its infancy an many of its today well established postulates at that time were heatedly debated. This means that even the state of normal conductor was not well understood.

2.2.1 *Bardeen-Cooper-Schrieffer theory*

A normal conductor is a material that posses inside an itinerant movement of electrical carriers which under the application of an electrical field will present an electrical current parallel to it. This electrical current is composed of electrons whose wave function follows Fermi-Dirac statistics. How was then possible that those electrons condensate to form a coherent macroscopic state? We should remember that such a mechanism was only possible through the ideas of the Bose-Einstein condensation (BEC) whose order parameter follows Bose statistics and therefore cannot be directly applied. The first attempt to apply those ideas to solve the problem of superconductivity was made by Schrafroth, Butler and Blatt. They formulate a theory of superconductivity as a Bose-Einstein condensate (BEC) [17, 109]. However, the pairing mechanism was different from the superconducting state. The main problem was that superconductivity is a bound state between electrons whose distance between them is large and they interact only weakly while in the BEC the distance between electrons is small and they interact strongly[2]. Parallel to this, there was the work of Frölich, Bardeen and Pines [9] that demonstrated that two electrons close to the Fermi surface can have an effective attractive interaction due to phonon exchange. Then, Leon N. Cooper, working as postdoc of John Bardeen, studied in more detail how this effective attraction could take place.

Cooper first considered a state described by the creation of two electrons $|\Psi>$ above the Fermi Surface:

$$|\Psi>= P^{\dagger}|S>, \quad P^{\dagger} = \sum_{\vec{k}} \phi_{\vec{k}} c^{\dagger}_{\vec{k}\uparrow} c^{\dagger}_{-\vec{k}\downarrow}, \quad |S>= \prod_{k<k_F} c^{\dagger}_{\vec{k}\uparrow} c^{\dagger}_{-\vec{k}\downarrow}|0>, \tag{2.1}$$

where $|0>$ is the vacuum and $|S>$ represents the Fermi sea of electrons filled up to the Fermi level with associated momentum k_F and the operator $P^{\dagger}$ creates a pair of electrons above the Fermi level. The momentum dependent function $\phi_{\vec{k}}$ is the Fourier transform of the spatial pair wave function. The properties of the pair wave function will be contained in $\phi_{\vec{k}}$ which for conventional pairing will have an isotropic s-wave function $\phi_{\vec{k}} \propto f(k)$.

2 Today, we know that for some cases, through the Feschbach resonance, we can tune the interaction between electrons and study the BCS-BEC crossover.

Qualitatively, the Hamiltonian of a pair of electrons above the Fermi surface have the following form:

$$H = \sum_{\vec{k}} \epsilon_{\vec{k}} c^{\dagger}_{\vec{k}\sigma} c_{\vec{k}\sigma} + \hat{V}. \tag{2.2}$$

where the potential $\hat{V}$ contains the effective electron-electron interaction. Now, the energy of a pair of electrons above the Fermi level will be given by

$$H|\Psi>= \sum_{|\vec{k}|>k_F} 2\epsilon_{\vec{k}}|\Psi> + \sum_{|\vec{k}|>k_F,\vec{k}'} |\Psi'><\Psi'|\hat{V}|\Psi>, \tag{2.3}$$

where the factor of two comes due to summation with respect to the spin degrees of freedom. In the interaction part, we have used the completeness relation $\sum_{k'} |\Psi'><\Psi'|$. Based on the previous work by Frölich, Bardeen and Pines, this scattering matrix $<\Psi'|\hat{V}|\Psi>$ should correspond to the electron-phonon propagator. Which in terms of Feynman diagrams is given by figure 2.2.

$$<\Psi'|\hat{V}|\Psi>= \hat{V}_{\vec{p}_1,\vec{p}_3} = g^2_{\vec{p}_1-\vec{p}_3} D(\vec{p}_1-\vec{p}_3, \epsilon_{\vec{p}_1}-\epsilon_{\vec{p}_3}) \tag{2.4}$$

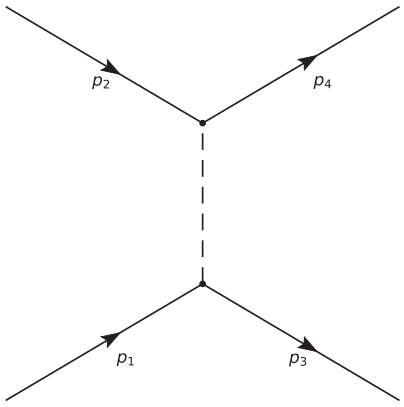

Figure 2.2: Phonon exchange between two electrons.

Explicitly, the electron-phonon propagator is given by the phonon D-function:

$$g^2_{\vec{p}_1-\vec{p}_3} D(\vec{p}_1-\vec{p}_3, \epsilon_{\vec{p}_1}-\epsilon_{\vec{p}_3}) = g^2_{\vec{p}_1-\vec{p}_3} \frac{u^2(\vec{p}_1-\vec{p}_3)^2}{(\epsilon_{\vec{p}_1}-\epsilon_{\vec{p}_3})^2 - u^2(\vec{p}_1-\vec{p}_3)^2}. \tag{2.5}$$

Cooper realized that the typical phonon exchange of electrons above the Fermi surface has a momentum difference much larger than the energy difference $u|\vec{p}_1-\vec{p}_3| >> |\epsilon_{\vec{p}_1}-\epsilon_{\vec{p}_3}|$, where u is constant factor with dimensions of velocity. Consequently the effective interaction

is reduced to $-g^2_{\vec{p}_1-\vec{p}_3}$ which is attractive. This is the argument to substitute the exchange interaction of two electrons close to the Fermi level by a negative contact potential which is constant in a small region defined by the Debye frequency Ω:

$$V_{\vec{k},\vec{k}'} = \begin{cases} -g_0/V, & |\epsilon_{\vec{k}}|, |\epsilon_{\vec{k}'}| < \Omega, \quad V \text{ is the volume,} \\ 0, & \text{otherwise.} \end{cases}$$

Under this condition the effective attraction will become energetically more favorable than the bare repulsion between electrons regardless of how weak the interaction is. This would imply in the emergence of a bosonic mode (Cooper pair) which reconstructs the ground state and introduces a gap opening in the excitation spectra of the electrons. This gap is then equal to the energy necessary to bound a pair of electrons.

After the insight of Cooper, Schrieffer came into play to describe the ground state of a superconductor. He described the wave function of a superconductor as a coherent state of Cooper pairs:

$$|\Psi_{BCS}> = \exp \sum_{\vec{k}} \phi_{\vec{k}} c^\dagger_{\vec{k}\uparrow} c^\dagger_{-\vec{k}\downarrow} |0> = \prod_{\vec{k}} \exp \phi_{\vec{k}} c^\dagger_{\vec{k}\uparrow} c^\dagger_{-\vec{k}\downarrow} |0>, \tag{2.6}$$

where $|\Psi_{BCS}>$ is the ground state of the superconductor. Applying the Pauli exclusion principle then we get

$$|\Psi_{BCS}> = \prod_{\vec{k}} (1 + \phi_{\vec{k}} c^\dagger_{-\vec{k}\uparrow} c^\dagger_{-\vec{k}\downarrow}) |0> . \tag{2.7}$$

Having the wave function and considering the Cooper pair operator we construct the BCS Hamiltonian

$$H_{BCS} = \sum_{\vec{k}} \epsilon_{\vec{k}} c^\dagger_{\vec{k}\sigma} c_{\vec{k}\sigma} + \sum_{\vec{k},\vec{k}'} V_{\vec{k},\vec{k}'} c^\dagger_{\vec{k}\uparrow} c^\dagger_{-\vec{k}\downarrow} c_{-\vec{k}'\downarrow} c_{\vec{k}'\uparrow}. \tag{2.8}$$

All those ideas were directed by John Bardeen who together with Cooper and Schrieffer received in 1972 the Nobel prize in physics for the theory of superconductivity or BCS theory [8].

2.2.2 *Gor'kov Green function formalism of superconductors*

During the development of the theory of superconductivity the former Soviet Union was very active and made many important contributions. The BCS theory was well received by the scientific community in the U.S.S.R where many of its remaining problems were immediately addressed. These problems were:

1. There was no clear definition of the superconducting order parameter and its symmetry.
2. The BCS theory only accounts for clean superconductors.
3. There was no relation between the BCS theory and its phenomenological counterpart heuristically derived by Ginzburg and Landau.
4. The theory needed to be generalized to materials with spatial non-homogeneous electronic structures.

Many of the above mentioned problems were solved with the Green function formalism and adapted Quantum Field Theory (QFT). These adaptations are required when one uses the QFT tools and machinery which are inherently Lorentz invariant to non-relativistic systems like in condensed matter physics. The adjustments include the identification of the Fermi sea at $T = 0$ K as a new QFT vacuum and the Wick rotation which introduces temperature as an imaginary time and with it the definition of Matsubara's frequencies for fermions and bosons.

In 1957, Bogoliubov gave a talk in the Kapitza Institute to Landau and his group were Gor'kov was a junior scientist. In that talk not only the canonical Bogoliubov transformations but also the Cooper instability and the nature of the new ground state were debated. Gor'kov noticed the emergence of bosonic mode and using the powerful Green function formalism solve some of the remaining problems of the BCS theory [52],

$$
\begin{aligned}
H &= H_{kin} + H_{int}, && (2.9)\\
H_{kin} &= \sum_{\sigma} \int d^3\vec{x}\psi^{\dagger}_{\sigma}(\vec{x}) T_{\vec{x}} \psi_{\sigma}(\vec{x}), && (2.10)\\
H_{int} &= \frac{1}{2} \int d^3\vec{x} d^3\vec{x}' V(\vec{x}-\vec{x}') \psi^{\dagger}_{\uparrow}(\vec{x}) \psi^{\dagger}_{\downarrow}(\vec{x}') \psi_{\downarrow}(\vec{x}') \psi_{\uparrow}(\vec{x}) \\
&+ \frac{1}{2} \int d^3\vec{x} d^3\vec{x}' V(\vec{x}-\vec{x}') \psi^{\dagger}_{\downarrow}(\vec{x}) \psi^{\dagger}_{\uparrow}(\vec{x}') \psi_{\uparrow}(\vec{x}') \psi_{\downarrow}(\vec{x}), && (2.11)
\end{aligned}
$$

where $T_{\vec{x}}$ is the kinetic energy operator. Using the result of the Fermi surface instability by Cooper and assuming that the scattering between electrons has the form of a contact potential $V(\vec{x}-\vec{x}') = -g\delta(\vec{x}-\vec{x}')$, we get

$$
H = \sum_{\sigma} \int d^3\vec{x}\psi^{\dagger}_{\sigma}(\vec{x}) T_{\vec{x}} \psi_{\sigma}(\vec{x}) + g \int d^3\vec{x}\psi^{\dagger}_{\uparrow}(\vec{x}) \psi^{\dagger}_{\downarrow}(\vec{x}) \psi_{\downarrow}(\vec{x}) \psi_{\uparrow}(\vec{x}). \quad (2.12)
$$

To deal with the interaction term, we use the Bogoliubov or mean-field approximation ($\psi_{\sigma}(\vec{x}) \equiv \psi_{\sigma}$):

$$
\psi^{\dagger}_{\uparrow}\psi^{\dagger}_{\downarrow}\psi_{\downarrow}\psi_{\uparrow} \approx < \psi^{\dagger}_{\uparrow}\psi^{\dagger}_{\downarrow} > \psi_{\downarrow}\psi_{\uparrow} + \psi^{\dagger}_{\uparrow}\psi^{\dagger}_{\downarrow} < \psi_{\downarrow}\psi_{\uparrow} > + const. \quad (2.13)
$$

The brilliance of Gor'kov was to choose precisely the form of the interaction term such as after the Bogoliubov approximation will give us the correlation $< \psi^\dagger_\uparrow(\vec{x})\psi^\dagger_\downarrow(\vec{x}) >$ which is non zero only in the superconducting state. This motivates the definition of the anomalous Green function $F(\vec{x}\tau, \vec{x}'\tau')$ together with the normal Green function $G(\vec{x}\tau, \vec{x}'\tau')$ with τ as the imaginary time, then:

$$G(\vec{x}\tau, \vec{x}'\tau') = -\frac{1}{\hbar}\left\langle T\psi_\uparrow(\vec{x}\tau)\psi^\dagger_\uparrow(\vec{x}'\tau')\right\rangle, \tag{2.14}$$

$$\bar{F}(\vec{x}\tau, \vec{x}'\tau') = -\frac{1}{\hbar}\left\langle T\psi^\dagger_\downarrow(\vec{x}\tau)\psi^\dagger_\uparrow(\vec{x}'\tau')\right\rangle, \tag{2.15}$$

$$\bar{G}(\vec{x}\tau, \vec{x}'\tau') = -\frac{1}{\hbar}\left\langle T\psi^\dagger_\downarrow(\vec{x}\tau)\psi_\downarrow(\vec{x}'\tau')\right\rangle, \tag{2.16}$$

$$F(\vec{x}\tau, \vec{x}'\tau') = -\frac{1}{\hbar}\left\langle T\psi_\uparrow(\vec{x}\tau)\psi_\downarrow(\vec{x}'\tau')\right\rangle, \tag{2.17}$$

where T represent the temporal ordering operator and $\hbar$ is the Planck constant divided by 2π.

From the definition of the anomalous Green function we can now define the superconducting OP,

$$\Delta(\vec{x}) = -g \lim_{(\tau',\vec{x}')\to(\tau,\vec{x})} F(\vec{x}\tau, \vec{x}'\tau'). \tag{2.18}$$

We notice the convenience of the formalism of Green functions, which allowed to introduce the OP elegantly in the Hamiltonian (2.12). Moreover, based on the definition of the superconducting OP, we underline the advantage of the Gor'kov formalism when one deals with a system in the presence of non-magnetic impurities. To see this consider the anomalous Green function averaged over the impurities:

$$F(\tau\vec{x}, \tau'\vec{x}') \propto F(\tau - \tau', \vec{x} - \vec{x}') \exp\left[-(\vec{x} - \vec{x}')/l\right], \tag{2.19}$$

where l is the mean free path. Although the anomalous Green function decays exponentially, qualitatively the superconducting OP remains the same when the system is isotropic [2], see Eqs. (2.18) and (2.19). This result is also known as the Anderson theorem [4].

Putting together Eqs. (2.12), (2.13) and (2.18), we obtain the mean-field Hamiltonian

$$H = \sum_\sigma \int d^3\vec{x}\psi^\dagger_\sigma(\vec{x})T_{\vec{x}}\psi_\sigma(\vec{x}) + \int d^3\vec{x}\left[\psi^\dagger_\uparrow(\vec{x})\psi^\dagger_\downarrow(\vec{x})\Delta(\vec{x}) + c.c\right]. \tag{2.20}$$

In the Heisenberg representation our fermionic fields can be represented as

$$\psi_\sigma(\vec{x}\tau) = e^{\frac{\hat{H}\tau}{\hbar}}\psi_\sigma(\vec{x})e^{-\frac{\hat{H}\tau}{\hbar}}, \tag{2.21}$$

$$\bar{\psi}_\sigma(\vec{x}\tau) = e^{\frac{\hat{H}\tau}{\hbar}}\psi^\dagger_\sigma(\vec{x})e^{-\frac{\hat{H}\tau}{\hbar}}, \tag{2.22}$$

where its corresponding equations of motion in matrix form are

$$-\hbar\partial_\tau \begin{pmatrix} \psi_\uparrow(\tau\vec{x}) \\ \bar{\psi}_\downarrow(\tau\vec{x}) \end{pmatrix} = \begin{pmatrix} T_{\vec{x}} & \Delta(\vec{x}) \\ \Delta^*(\vec{x}) & -T_{\vec{x}} \end{pmatrix} \begin{pmatrix} \psi_\uparrow(\tau\vec{x}) \\ \bar{\psi}_\downarrow(\tau\vec{x}) \end{pmatrix}. \tag{2.23}$$

We have everything in our disposal to calculate the temporal evolution of the two point correlation functions. Using (2.23) we obtain

$$\begin{aligned} -\hbar\partial_\tau G(x,x') &= \delta(x-x') + T_{\vec{x}}G(x,x') + \Delta(\vec{x})\bar{F}(x,x'), && (2.24)\\ -\hbar\partial_\tau \bar{F}(x,x') &= -T^*_{\vec{x}}\bar{F}(x,x') + \Delta^*(\vec{x})G(x,x'), && (2.25)\\ -\hbar\partial_\tau \bar{G}(x,x') &= \delta(x,x') - T^*_{\vec{x}}\bar{G}(x,x') + \Delta^*(\vec{x})F(x,x'), && (2.26)\\ -\hbar\partial_\tau F(x,x') &= T_{\vec{x}}F(x,x') + \Delta(\vec{x})\bar{G}(x,x'), && (2.27) \end{aligned}$$

where $x \equiv (\tau, \vec{x})$.

We proceed by applying the Fourier transforms. From the imaginary time we go to the frequency domain $(\tau - \tau') \to \omega$. Then, from the coordinate space we go to momentum space $\vec{x} \to (\vec{k} - \vec{k}')$, $(\vec{x} - \vec{x}') \to \vec{k}$. Therefore, Eqs. (2.24)-(2.27) become

$$\begin{aligned} \delta(\vec{k}-\vec{k}')(i\hbar\omega - \xi_{\vec{k}'})G_{\omega,\vec{k}'} &= \delta(\vec{k}-\vec{k}') + \Delta(\vec{k}-\vec{k}')\bar{F}_{\omega,\vec{k}'}, && (2.28)\\ \delta(\vec{k}-\vec{k}')(i\hbar\omega + \xi_{\vec{k}'})\bar{F}_{\omega,\vec{k}'} &= \Delta^*(\vec{k}-\vec{k}')G_{\omega,\vec{k}'}, && (2.29)\\ \delta(\vec{k}-\vec{k}')(i\hbar\omega + \xi_{\vec{k}'})\bar{G}_{\omega,\vec{k}'} &= \delta(\vec{k}-\vec{k}') + \Delta^*(\vec{k}-\vec{k}')F_{\omega,\vec{k}'}, && (2.30)\\ \delta(\vec{k}-\vec{k}')(i\hbar\omega - \xi_{\vec{k}'})F_{\omega,\vec{k}'} &= \Delta(\vec{k}-\vec{k}')\bar{G}_{\omega,\vec{k}'}, && (2.31) \end{aligned}$$

where ω is the fermionic Matsubara frequency and $\xi_{\vec{k}}$ is the kinetic operator in momentum representation. Now, we assume that our OP is homogeneous:

$$\Delta(\vec{k}-\vec{k}') = \delta(\vec{k}-\vec{k}')\Delta_0. \tag{2.32}$$

Finally we obtain the Nambu-Gor'kov equations in the momentum representation ($f_{\vec{k}} \to f(\vec{k})$, $\Delta_0 \to \Delta$) :

$$\begin{aligned} (i\hbar\omega - \xi_{\vec{k}})G_\omega(\vec{k}) &= 1 + \Delta\bar{F}_\omega(\vec{k}), && (2.33)\\ (i\hbar\omega + \xi_{\vec{k}})\bar{F}_\omega(\vec{k}) &= \Delta^* G_\omega(\vec{k}), && (2.34)\\ (i\hbar\omega + \xi_{\vec{k}})\bar{G}_\omega(\vec{k}) &= 1 + \Delta^* F_\omega(\vec{k}), && (2.35)\\ (i\hbar\omega - \xi_{\vec{k}})F_\omega(\vec{k}) &= \Delta\bar{G}_\omega(\vec{k}). && (2.36) \end{aligned}$$

Combining the last two equations (2.35) and (2.36), we obtain $F_\omega(\vec{k})$:

$$F_\omega(\vec{k}) = -\frac{1}{2\varepsilon}\left(\frac{1}{i\hbar\omega + \varepsilon}\right) + \frac{1}{2\varepsilon}\left(\frac{1}{i\hbar\omega - \varepsilon}\right), \tag{2.37}$$

where $\varepsilon^2 = \xi_{\vec{k}}^2 + |\Delta|^2$. To obtain the equation for the OP we need to sum over the Matsubara's frequencies and integrate over the $\vec{k}$ momentum (the inverse Fourier transform):

$$\Delta = -\frac{g}{\beta}\sum_{\omega} e^{i\omega 0^+}\int \frac{d^3\vec{k}}{(2\pi)^3}F_{\omega}(\vec{k}). \tag{2.38}$$

The sum over the Matsubara frequencies for simple poles is

$$\sum_{\omega}\frac{e^{i\omega 0^+}}{i\hbar\omega - x} = \frac{\beta}{e^{\beta x}+1}, \quad \beta = \frac{1}{k_B T}, \tag{2.39}$$

where k_B is the Boltzmann constant. Finally, we obtain the equation for the OP,

$$\Delta = g\int \frac{d^3\vec{k}}{(2\pi)^3}\frac{\Delta \tanh\left(\frac{\beta\varepsilon}{2}\right)}{2\varepsilon}. \tag{2.40}$$

The above Eq.(2.40) can be solved self consistently and there are two particular cases for which we can get analytic solutions, those are:

- At $T = T_c$, therefore $\Delta \to 0$
- At $T = 0$ K, therefore $\tanh(\frac{\beta\varepsilon}{2}) \to 1$

Before we proceed, we make the following substitution $k \to \xi_{\vec{k}}$, where $\xi_{\vec{k}} = \vec{k}^2/2m - \mu$, then

$$\int \frac{d^3\vec{k}}{(2\pi)^3} = \int_0^{\Omega}\frac{dk}{2\pi^2} = \int_{-\Omega}^{\Omega} d\xi_{\vec{k}}\left(\frac{m\sqrt{2m(\xi_{\vec{k}}+\mu)}}{2\pi^2}\right), \tag{2.41}$$

now using the fact that close to the Fermi level $\sqrt{2m(\xi_{\vec{k}}+\mu)} \approx \sqrt{2m\mu} = k_F$, we have

$$\int \frac{d^3\vec{k}}{(2\pi)^3} \approx N(0)\int_{-\Omega}^{\Omega} d\xi_{\vec{k}}, \tag{2.42}$$

where $N(0) = \frac{mk_F}{2\pi^2}$ is the density of states at the Fermi level.

Hence, the above approximation Eq. (2.42), give us the solution for both cases:

- For $T = T_c$, we have

$$\frac{1}{gN(0)} = \int_{-\Omega}^{\Omega} d\xi_{\vec{k}}\frac{\tanh\left(\frac{\beta_c\xi_{\vec{k}}}{2}\right)}{2\xi_{\vec{k}}} \approx \ln\left(\frac{2e^{\gamma}\Omega}{\pi T_c}\right), \tag{2.43}$$

  where γ is the Euler's constant. The expression for Tc is

$$k_B T_c = \frac{2e^{\gamma}}{\pi}\Omega e^{-\frac{1}{gN(0)}}. \tag{2.44}$$

- For $T = 0$ K, we have

$$\frac{1}{gN(0)} = \int_{-\Omega}^{\Omega} d\xi_{\vec{k}} \frac{1}{\sqrt{\xi_{\vec{k}^2+|\Delta|^2}}} = \sinh^{-1}\left(\frac{\Omega}{\Delta}\right), \tag{2.45}$$

  the expression for Δ is

$$\Delta = \frac{\Omega}{\sinh\left(\frac{1}{gN(0)}\right)} \approx 2\Omega e^{-\frac{1}{gN(0)}}, \tag{2.46}$$

  where we have used the weak coupling limit, meaning gN(0)«1.

The above solutions help us to calculate the ratio of the OP at zero temperature with the critical temperature T_c

$$\frac{\Delta(0)}{k_B T_c} = 1.764. \tag{2.47}$$

If the gap opening in the normal conductance is given by 2Δ, then we obtain the famous BCS ratio of $2\Delta(0)/k_B T_c = 3.53$.

2.3 PHENOMENOLOGICAL THEORY OF SUPERCONDUCTIVITY

In the previous section we have reviewed the principles of the BCS theory and its remaining problems where two of them were addressed using the Gor'kov Green function formalism. One of the problems was solved by the definition of the order parameter given by the contraction of the anomalous Green function Eq. (2.18) which together with Eq. (2.19) validates the BCS theory also in the dirty limit. Now, in this section we will focus on the relation of the microscopic theory of superconductivity with its phenomenological counterpart.

2.3.1 *London model*

In superconductors when an external magnetic field is applied, the vanishing of resistance at T_c is accompanied by the expulsion of the magnetic field in its interior . This property, which is used for magnetic levitated transportation, originates from the perfect diamagnetism present in superconductivity. Indicators of this property were observed soon after the discovery of superconductivity in the Kamerlingh Onnes laboratory, where superconductivity disappeared if an applied magnetic field surpasses the value of 0.04 Teslas (upper critical field for Hg). However, the discovery of the magnetic repulsion in superconductors was reported only in 1933 by two German physicists, Walther Meissner and Robert Ochsenfeld (the Meissner-Ochsenfeld effect). They studied the magnetic flux configuration around a superconducting sample when an external magnetic field is applied [85],

see fig. 2.3. Based on the magnetic repulsion and infinite conductivity, we can characterize a superconductor as a material which presents no resistance and perfect diamagnetism.

A superconductor is a state of matter which presents no resistance and perfect diamagnetism.

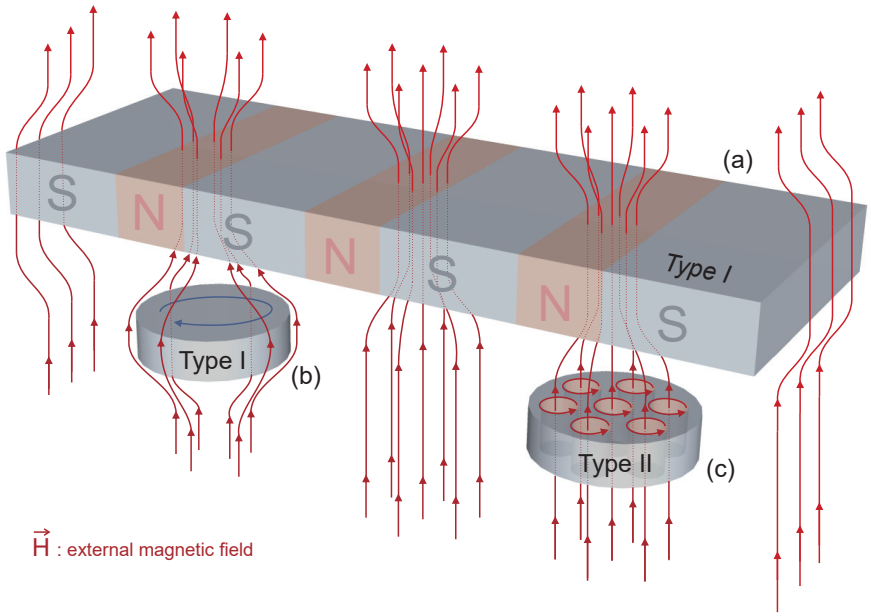

Figure 2.3: The Meissner effect in superconductors. The repulsion of the magnetic field depends on the geometry of the superconductor (a) and the way how the magnetic field penetrates the superconductor defines type I (b) and type II (c) superconductors.

The definition of the type of the superconductor in Fig. 2.3 will be introduced in the next Section. when we present the GL theory.

The Meissner-Ochsenfeld effect gave physicists more clues to elucidate the superconducting phase when no microscopic theories were available. Then, it is not surprising that historically the first progress towards a theory of superconductivity was done by the London brothers in 1935 [76]. They were inspired by the diamagnetic part of a quantum mechanical current and gave the first explanation to the perfect diamagnetism of superconductors. To see this, consider the wave function $\psi(\vec{x})$[3] that couples minimally with electromagnetism, then the Ampère current is given by

$$\vec{j} = \frac{\hbar e}{2mi}\left(\psi^*\vec{\nabla}\psi - \psi\vec{\nabla}\psi^*\right) - \frac{e^2}{mc}\psi^*\psi\vec{A}, \tag{2.48}$$

where $\vec{A}$ is the vector potential. The London brothers observed that if the wave function is rigid, meaning $\psi(\vec{x}) = \psi$, then the current is

$$\vec{j} = -\frac{e^2}{mc}|\psi|^2\vec{A}. \tag{2.49}$$

3 Here the wave function $\psi(\vec{x})$ does no longer describe a single electron but, as we will see later, the pair correlation between two electrons.

Replacing the London current (2.49) in the Ampère law we get

$$\vec{\nabla} \times \vec{h} = -4\pi \frac{e^2}{mc^2} |\psi|^2 \vec{A}. \tag{2.50}$$

Taking the rotational of the above equation and using $\vec{\nabla}.\vec{h} = 0$, we have

$$\left(\vec{\nabla}^2 - \frac{1}{\lambda_L^2}\right) \vec{h} = 0, \tag{2.51}$$

where λ_L^2 is defined as

$$\lambda_L^2 = \frac{mc^2}{4\pi e^2 |\psi|^2}. \tag{2.52}$$

λ_L is the London penetration depth which determines the length that the magnetic field reaches inside the superconductor.

For a planar superconductor, the solution of (2.51) is given by

$$\vec{h}(\vec{x}) = \vec{h}_0 e^{-x_3/\lambda_L}, \tag{2.53}$$

where x_3 is the direction perpendicular to the surface of the superconductor and $\vec{H}_0$ is the magnetic field parallel to its surface.

Equation (2.51) is the non-relativistic version of the Proca equation which correspond to a field with mass and spin 1. To see this, we use the Coulomb or London gauge $\vec{\nabla}.\vec{A} = 0$ and we obtain:

$$\left(\vec{\nabla}^2 - \frac{1}{\lambda_L^2}\right) \vec{A} = 0. \tag{2.54}$$

The above Eq. (2.54) describes a massive mediator of the magnetic interaction. Usually the Meissner effect in a superconductors is depicted by the presence of spontaneous currents in its surface. Nonetheless, it was the interpretation of mass generation that later inspired particle physicists for the formulation of the Higgs mechanism.

The solution of the London equation describes a massive mediator of the magnetic interaction and therefore it is short ranged.

2.3.2 *Ginzburg-Landau theory*

There were a few problems with the London model. First, it gave no explanation why superconductivity vanishes in thin films after the applied magnetic field or current exceed their particular critical values: $\vec{H}_c$, $\vec{j}_c$. Second, if we were to calculate the surface energy at the boundary separating the superconducting and normal phases, using Eq. (2.53) we would obtain a negative surface energy. The surface energy is equal to the bulk free energy per unit volume times a length

of the order of atomic dimensions, which following the London model will be equal to $-\lambda_L \vec{h}_c^2/8\pi$.[4]

To solve the London model problems, Ginzburg and Landau realized that they need to substantially change the current set of equations, which they did brilliantly based on two physical principles [46, 47]:

1. *Introduction of a complex order parameter, $\psi(\vec{x})$.* From the specific heat measurements of superconductors it was known that the phase transition was of the second kind. All second order phase transitions are accompanied by the emergence of a phenomenological OP which changes from zero to non-zero when the system goes from the disordered to the ordered phase. In this context, this new field $\psi(\vec{x})$ will describe the wave function of the superconducting electrons which needs to be complex to minimally couple to the electromagnetic interaction and to properly describe charged particles.

2. *Preservation of gauge symmetry.* To accommodate a second order phase transition in the free energy, you are constrained by gauge symmetry. In terms of $\psi(\vec{x})$, this implies that its phase is not present in the free energy and its derivatives are covariant under a gauge transformation:

$$\frac{\hbar}{i}\vec{\nabla}\psi(\vec{x}) \to \left(\frac{\hbar}{i}\vec{\nabla} - \frac{e}{c}\vec{A}\right)\psi(\vec{x}). \tag{2.55}$$

Following the above two principles and assuming ψ is small, which is reasonable when we are close to T_c, then the Gibbs free energy of a superconductor is given by

$$f = f_{n0} + \frac{1}{2m}\left|\left(\frac{\hbar}{i}\vec{\nabla} - \frac{e}{c}\vec{A}\right)\psi\right|^2 + \alpha|\psi|^2 + \frac{\beta}{2}|\psi|^4 + \frac{\vec{h}^2}{8\pi}, \tag{2.56}$$

where $f_{n0} = f_n|(T = T_c)$ is the free energy of the normal phase without any applied field and m and e are the bare mass and charge of the electron[5] and $\vec{h} = \vec{\nabla} \times \vec{A}$.

Now we calculate the surface energy which is the free energy difference between its surface and the bulk.

In the bulk we assume that the superconductor OP is constant ($\psi_b = const$). Then, if there is no applied magnetic field, the free energy becomes

4 When the GL was first formulated, no superconductors with negative surface energy were reported (type II superconductors).

5 Ginzburg and Landau had no reason to assume otherwise even when they found that there was a discrepancy with the experiment by a factor of ~ 2. Landau assumed that those effects came from the dressing of $e \to e^*$ and $m \to m^*$ which are always present in a Fermi liquid theory. Later, was Gor'kov who made a correction of this factor after the BCS theory was formulated.

$$f_s = f_{n0} + \alpha|\psi|^2 + \frac{\beta}{2}|\psi|^4, \quad f_n = f_{n0} \tag{2.57}$$

$$f_s - f_n = \alpha|\psi|^2 + \frac{\beta}{2}|\psi|^4. \tag{2.58}$$

In this case, Eq. (2.58) is in equilibrium when $\partial f/\partial|\psi|^2 = 0$ and $\partial^2 f/\partial|(\psi|^2)^2 > 0$, therefore

$$\alpha + \beta|\psi|^2 = 0, \quad \beta > 0, \quad \rightarrow \quad |\psi_b|^2 = -\frac{\alpha}{\beta}, \tag{2.59}$$

which implies that when $T < T_c$, $\alpha < 0$ and when $T = T_c$, $\alpha_c = 0$. If we substitute (2.59) into (2.58) we get

$$f_s - f_n = -\frac{\alpha^2}{2\beta}. \tag{2.60}$$

Now we proceed to calculate the free energy of the surface which is equivalent to the bulk free energy if the magnetic field reaches its critical value ($\vec{h} = \vec{H}_c$), then

$$f_s = f_{n0}, \quad f_n = f_{n0} + \frac{\vec{h}^2}{8\pi} \tag{2.61}$$

$$f_s - f_n = -\frac{\vec{h}^2}{8\pi}. \tag{2.62}$$

From (2.60) and (2.62), we obtain $\vec{H}_c$

$$-\frac{\alpha^2}{2\beta} = -\frac{\vec{h}^2}{8\pi} \quad \rightarrow \quad \vec{H}_c^2 = \frac{4\pi}{\beta}\alpha^2. \tag{2.63}$$

To calculate α we make its Taylor expansion around $T \rightarrow T_c$

$$\alpha(T) = \alpha_c + (T - T_c)\frac{\partial\alpha}{\partial T}\Big|_{T=T_c} + \ldots \tag{2.64}$$

The condition of equilibrium requires $\alpha_c = 0$, which gives us

$$\vec{H}_c^2 = 4\pi\frac{(T - T_c)^2}{\beta}\left(\frac{\partial\alpha}{\partial T}\right)\Big|^2_{T=T_c}. \tag{2.65}$$

Eq. (2.65) is in agreement with experiment and solves one of the issues of the London model regarding the existence of an upper critical field, $\vec{H}_c$.

An interesting fact coming from the expression α is that qualitatively changes the shape of the potential $V(\psi) = \alpha|\psi|^2 + \beta|\psi|^4/2$ for $T > T_c$ and $T < T_c$, see Fig 2.4.

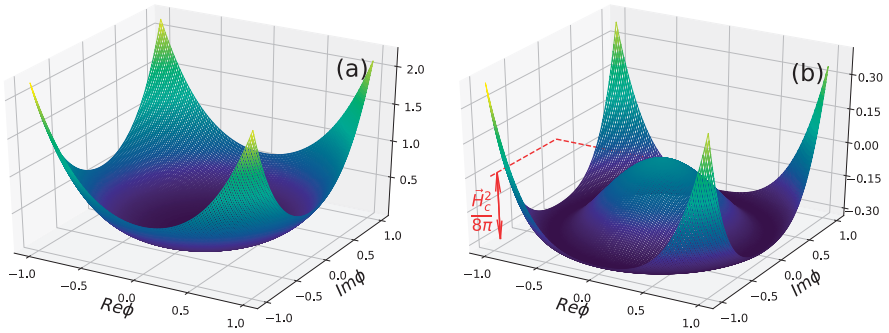

Figure 2.4: $V(\psi)$ for: (a) $\alpha > 0$ and (b) $\alpha < 0$.

Experimentally we can obtain values of α and β by measuring $\vec{H}_c$ and λ_L. Using Eqs. (2.52), (2.59) and (2.63) we get

$$\alpha = -\frac{e^2}{mc^2}\vec{H}_c^2\lambda_L^2, \tag{2.66}$$

$$\beta = 4\pi\frac{e^4}{m^2c^4}\vec{H}_c^2\lambda_L^4. \tag{2.67}$$

Taking the variational principle from (2.56) we get the Ginzburg-Landau equations

$$\left[\frac{1}{2m}\left(\frac{\hbar}{i}\vec{\nabla} - \frac{e}{c}\vec{A}\right)^2 + \alpha + \beta|\psi|^2\right]\psi = 0, \tag{2.68}$$

$$\vec{\nabla}\times\vec{h} = \frac{4\pi}{c}\left[\frac{e\hbar}{2mi}\left(\psi^*\vec{\nabla}\psi - \psi\vec{\nabla}\psi^*\right) - \frac{e^2}{mc}|\psi|^2\vec{A}\right]. \tag{2.69}$$

To have an idea of the solution of Eq. (2.68), we take $\vec{A} = 0$ and solve it in one dimension $\psi = \psi(x)$,

$$-\frac{\hbar^2}{2m|\alpha|}\frac{\partial^2}{\partial x^2}\psi - \psi + |\psi|^3 = 0, \tag{2.70}$$

where we have normalized the function with its bulk value, $\psi \to \sqrt{-\frac{\beta}{\alpha}}\psi$. Eq. (2.70) has an analytic solution:

$$\psi(x) = \tanh\left(\frac{x}{\sqrt{2}\xi_{GL}}\right), \tag{2.71}$$

where $\xi_{GL} = \sqrt{\frac{\hbar^2}{2m|\alpha|}}$ is the GL coherence length which characterize the OP profile from the surface to the bulk of the superconductor.

Therefore, the GL theory contains two characteristic lengths: the London penetration depth λ_L and the coherence length ξ_{GL}. Their physical significance is better depicted if we consider the interface between the normal (N) and superconducting phases (S), see fig. 2.5.

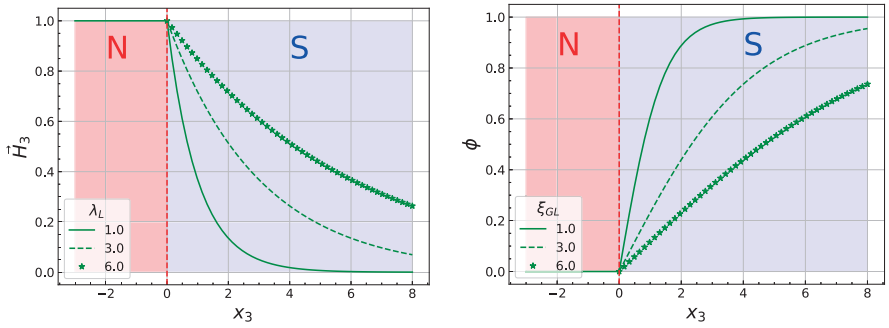

Figure 2.5: Characteristic lengths of GL: (left) the London penetration depth and (right) coherence length.

Once we have defined λ_L and ξ_{GL}, an important classification of superconductors comes with the introduction of the GL paremeter:

$$\kappa = \frac{\lambda_L}{\xi_{GL}}. \tag{2.72}$$

To see better the importance of κ, we write the expression for the surface energy, but this time for position dependent $\psi(x)$. The Gibbs free energy at the surface is given by

$$g_{surface} = f_{surface} - \frac{\vec{h}.\vec{H}_c}{4\pi}. \tag{2.73}$$

On the other hand, deep in the bulk of the superconductor the Gibbs free energy is

$$g_{bulk} = g_{n0} - \frac{\vec{H}_c^2}{8\pi}, \tag{2.74}$$

where g_{n0} is the Gibbs energy of the normal phase. Now, the surface energy E_S is simply the difference (2.73) - (2.74)

$$E_S = g_{surface} - g_{bulk} = f_{surface} - \frac{\vec{h}.\vec{H}_c}{4\pi} - g_{n0} + \frac{\vec{H}_c^2}{8\pi}. \tag{2.75}$$

Simplifying further we get

$$E_S = \frac{1}{2m}\left|\left(\frac{\hbar}{i}\vec{\nabla} - \frac{e}{c}\vec{A}\right)\psi\right|^2 + \alpha|\psi|^2 + \frac{\beta}{2}|\psi|^4 + \frac{\left(\vec{h}-\vec{H}_c\right)^2}{8\pi}. \tag{2.76}$$

If we subtract Eq. (2.68) from Eq. (2.76) and then integrate over the coordinate perpendicular to the interface, we get

$$\gamma = \int_{-\infty}^{\infty} dx_3 \left[-\frac{\beta}{2}|\psi|^4 + \frac{\left(\vec{h}-\vec{H}_c\right)^2}{8\pi}\right]. \tag{2.77}$$

The integrated surface energy γ(2.77) shows a clear competition between the condensation energy which is negative (takes energy to form Cooper pairs) $-\frac{\beta}{2}|\psi|^4$ and the diamagnetic energy which is positive $(\vec{h}-\vec{H}_c)^2/8\pi$. Comparing (2.53) with (2.71) we see that if $\kappa << 1$ ($\lambda_L << \xi_{GL}$), then the diamagnetic energy is dominant over the condensation energy and the surface energy is positive. On the other hand, if $\kappa >> 1$ ($\lambda_L >> \xi_{GL}$), then the condensation energy is dominant and the surface energy is then negative. This division introduces a classification in the superconductors in two types, type I with $\kappa << 1$ and type II with $\kappa >> 1$. Numerical calculations of the GL equations showed that the transition point occurs for $\kappa = \frac{1}{\sqrt{2}}$.

2.3.3 *Gor'kov derivation of the Ginzburg-Landau theory*

Gor'kov showed that the GL theory can formally be derived microscopically by the expansion of the order parameter close to the transition $T = T_c$ [53], [54] for an arbitrary magnetic field below $\vec{H}_c$ where $\lambda_L > \xi_{GL}$ (type II superconductors). To see Gor'kov's derivation, we start by taking the time Fourier transform of equations (2.26) and (2.27) and minimally couple them with electromagnetism (2.55):

$$\left(-i\hbar\omega + \frac{1}{2m}\vec{D}^{*2} + \mu\right)\bar{G}_\omega = \delta(\vec{x}-\vec{x}') + \Delta^*(\vec{x})F_\omega, \quad (2.78)$$

$$\left(i\hbar\omega + \frac{1}{2m}\vec{D}^{2} + \mu\right)F_\omega = \Delta(\vec{x})\bar{G}_\omega, \quad (2.79)$$

where $\vec{D} = \hbar/i\vec{\nabla} - e/c\vec{A}$ and $\bar{G}_\omega \equiv \bar{G}_\omega(\vec{x},\vec{x}')$, $F_\omega \equiv F_\omega(\vec{x},\vec{x}')$. Note that we cannot take directly the Fourier transform of the coordinates due to the presence of the magnetic potential $\vec{A}$. Now, equations (2.78) and (2.79) can be writen in an integral form as follows

$$F_\omega(\vec{x},\vec{x}') = \int d^3y G^0_\omega(\vec{x},\vec{y})\Delta(\vec{y})\bar{G}_\omega(\vec{y},\vec{x}'), \quad (2.80)$$

$$\bar{G}_\omega(\vec{x},\vec{x}') = \bar{G}^0_\omega(\vec{x},\vec{x}') + \int d^3y \bar{G}^0_\omega(\vec{x},\vec{y})\Delta^*(\vec{y})F_\omega(\vec{y},\vec{x}'), \quad (2.81)$$

where $G^0_\omega(\vec{x},\vec{y})$ is the normal Green function for metals in absence of a magnetic field:

$$G^0_\omega(\vec{x},\vec{y}) = \int \frac{d^3k}{(2\pi)^3}\frac{e^{i\vec{k}.(\vec{x}-\vec{y})}}{i\hbar\omega - \xi_k}. \quad (2.82)$$

We can solve (2.80) and (2.81) by iteration, but first we need to establish a criteria for truncation of the iterative process. Close to T_c

our OP vanishes as any other phase transition[6], therefore relations (2.59) and (2.64) hold and we have

$$\psi = \sqrt{\frac{T_c}{\beta}}\tau^{1/2}, \quad \tau = 1 - \frac{T}{T_c}. \tag{2.83}$$

Now, let's assume that the microscopic and macroscopic OP are related, $\psi \propto \Delta$ and use τ as a control parameter of the iterative process. Furthermore, because of the coherence length $\xi_{GL} = \sqrt{-\hbar^2/2m\alpha}$, the coordinates will also be scaled.

$$\Delta \to \tau^{1/2}\Delta \quad \vec{x} \to \tau^{-1/2}\vec{x}, \quad \vec{\nabla} \to \tau^{1/2}\vec{\nabla}, \tag{2.84}$$

The above scaling of the coordinates was not introduced by Gor'kov. Formally it is not needed if one deals only with the canonical GL derivation which goes to the order $\tau^{3/2}$ of the iterative process. However, there are two situations where this scaling is needed to keep control of the iterative process:

1. When we take the next order iteration of the GL expansion, then we must introduce a transformation also in the coordinates to control the truncation of higher order derivatives [130, 131].
2. If we deal with multicomponent GL models where the coupling between them introduce higher orders terms beyond the GL domain (truncation up to $\tau^{3/2}$) [67, 114].

Solving by iteration (2.80) and (2.81) up to $\tau^{3/2}$, we get an expression for the anomalous Green function $F_\omega(\vec{x}, \vec{x}')$,

$$F_\omega(\vec{x}, \vec{x}') = I_1 + I_2, \tag{2.85}$$

$$I_1 = \int d^3y G^0_\omega(\vec{x}, \vec{y})\Delta(\vec{y})\bar{G}^0_\omega(\vec{y}, \vec{x}'), \tag{2.86}$$

$$I_2 = \int d^3y_1 d^3y_2 d^3y_3 G^0_\omega(\vec{x}, \vec{y}_1)\Delta(\vec{y}_1)\bar{G}^0_\omega(\vec{y}_1, \vec{y}_2)\Delta^*(\vec{y}_2) \times \\ \times G^0_\omega(\vec{y}_2, \vec{y}_3)\Delta(\vec{y}_3)\bar{G}^0_\omega(\vec{y}_3, \vec{x}'). \tag{2.87}$$

Although the anomalous Green function (2.85) depends on two unknown functions: $G_\omega(\vec{x}, \vec{y})$ and $\bar{G}_\omega(\vec{x}, \vec{y})$, the normal green functions can be related through the charge, parity and time (CPT) transformation[7]. This means that

$$\bar{G}_\omega(\vec{x}, \vec{y}) = -G_{-\omega}(\vec{y}, \vec{x}). \tag{2.88}$$

6 Even first order transitions can be described by an OP. For example, in the transition gas/liquid of water we can define the order parameter as the density difference of the two phases.

7 The CPT transformation is used because we have symmetry under the simultaneous transformation of charge conjugation $\bar{G}_\omega(\vec{x}, \vec{y}) = G_\omega(\vec{x}, \vec{y})$, parity inversion $G_\omega(\vec{x}, \vec{y}) = -G_\omega(\vec{y}, \vec{x})$ and time reversion $G_\omega(\vec{x}, \vec{y}) = G_{-\omega}(\vec{x}, \vec{y})$.

Before we calculate the integrals I_1 and I_2 from (2.85) we need to take into account three considerations:

1. The normal Green function in presence of a magnetic field will be related by a phase factor to the normal Green function with $\vec{B} = 0$ as

$$G_\omega(\vec{x},\vec{x}')\Big|_{\vec{B}\neq 0} = e^{\frac{i}{\hbar}\frac{e}{c}\int_{\vec{x}'}^{\vec{x}}\vec{A}.d\vec{l}} G_\omega(\vec{x},\vec{x}')\Big|_{\vec{B}=0}. \tag{2.89}$$

   Eq. (2.89) assures that $G_\omega(\vec{x},\vec{x}')$ transform covariantly under a local gauge transformation and therefore satisfies (2.78) and (2.79). Furthermore, the phase $\int_{\vec{x}'}^{\vec{x}}\vec{A}.d\vec{l}$ in terms of the path integral formalism can be expanded around the classical trajectory which is the straight line $\vec{x}-\vec{x}'$,

$$e^{\frac{i}{\hbar}\frac{e}{c}\int_{\vec{x}'}^{\vec{x}}\vec{A}.d\vec{l}} \approx e^{\frac{i}{\hbar}\frac{e}{c}\vec{A}.(\vec{x}-\vec{x}')}. \tag{2.90}$$

   The above approximation is enough in terms of the expansion up to $\tau^{3/2}$. Nonetheless if we need to extend the GL equation then we should go beyond the classical trajectory [130]. Due to the minimal coupling with electromagnetism (2.55), the vector potential is rescaled by τ

$$\vec{A} \to \tau^{1/2}\vec{A}, \quad \Longrightarrow \vec{H} \to \tau\vec{H}. \tag{2.91}$$

2. The Taylor expansions $\Delta(y)$ around $\vec{x}$ inside the integrals I_1 and I_2 can be performed as follows:

$$\Delta(\vec{y}) = \Delta(\vec{r}+\vec{z}) = \sum_{n=0}^{\infty}\frac{1}{n!}(\vec{z}.\vec{\nabla})^n\Delta(\vec{r}), \tag{2.92}$$

   where $\vec{z} = \vec{y}-\vec{r}$. The above expression will allow us to put all the $\Delta(\vec{y})$ out of the integrals (2.86, 2.87).

3. The anomalous Green function in Eq. (2.85) contains the full solution for all n-orders of $\tau^{n/2}$. Therefore, when we calculate the order parameter from it we need to expand it again in terms of τ:

$$\lim_{\vec{x}\to\vec{x}'}\sum_{\omega} F_\omega(\vec{x}-\vec{x}') = \Delta(\vec{x}) = \Delta_0 + \tau\Delta_1 + ..., \tag{2.93}$$

   the lowest order in the expansion will give us two equations by collecting the the factors proportional to $\tau^{1/2}$ and $\tau^{3/2}$ respectively.

Finally, we can proceed to calculate the integrals I_1 and I_2 for the OP. Summing over Matsubara's frequencies and taking the corresponding limit, $\lim_{\vec{x}\to\vec{x}'} gT\sum_\omega I_1$ is equal to

$$gT\sum_\omega \int d^3y \left(e^{\frac{i}{\hbar}\frac{e}{c}\tau^{1/2}\vec{A}(\vec{x}).(\vec{x}-\vec{y})} \int \frac{d^3k_1}{(2\pi)^3}\frac{e^{i\vec{k}_1.(\vec{x}-\vec{y})}}{i\omega-\xi_{k_1}} \right) \tau^{1/2}\Delta(\vec{y}) \times \left(e^{-\frac{i}{\hbar}\frac{e}{c}\tau^{1/2}\vec{A}(\vec{x}).(-\vec{x}+\vec{y})} \int \frac{d^3k_2}{(2\pi)^3}\frac{e^{-i\vec{k}_2.(\vec{x}-\vec{y})}}{-i\omega-\xi_{k_2}} \right), \quad (2.94)$$

where we have used the CPT transformation for $\bar{G}^0_\omega$ and the Fourier representation of all normal Green functions. The expansion for $\Delta(y)$ up to $\tau^{3/2}$ is then given by

$$\tau^{1/2}\Delta(\vec{y}) = \tau^{1/2}\Delta(\vec{x}) + \tau(\vec{z}.\vec{\nabla})\Delta(\vec{x}) + \tau^{3/2}\frac{(\vec{z}.\vec{\nabla})^2}{2}\Delta(\vec{x}), \quad (2.95)$$

where $\vec{z} = \vec{y} - \vec{x}$. The expansion of the exponentials in (2.94) are taken up to $\tau^{1/2}$ because next order would introduce terms beyond the original GL equation derivation. Substituting Eq. (2.95) into (2.94) we get

$$gT\sum_\omega \int d^3y \left(\int \frac{d^3k_1}{(2\pi)^3}\frac{e^{i\vec{k}_1.(\vec{x}-\vec{y})}}{i\omega-\xi_{k_1}} \right) \left(\int \frac{d^3k_2}{(2\pi)^3}\frac{e^{-i\vec{k}_2.(\vec{x}-\vec{y})}}{-i\omega-\xi_{k_2}} \right) \times \left(\tau^{1/2}\Delta(\vec{x}) + \tau^{3/2}\frac{(\vec{z}.\vec{D})^2}{2}\Delta(\vec{x}) \right), \quad (2.96)$$

where we have neglected terms odd in $\vec{z}$ because the limits of integration are symmetric. Note that in the above expression the covariant derivative, $\vec{D} = \hbar/i\vec{\nabla} - 2e/c\vec{A}$ contains now an electric charge of $2e$, different from the single e as was originally proposed by Ginzburg and Landau. This does not invalidate the original proposed GL theory which remains formally correct, however many of the observables that depend on the electric charge will have mismatch by 2 with the experiment.

The term proportional to $\tau^{1/2}$ in Eq.(2.96) becomes

$$\tau^{1/2}gN(0)\ln\left(\frac{2e^\gamma\Omega}{\pi T}\right)\Delta(\vec{x}), \quad (2.97)$$

$$\tau^{1/2}gN(0)\left[\ln\left(\frac{2e^\gamma\Omega}{\pi T_c}\right) + \ln\left(\frac{T_c}{T}\right)\right]\Delta(\vec{x}), \quad (2.98)$$

$$\tau^{1/2}gN(0)\ln\left(\frac{2e^\gamma\Omega}{\pi T_c}\right)\Delta(\vec{x}) + \tau^{3/2}gN(0)\Delta(\vec{x}), \quad (2.99)$$

where we have used the Taylor expansion of $\ln(T_c/T) = \tau + 1/2\tau^2 + ...$ and kept terms whose contribution introduces orders not higher than the $\tau^{3/2}$ of the canonical GL equation.

To calculate the term proportional to $\tau^{3/2}$ in Eq.(2.96), we first integrate over $\vec{k}_1$ and $\vec{k}_2$ as follows:

$$\int \frac{d^3k_i}{(2\pi)^3}\frac{e^{i\vec{k}_i.(\vec{x}-\vec{y})}}{i\omega-\xi_{k_i}} = -\frac{m_i}{2\pi|\vec{x}-\vec{y}|}e^{\left(i\frac{\omega}{|\omega|}p_F-\frac{|\omega|}{v_F}\right)|\vec{x}-\vec{y}|}, \tag{2.100}$$

where p_F, v_F are the Fermi momentum and velocity. Using Eq. (2.100), the term proportional to $\tau^{3/2}$ of Eq.(2.96) becomes

$$\tau^{3/2}\frac{gT}{2}\int d^3y\sum_\omega\left(\frac{m}{2\pi|\vec{x}-\vec{y}|}\right)^2 e^{-\frac{2|\omega|}{v_F}|\vec{x}-\vec{y}|}\left[(\vec{x}-\vec{y}).\vec{D}\right]^2\Delta(\vec{x}), \tag{2.101}$$

$$\tau^{3/2}\frac{gT}{2}\int d^3y\frac{\left(\frac{m}{2\pi|\vec{x}-\vec{y}|}\right)^2}{\sinh\left(\frac{2\pi T}{v_F}|\vec{x}-\vec{y}|\right)}\frac{1}{2}\left[(\vec{x}-\vec{y}).\vec{D}^2\right]^2\Delta(\vec{x}), \tag{2.102}$$

$$\tau^{3/2}\frac{gT}{2}\left(\frac{m}{2\pi}\right)^2\frac{4\pi}{3}\frac{v_F}{2\pi T}\int_0^\infty dy\left(\frac{v_F^2y^2}{(2\pi T)^2\sinh y}\right)\vec{D}^2\Delta(\vec{x}), \tag{2.103}$$

$$\tau^{3/2}g\frac{v_F^2}{6}N(0)\frac{7\zeta(3)}{8\pi^2T^2}\vec{D}^2\Delta(\vec{x}), \tag{2.104}$$

where again we expand the temperature dependence of Eq.(2.104) around T_c and obtain

$$\frac{T_c^2}{T^2} = 1+2\tau-3\tau^2+..., \tag{2.105}$$

with only the first term contributing to the canonical derivation of the GL equation. Then, term proportional to $\tau^{3/2}$ in Eq.(2.96) is

$$\tau^{3/2}g\frac{v_F^2}{6}N(0)\frac{7\zeta(3)}{8\pi^2T_c^2}\vec{D}^2\Delta(\vec{x}). \tag{2.106}$$

Putting together Eqs. (2.99) and (2.106) we get that the integral given by Eq.(2.86) is equal to

$$gN(0)\left[\tau^{1/2}\ln\left(\frac{2e^\gamma\Omega}{\pi T_c}\right)+\tau^{3/2}+\tau^{3/2}\frac{v_F^2}{6}\frac{7\zeta(3)}{8\pi^2T_c^2}\vec{D}^2\right]\Delta(\vec{x}), \tag{2.107}$$

where $\zeta(x)$ is the Riemann zeta function.

We proceed by taking the limit and summing over Matsubara's frequencies the second integral I_2, see Eq.(2.87). $\lim_{\vec{x}\to\vec{x}'} gT\sum_\omega I_2$

$$\tau^{3/2}gT\sum_\omega\int d^3y_1d^3y_2d^3y_3G^0_\omega(\vec{x},\vec{y}_1)\Delta(\vec{y}_1)G_{-\omega}(\vec{y}_2,\vec{y}_1)\times$$
$$\Delta^*(\vec{y}_2)G^0_\omega(\vec{y}_2,\vec{y}_3)\Delta(\vec{y}_3)G^0_{-\omega}(\vec{x},\vec{y}_3), \tag{2.108}$$

where we have used the CPT symmetry given by Eq.(2.88). The Taylor expansion for $\Delta(\vec{y}_i)$ is equal to $\Delta(\vec{x})$ if we are constrained to terms up to the order $\tau^{3/2}$. Therefore, the expression (2.108) becomes

$$\tau^{3/2} g T \sum_{\omega} \int d^3y_1 d^3y_2 d^3y_3 G^0_{\omega}(\vec{x},\vec{y}_1) G_{-\omega}(\vec{y}_2,\vec{y}_1) \times$$
$$G^0_{\omega}(\vec{y}_2,\vec{y}_3) G^0_{-\omega}(\vec{x},\vec{y}_3) |\Delta(\vec{x})|^2 \Delta(\vec{x}). \tag{2.109}$$

Using the Fourier representation of all normal Green functions of the above expression and integrating all variables we get:

$$-\tau^{3/2} g N(0) \frac{7\zeta(3)}{8\pi^2 T_c^2} |\Delta(\vec{x})|^2 \Delta(\vec{x}). \tag{2.110}$$

Putting together Eq(2.107) and Eq.(2.110) and collecting the terms proportional to $\tau^{1/2}$ and $\tau^{3/2}$ we get

$$\tau^{1/2}\Delta(\vec{x}) = \tau^{1/2} g N(0) \ln\left(\frac{2e^{\gamma}\Omega}{\pi T_c}\right) \Delta(\vec{x}) +$$
$$+\tau^{3/2} g N(0) \left[\frac{v_F^2}{6} \frac{7\zeta(3)}{8\pi^2 T_c^2} \vec{D}^2 + 1 - \frac{7\zeta(3)}{8\pi^2 T_c^2} |\Delta(\vec{x})|^2\right] \Delta(\vec{x}). \tag{2.111}$$

Now using the τ expansion for the OP given by Eq.(2.93), we obtain

$$\tau^{1/2}\Delta_0(\vec{x}) + \tau^{3/2}\Delta_1(\vec{x}) = \tau^{1/2} g\mathcal{A}\Delta_0(\vec{x}) + \tau^{3/2} g\mathcal{A}\Delta_1(\vec{x}) +$$
$$+\tau^{3/2} g \left[K\vec{D}^2 + a - b|\Delta_0(\vec{x})|^2\right] \Delta_0(\vec{x}). \tag{2.112}$$

where $a = N(0)$ is the density of states at the Fermi energy and

$$K = a\frac{v_F^2}{6}\frac{7\zeta(3)}{8\pi^2 T_c^2}, \quad \mathcal{A} = a\ln\left(\frac{2e^{\gamma}\Omega}{\pi T_c}\right), \quad b = a\frac{7\zeta(3)}{8\pi^2 T_c^2}. \tag{2.113}$$

Terms proportional to $\tau^{1/2}$ give us the equation for T_c:

$$\tau^{1/2}\left(1 - g\mathcal{A}\right)\Delta_0(\vec{x}) = 0, \tag{2.114}$$
$$T_c = \frac{2e^{\gamma}}{\pi}\Omega e^{-\frac{1}{gN(0)}}. \tag{2.115}$$

The terms proportional to $\tau^{3/2}$ will give us two equations, one for Δ_0 and another for Δ_1. The latter does not contribute when we deal with the canonical derivation of the GL equation, this can be seen as the kernel of the equation is proportional to $1 - g\mathcal{A}$ which is identical zero because is constraint by the T_c equation (2.114). Therefore, the equation for Δ_0 becomes:

$$\left[-K\vec{D}^2 - a\tau + b|\Delta_0(\vec{x})|^2\right]\Delta_0(\vec{x}) = 0, \tag{2.116}$$

where we have multiplied Eq.(2.116) by $\tau^{3/2}$ and scaled back using Eq.(2.84).

To obtain Ampere's law is more elegant to build the free energy knowing the microscopically derived Ginzburg-Landau equation and

later take the variational procedure with respect to the vector potential $\vec{A}$. The overall result will give us the two Ginzburg-Landau equations, (2.68) and (2.69) which are now microscopically well founded. This derivation will be repeated in the next two Chapters for a multiband system with only intraband pairing and for the case where one includes crosspairing in a two-band system.

2.3.4 *The vortex state*

To finalize this Chapter we will present a solution for the GL equation for extreme type-II superconductors or $\kappa >> 1/\sqrt{2}$. Historically, the original proposed GL theory assumed only positive surface energy $\kappa < 1/\sqrt{2}$ as it was suggested by the Meissner effect. Nevertheless experiments performed by Nikolay Zavaritskii and Alexander Shalnikov showed that the ratio of the thickness to the London penetration depth did not follow the prediction of the original GL theory. In this context, A. A. Abrikosov who was a friend of Nikolay tried to make sense of the experimental results within the GL framework. He was convinced that the GL theory cannot be wrong due to its beauty and because correctly fitted previous experimental data. Therefore, Abrikosov motivated by this tried successfully to relax the condition that the surface energy has to be positive [1] and investigated solutions with $\kappa > 1/\sqrt{2}$.

To obtain the solution with Abrikosov vortices we will follow the method indicated in Ref. [87]. We start by writing the dimensionless Gibbs energy which contains the GL equation:

$$F = \frac{\vec{H}_c^2}{4\pi}\int dV\left[\frac{1}{2}|(\frac{\vec{\nabla}}{i}-\vec{A})\psi|^2 - |\psi|^2 + \frac{1}{2}|\psi|^4 + \kappa^2(\vec{h}-\vec{H}_0)^2\right], \tag{2.117}$$

where $\kappa = \lambda/\xi$, $\vec{H}_0$ is the applied magnetic field. All distances are normalized with respect to the coherence length ξ and the magnetic field in units of $\vec{H}_{c2} = c\hbar/2e\xi^2$. The order parameter is normalized with respect to is homogeneous bulk value $\psi_b = \sqrt{-\alpha/\beta}$. Using the variational principle we obtain the dimensionless GL equation from the Gibbs free energy (2.117),

$$-(\frac{\vec{\nabla}}{i}-\vec{A})^2\psi - (|\psi|^2-1)\psi = \frac{\partial\psi}{\partial t}, \tag{2.118}$$

where we have introduced by hand on the r.h.s a time derivative[8]. Because we will solve Eq. (2.118) self-consistently, the introduction of the time dependence can be seen as the iterative equation scaled

8 This time derivative could also be included from the very beginning in the dimensionless Gibbs energy.

by the time-step dt. This artificial introduction dt allow us to control the convergence of the solution when more fine iterations are needed (smaller time-step). In a two dimensional (2D) numerical grid the gauge invariance is naturally broken due to the lattice discretization. To restore this symmetry one could represent the phase of the order parameter in terms of the link variables:

$$U_{\mu}^{\vec{r}_1,\vec{r}_2} = \exp\left[-i\int_{\vec{r}_1}^{\vec{r}_2}\vec{A}(\vec{r}).d\vec{r}\right], \tag{2.119}$$

where $\vec{r}$ is the position vector with 2D Cartesian coordinates. Now we proceed to solve Eq. (2.118) self-consistently by imposing periodic boundary conditions. The periodicity of the system is always granted in homogeneous superconductors whose dimensions are larger than the coherence length ξ. Now, given all the above considerations we can address the question of what could emerge when two competitive orders are force to coexist? Well for the case of magnetism and superconductivity, we have two answers: (a) They either total annihilate like the Meissner effect in type-I superconductors or (b) they coexist by allowing some magnetic flux to penetrate the superconductor which reduces the competition between the two orders (type-II superconductors). The latter is characterized by an ordered penetration of magnetic flux, which is called the Abrikosov lattice of vortices.

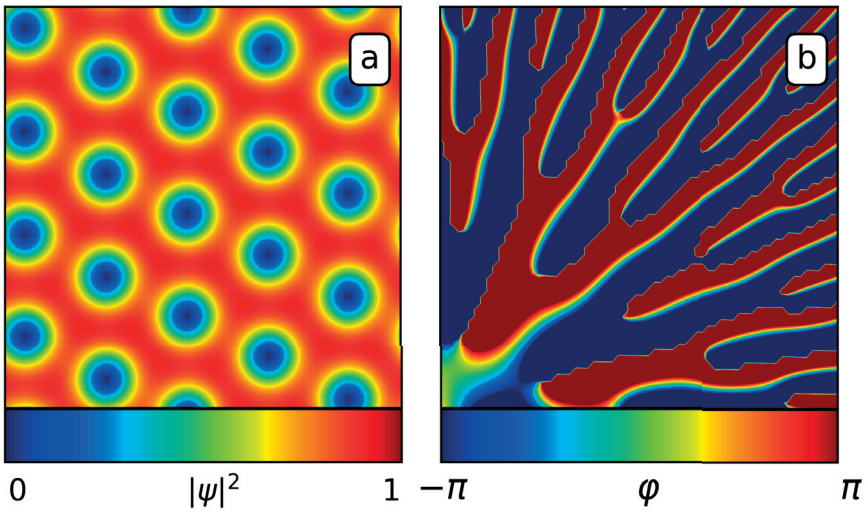

Figure 2.6: (a) Cooper-pair density and (b) phase of the order parameter, $\psi = |\psi|e^{i\varphi}$. The dimensions of the superconducting square is $20\xi \times 20\xi$ which is under the influence of constant perpendicular magnetic field of $0.31\vec{H}_c$.

Fig. 2.6a shows the most distinctive feature of type-II superconductors which consists in the nucleation of vortices which arrange themselves in a triangular lattice. Other arrangements like the square

lattice are higher energy configurations. This can be seen by the tendency of vortex nucleation along the diagonals of the square which are $\sqrt{2}$ more times separated than the side of the square. The nucleation of vortices in the middle of the square will deform the whole lattice until it reaches its triangular configuration. Fig. 2.6b displays the phase discontinuity which characterize the winding number of vortices.

The Ginzburg-Landau theory has applications beyond the scope of superconductivity, quantum electrodynamics (QED) and quantum cromodynamics (QCD) qualitatively have the same set of equations when coupled to any charged boson and present different phases with multiple orders and different topological defects. Also systems with diffusion dynamics and pattern formation, e.g. tissue of animals, can also be described with the Ginzburg-Landau equation.

In this Chapter we have reviewed the theoretical framework of this thesis which include the microscopic BCS theory using the Green function formalism and the Gor'kov derivation of the GL theory. The interplay between the magnetic order and the superconducting order in type II superconductors promotes the formation of the Abrikosov vortices. Those vortices arrange themselves in a triangular lattice as is the configuration that minimizes the free energy. In the following Chapter we will revisit the main ideas here presented when one has non-homogeneous electronic structures which induce multigap and/or multicomponent superconductivity.

3

MULTIGAP AND MULTICOMPONENT SUPERCONDUCTIVITY

"The whole is greater than the sum of its parts" (Aristoteles)

In the previous Chapter we introduced the Gor'kov Green function formalism of superconductors and listed four remaining problems after the BCS formulation. The fourth problem was the need to generalize the BCS theory to materials with spatial non-homogeneous electronic structures. These inhomogeneities can have several origins: different band dimensionality as in bulk MgB_2 [119], 2D quantum confinement which promotes a multiband scenario [10, 18, 116], electron-phonon anisotropy at the FS as in Pb [37] or the presence of multiple Fermi-surface pockets dictated by crystal symmetry as in $FeSe_xTe_{1-x}$ [78]. All these examples require new variables which need to be properly formulated beyond the single-gap BCS and single-component GL theories.

3.1 MULTIGAP SUPERCONDUCTORS

Within Gor'kov Green function formalism the implementation of inhomogeneities of the OP with only IBP is straightforward:

$$\Delta_i(\vec{x}) = -\lim_{(\tau',\vec{x}')\to(\tau,\vec{x})} \sum_j g_{ij} F_j(\vec{x}\tau, \vec{x}'\tau'), \tag{3.1}$$

$$F_j(\vec{x}\tau, \vec{x}'\tau') = -\frac{1}{\hbar} \left\langle T\psi_{j\uparrow}(\vec{x}\tau)\psi_{j\downarrow}(\vec{x}'\tau') \right\rangle, \tag{3.2}$$

where the Latin indices $i, j, ..., N = 1, 2, \ldots$ represent the band index, g_{ij} is the $N \times N$ matrix of interaction elements and N is the total number of bands.

Eq.(3.1) is the generalization of the order parameter in presence of multiple bands. Taking into account the band index, the BCS Hamiltonian is usually extended as follows:

$$\begin{aligned} H &= \sum_{\sigma,i} \int d^3\vec{x} \psi^\dagger_{i\sigma}(\vec{x}) T_{i\vec{x}} \psi_{i\sigma}(\vec{x}) + \\ &+ \sum_i \int d^3\vec{x} \left[\psi^\dagger_{i\uparrow}(\vec{x}) \psi^\dagger_{i\downarrow}(\vec{x}) \Delta_i(\vec{x}) + c.c \right]. \end{aligned} \tag{3.3}$$

The above Hamiltonian Eq.(3.3) can describe a two-gap superconductors when the band index assumes two values $i, j = 1, 2$. This

band index can represent electrons with different orbital character as initially proposed by Suhl, Matthias and Walker [122].

For clarity and to understand better the multigap effects, we will study a two-gap superconductor whose interaction matrix g_{ij} has the following form:

$$\begin{pmatrix} g_{11} & g_{12} \\ g_{21} & g_{22} \end{pmatrix}. \tag{3.4}$$

In the above matrix the diagonal elements represent the effective attraction between electrons belonging to the same band and the off-diagonal elements will describe the scattering between electrons belonging to different bands. In our case, $g_{11} > 0$ and $g_{22} > 0$ based on the assumption that the Cooper pair instability holds for both bands. However, this assumption does not longer hold for the off-diagonal elements g_{12} and g_{21} which can acquire both positive and negative values.

From the Hamiltonian (3.3) with two bands ($i, j = 1, 2.$), we obtain the two gap equations (see Appx. A.1 for details)

$$\Delta_1 = g_{11} \int \frac{d^3\vec{k}}{(2\pi)^3} \frac{\Delta_1 \tanh\left(\frac{\beta\varepsilon_1}{2}\right)}{2\varepsilon_1} + g_{12} \int \frac{d^3\vec{k}}{(2\pi)^3} \frac{\Delta_2 \tanh\left(\frac{\beta\varepsilon_2}{2}\right)}{2\varepsilon_2}, \tag{3.5}$$

$$\Delta_2 = g_{21} \int \frac{d^3\vec{k}}{(2\pi)^3} \frac{\Delta_1 \tanh\left(\frac{\beta\varepsilon_1}{2}\right)}{2\varepsilon_1} + g_{22} \int \frac{d^3\vec{k}}{(2\pi)^3} \frac{\Delta_2 \tanh\left(\frac{\beta\varepsilon_2}{2}\right)}{2\varepsilon_2}, \tag{3.6}$$

where $\varepsilon_i = \sqrt{\zeta_i^2 + |\Delta_i|^2}$ is the electron excitation spectra with gap opening Δ_i associated to each band and $\zeta_i(\vec{k}) = \vec{k}^2/2m_i - \mu$ is the kinetic energy of the electron with chemical potential μ.

We underline that the system of Eqs. (3.5) and (3.6) is phase-dependent as given by the following equation:

$$\Delta_i = \Theta(\Omega - |\zeta_i|)|\Delta_i|e^{i\varphi_i}, \tag{3.7}$$

here the wave-vector structure of the interaction matrix elements is approximated by a separable potential, in which the interaction among the electrons is active only for an energy window Ω around the Fermi surface. This permits to model the cutoff with a step-like function, which induces a step-like behavior in the pair amplitudes.

Interestingly, the value of the scattering between the bands can acquire positive or negative values: $g_{12} > 0$ or $g_{12} < 0$ which will induce a phase shift of π between Δ_1 and Δ_2. This can be seen as the system of equations (3.5) and (3.6) is symmetric under the change of sign of g_{12} and the phase change of one of the gaps to π with respect to the other gap, i.e. $\varphi_1 - \varphi_2 = \pi$.

Now we define the s^{++} and s^{+-} states. When one has attractive scattering between the bands, i.e. $g_{12} > 0$, then $sgn(\Delta_1) = sgn(\Delta_2)$ which we will call the s^{++} state. On the other hand for repulsive scattering between the bands, i.e. $g_{12} < 0$, we have $sgn(\Delta_1) = -sgn(\Delta_2)$ which we will denote as the s^{+-} state.

Similarly to the BCS-gap equation we can substitute the integral variable of the gap equations from momentum to energy:

$$\Delta_1 = \lambda_{11} \int d\zeta \frac{\Delta_1 \tanh\left(\frac{\beta\varepsilon_1}{2}\right)}{2\varepsilon_1} + \lambda_{12} \int d\zeta \frac{\Delta_2 \tanh\left(\frac{\beta\varepsilon_2}{2}\right)}{2\varepsilon_2}, \tag{3.8}$$

$$\Delta_2 = \lambda_{21} \int d\zeta \frac{\Delta_1 \tanh\left(\frac{\beta\varepsilon_1}{2}\right)}{2\varepsilon_1} + \lambda_{22} \int d\zeta \frac{\Delta_2 \tanh\left(\frac{\beta\varepsilon_2}{2}\right)}{2\varepsilon_2}, \tag{3.9}$$

where $\lambda_{ij} = g_{ij}N_j(0)$ are the dimensionless effective couplings which depend on the density of states $N_j(0)$ of each band respectively.

At $T = T_c$, the system of equations (3.8) and (3.9) simplifies and give us a second order equation. Mathematically the roots of this equation will give an expression for the two band-dependent critical temperatures

$$k_B T_c^{\pm} = 1.13\Omega e^{-\frac{1}{\lambda_{\pm}^*}}, \tag{3.10}$$

where $\lambda_{\pm}^*$ is given by

$$\lambda_{\pm}^* = \frac{\lambda_{11} + \lambda_{22} \pm \sqrt{(\lambda_{11} - \lambda_{22})^2 + 4\lambda_{12}\lambda_{21}}}{2(\lambda_{11}\lambda_{22} - \lambda_{12}\lambda_{21})}, \tag{3.11}$$

and $\lambda_{ij} = g_{ij}N_j(0)$ are the dimensionless effective couplings which depend on the density of states $N_j(0)$ of each band respectively.

Physically, the critical temperature of the system will be given by T_c^+, which corresponds to the highest T_c given in Eq.(3.10). This will be seen more clearly when we present the finite temperature numerical solutions. If the system becomes decoupled, $\lambda_{12} = \lambda_{21} = 0$, we recover two critical temperatures from each condensate respectively:

$$k_B T_{c_1} = 1.13\Omega e^{-\frac{1}{\lambda_{11}}}, \quad k_B T_{c_2} = 1.13\Omega e^{-\frac{1}{\lambda_{22}}} \tag{3.12}$$

However, real systems with different bands crossing the Fermi level become connected due to electronic interband scattering. Therefore, the critical temperature of the system will be dictated by the both bands and its respective couplings λ_{11}, λ_{22}, λ_{12} and λ_{21}.

To illustrate better the role of the interband couplings lets consider with no specific material in mind the following parameters $\mu = 500$ meV, $\Omega = 50$ meV and the following matrix of effective couplings:

$$\begin{pmatrix} 0.3 & \lambda_{12} \\ \lambda_{21} & 0.2 \end{pmatrix}. \tag{3.13}$$

The off-diagonal elements of the interaction matrix (3.13) are also called Josephson-like coupling due to its similarity with Josephson effect and its coupling between two superconductors. In what follows we assume $\lambda_{12} = \lambda_{21}$ as a sole parameter for the discussion of the solutions at zero and finite temperature. Therefore for here on we refer to this coupling between different bands as Josephson-like coupling which in our case is given only by λ_{12}.

3.1.1 *Two-gaps at zero temperature*

The critical temperature in a two-gap system is not sensitive to whether the scattering of electrons between band 1 and band 2 is attractive or repulsive.

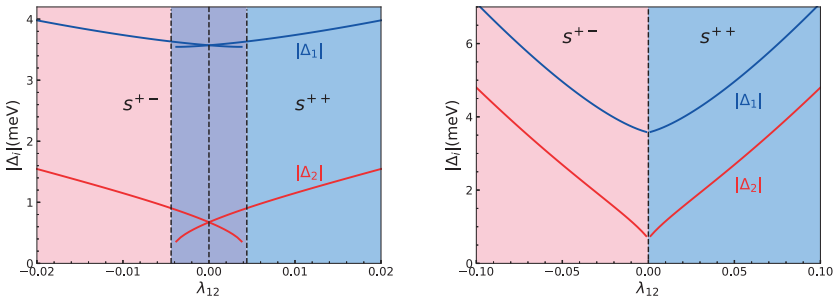

(a) $s^{+-} \leftrightarrow s^{++}$ transition with degenerate solutions. The colored blue and pink regions denote the s^{++} and s^{+-} states respectively.

(b) $s^{+-} \leftrightarrow s^{++}$ transition. Degenerate solutions were removed for illustrative purposes to show that the gaps are an even function with respect to λ_{12}.

Figure 3.1: Gaps as function of λ_{12}. The s^{+-} region corresponds to $\varphi_1 - \varphi_2 = \pi$, while the s^{++} region corresponds to $\varphi_1 - \varphi_2 = 0$. The transition $s^{+-} \leftrightarrow s^{++}$ is always not smooth and can be discontinuous (a) or continuous (b).

In the solutions shown in Fig.(3.1), we have adopted the interaction matrix defined previously in Eq. (3.13). The shadow pink and blue regions denote the s^{+-}-state and s^{++}-state, respectively. The purple area in Fig.(3.1a) describes degeneracy of solutions with two possible values for $|\Delta_1|$, two values for $|\Delta_2|$ and two distinct phases given by the s^{++} and s^{+-} states. Fig.(3.1b) presents the same solutions but where the degenerated solutions were removed to illustrate that the gap modulus are an even function with respect to λ_{12}. Interestingly for both figures, the values of the gaps $|\Delta_1|$ and $|\Delta_2|$ remain symmetric under the change of sign of λ_{12}. This means that the critical temperature of the system is non-sensitive to whether the scattering of electrons between band 1 and band 2 is attractive or repulsive. This can be clearly seen from Eq.(3.10) where T_c in a two-gap system is an even function of λ_{12}.

In Fig.(3.1a) at weak coupling $|\lambda_{12}| < 0.005$, we have two sets of solutions. The first one is given by the increment of both $|\Delta_1|$, $|\Delta_2|$ as $|\lambda_{12}|$ increases. The second set of solutions is given by reduction of

both $|\Delta_1|$, $|\Delta_2|$ as $|\lambda_{12}|$ increases. We will assume that the former is the stable solution and the latter is unstable. However, the second solution can be reached as steady state if we excite the system with light pulses. Experimentally those light pulses will induce an oscillation of the measured gaps in the modulus and in the phases. In the literature those oscillations in the gap modulus and phases are denoted as gap resonances [48, 69]. Specifically the gap resonances in the modulus are identified as the Higgs modes and the gap resonances in the phase with $\varphi_1 - \varphi_2$ changing between 0 and π are identified as Leggett modes. Therefore we expect that the $s^{+-} \leftrightarrow s^{++}$ transition will be accompanied by Higgs [66] and Leggett [71] modes. We emphasize that this gap resonance is only present due to nonzero interband coupling and is an emergent phenomenon non present in single-gap superconductors. Interestingly, the Higgs oscillation is more pronounced for the smaller gap Δ_2 than for the larger gap Δ_1 and both modes Leggett and Higgs disappear as the interband coupling λ_{12} increases, see Fig. (3.1a). The Higgs and Legget modes in two-gap superconductors have been proposed and detected experimentally in [69] and [48], see Fig. 3.2.

Gap resonances accompanied by oscillatory Higgs and Leggett modes is an emergent phenomenon not present in single-gap superconductors.

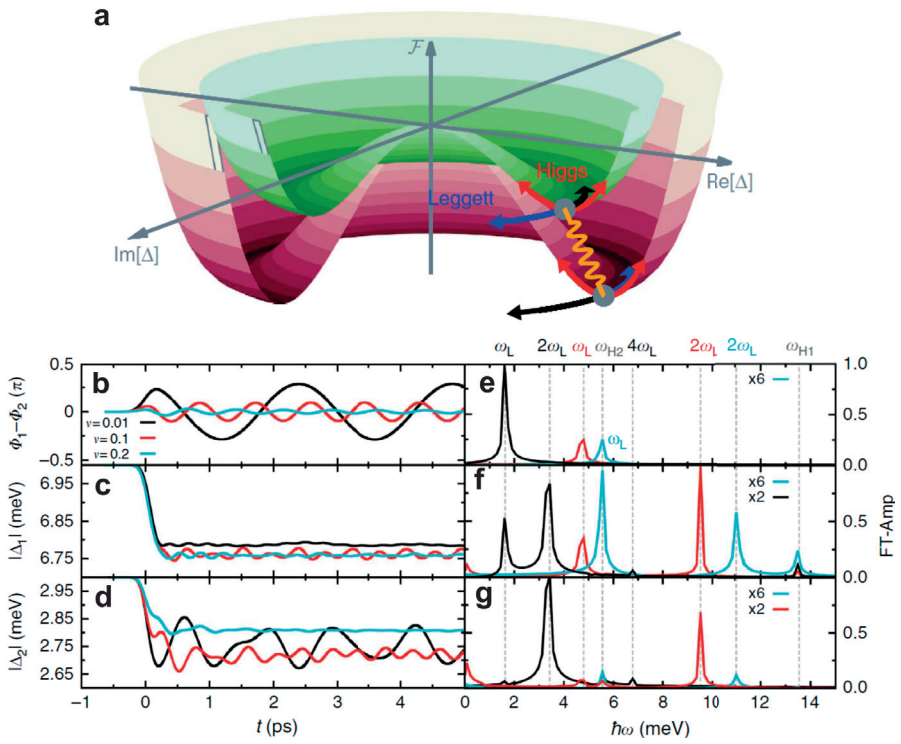

Figure 3.2: (**a**) Effective free-energy landscape $\mathcal{F}$ for a two gap superconductor, with green and red representing the Mexican-hat potentials of the smaller and larger gaps, respectively. (**b**, **c**, **d**) Phase difference $\Phi_1 - \Phi_2$ between the two gaps and magnitude of the gaps as a function of time t for various interband couplings strengths v. (**e**, **f**, **g**) Fourier spectrum of the oscillations in **b**, **c**, **d**. From Ref. [69].

3.1.2 *Two-gaps at finite temperature*

In this Section we will adopt the parameters defined for a two-band system given by Eq.(3.13) and obtain numerical solution by changing both the temperature and the interband coupling λ_{12}. Particularly we will focus on positive values of interband coupling which means we will describe only the s^{++}-state.

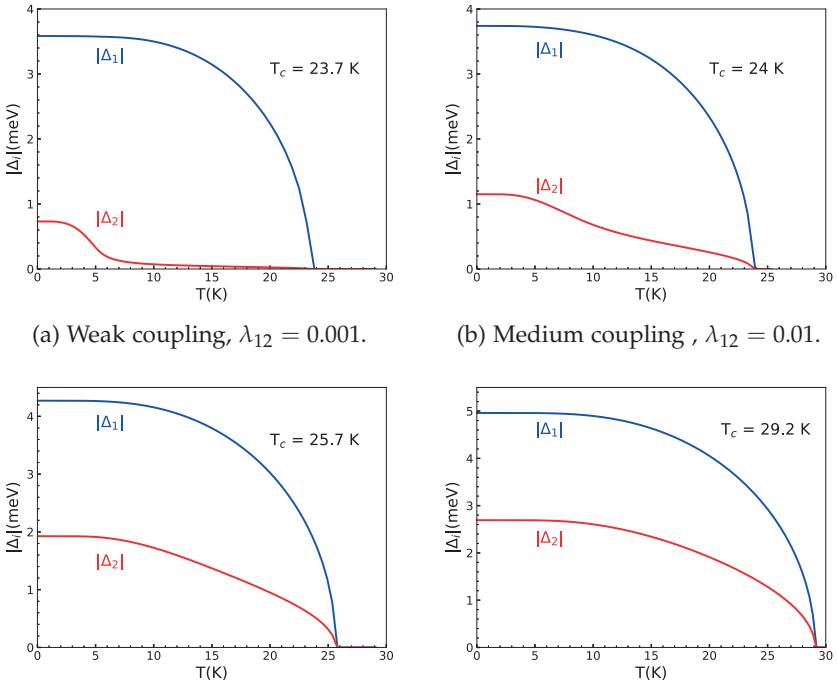

(a) Weak coupling, $\lambda_{12} = 0.001$.

(b) Medium coupling , $\lambda_{12} = 0.01$.

(c) Strong coupling , $\lambda_{12} = 0.03$.

(d) Very strong coupling , $\lambda_{12} = 0.05$.

Figure 3.3: Gaps versus temperature from weak (a) to strong coupling (d).

For an interband coupling equal to zero ($\lambda_{12} = 0$) the system is decoupled and we have two critical temperatures. On the other hand any interband coupling different from zero ($\lambda_{12} \neq 0$) yields to a single T_c. From Fig. (3.3)a, $\lambda_{12} = 0.001$, we can see that we have a single T_c due to a small but non vanishing interband coupling $\lambda_{12} \neq 0$ [122]. When the interband coupling goes to zero, $\lambda_{12} \to 0$ the systems becomes decoupled and we obtained two critical temperatures, around $T_{c1} \approx 23$ K for Δ_1 and around $T_{c2} \approx 5$ K for Δ_2. In Fig. (3.3)(b), we increase the value of the interband coupling, $\lambda_{12} = 0.01$, the change on T_c is small and of the order of ~ 1 K. Nonetheless the smaller gap Δ_2 presents a substantial different profile as a function of temperature. For strong coupling, Figs. (3.3)(c,d), $\lambda_{12} \geq 0.03$, the gaps profile start deviating from the conventional BCS. This deviation can be estimated by calculating the BCS-ratio between the gap and T_c, see Table 3.1.

The role of the interband coupling λ_{12} in two-gap superconductors is to enhance T_c as λ_{12} increases. For example, when $\lambda_{12} \leq 0.01$, T_c is

λ_{12} \ BCS RATIO	$\frac{2\Delta_1}{k_B T_c}$	$\frac{2\Delta_2}{k_B T_c}$	$\frac{2\Delta_{av}}{k_B T_c}$
0.001	3.50	0.76	2.13
0.01	3.60	1.13	2.37
0.03	3.90	1.70	2.58
0.05	3.95	2.13	3.04

Table 3.1: BCS-ratio from weak to strong coupling. Δ_{av} is given by the average ratio between the two gaps. The single-gap BCS-ratio is 3.53.

dictated by the larger gap which will have a BCS-ratio. For intermediate couplings ($0.01 < \lambda_{12} \leq 0.03$), the second band with the smaller gap becomes relevant and begins to change significantly the value of T_c. In this regime neither the larger nor the gap average will have a BCS-ratio. Finally at strong coupling ($\lambda_{12} > 0.03$) is the gap average that controls the value of T_c and follows a BCS-ratio. See Table 3.1 and Fig. 3.4.

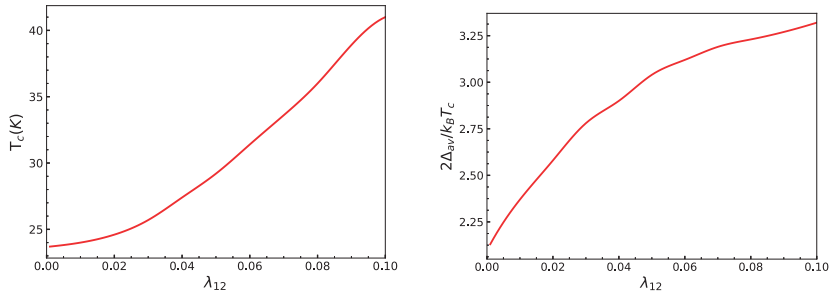

(a) Critical temperature T_c versus λ_{12}. Presents a quadratic behavior approximately up to $\lambda_{12} = 0.05$ and then becomes linear.

(b) BCS-ratio of the gap average versus λ_{12}. As the interband coupling increases it approaches its single-gap value of 3.53.

Figure 3.4: T_c and BCS-ratio versus λ_{12} from weak to strong coupling.

3.1.3 *Shape-Resonant Superconductivity in Nanofilms*

This Section contains my contribution to the study of shape resonances in superconducting nanofilms published in Ref. [22].

Films are becoming powerful platforms to find mechanisms for the enhancement of superconductivity. Furthermore superconductivity in strongly confined systems at the nano or atomic scale is attracting a growing interest after the recent observation of a sizable enhancement of the critical temperature in superconducting FeSe systems when reduced to monolayers [43] and the observation of superconductivity above 5 K in graphene doped with Potassium [136]. The multiband nature of the superconductivity in doped FeSe can also lead to amplifications of the superconducting parameters when the chemical

potential crosses a Lifshitz transition [118] as well as to BCS-BEC crossover phenomena [98, 99] in a multigap configuration [57, 65, 78, 94]. In this context, superconducting properties are evaluated at mean field level as a function of the thickness of the nanofilm, in order to characterize the shape resonances in the superconducting gap.

The objective of this Section is to identify the parameter regime in which future experiments should directly detect multiple gaps from weak to strong coupling. Strong enhancement of superconductivity has been also predicted and observed when all the lateral dimensions of a bulk superconductor are reduced to the nanoscale, as in nanoparticles, nanoclusters, and nanocubes [19, 42, 82, 83]. Predictions of large amplifications of the superconducting critical temperature and of multigap BCS-BEC crossover phenomena point toward superstripes, i.e., a system of periodic stripes organized in a superlattice, as an ideal candidate system to control and enhance superconductivity at the nanoscale [13–15]. Motivated by the fact that many different bulk superconducting materials can be used as a starting system to realize nanostructures, for instance by nanosculpting lithography [38], we can investigate theoretically the nature of the superconducting shape resonances in metallic nanofilms, tuning the parameters of the pairing interaction from weak to strong coupling, and considering different values of the energy scale of the pairing. For a review on theory and experiments discussing the multiband and multigap physics of superconducting nanofilms, see Refs. [86, 116]. The shape resonances in the superconducting gaps at zero temperature are characterized in terms of the amplification with respect to the bulk value of the gap and the width of the resonance, where formation of a multicondensate with multiple gaps can be observed. We find that the most pronounced shape resonances are generated for weakly coupled superconductors, while approaching the strong coupling regime the shape resonances are rounded by a mixing of the subbands due to the large energy gaps extending over large energy scales. Finally, we find that the spatial profile, transverse to the nanofilm, of the superconducting gap acquires a flat behavior in the shape resonance region, indicating that a robust and uniform multigap superconducting state can arise at resonance.

In 2004 shape resonances were observed in superconducting metallic nanofilms of Pb [36, 59, 105] and first evidences of shape resonances in the superconducting critical temperature in metallic nanowires of Sn and Al [3, 113, 117] clearly established the importance of the interplay between quantum size effects and superconductivity when the lateral dimensions of the system are reduced to the order of the interparticle distance or the pair correlation length [18, 86, 100, 116, 125]. It is important to note that current experiments on nanofilms reporting shape resonances in the gap and in the critical temperature [36, 59,

105] do not find evidences for multigap superconductivity close to the shape resonances.

It is known that the amplification of the resonances is controlled by the pairing strength, while the width of the resonance depends on the energy cutoff of the pairing interaction. Note that recently a heterostructure of superconductors and insulating barriers has been proposed to generate multigap superconductivity also outside the shape resonance region [33]. The chemical potential renormalization at fixed density is also explored, which is important when the system is close to a shape resonance and the gap becomes a large energy scale with respect to the distance of the chemical potential to the Lifshitz transitions [63, 102]. In this situation, a mixture of BCS-like and crossover BCS-BEC pairs is realized [23, 58, 115], providing the best condition to stabilize the detrimental superconducting fluctuations [101] which can be strong in reduced dimensionality [79]. We also investigate the spatial profile of the superconducting gap parameter and of the density of electrons. We find that the shape resonant superconductivity is characterized by a flat behavior of the gap profile, to be contrasted with a many-peak gap outside resonance. Resonant superconductivity is therefore the most robust phase of superconducting nanofilms in the strong quantum confinement regime.

Our system will consist of electrons confined in a thin metallic slab with infinite potential walls. In the direction parallel to the film, the electrons have a parabolic dispersion with an effective mass equal to the bare mass of the electrons. In the direction perpendicular to the film the motion of the electrons is quantized, with formation of discrete single-particle energy levels, as given by the solution of the uni-dimensional Schrödinger equation [3, 18]. Hence, the electronic subbands have the following form:

$$\xi_n(\vec{k}) = \frac{|\vec{k}|^2}{2m} + E_n - \mu; \quad E_n = \frac{1}{2m}\left(\frac{n\pi}{L}\right)^2, \tag{3.14}$$

where $\vec{k}$ is the wave-vector of the electrons parallel to the film, m is the effective mass, μ is the chemical potential, and E_n are the discrete energies of the subband bottoms. The index $n = 1, 2, ...$ labels the electronic subbands. For a given chemical potential, the Fermi surface exhibits a number of concentric circular 2D Fermi sheets. The reduced Planck constant ($h/2\pi$) is taken equal to unity throughout this Section. The electrons interact via an effective attraction characterized by an interaction strength V^0 and an energy cutoff ω_0. The effective pairing attraction of the bulk system is taken in a separable form, as in [18]. Moreover, because in the case of nanofilms, the motion along the z-axis is tightly bound, the bare strengths of the potential that control the

CBPs, and the interband exchange (Josephson-like) pairing between the two subbands are related by

$$V^0_{nm} = V^0(1 + \frac{1}{2}\delta_{nm}). \tag{3.15}$$

This expression is due to the overlap integral of the single-particle wave-functions, as arising from the Anderson approximation to the full Bogoliubov - de Gennes (BdG) equations (a detailed derivation of the above expression and other equations of this Section can be found in Ref. [34]). A comparison between the Anderson approximation and the exact BdG solution is available in [124]. Therefore, the quantum confinement in superconducting nanofilms is able to generate different intraband and pair exchange interactions, but the partial condensates of each subband are strongly coupled by the pair exchange terms, being the intraband term only 50 % larger than the pair exchange. As we will see below, this behavior is at the origin of a not too evident multigap structure in single superconducting nanofilms. We note also that this large pair-exchange interaction will prevent the resonant condensate to enter the BEC regime at strong coupling [57]. The pairing potential can be written as

$$V_{nm}(\vec{k},\vec{k}') = -V^0\left(1 + \frac{\delta_{nm}}{2}\right)\Theta(\omega_0 - |\xi(\vec{k})|)\Theta(\omega_0 - |\xi(\vec{k}')|), \tag{3.16}$$

where V^0 is the (positive) strength of the attractive potential. The $\vec{k}$-dependence of the (isotropic s-wave) gaps is a consequence of the separable form of the interaction of Eq. (3.16) and its given by

$$\Delta_n(\vec{k}) = \Delta_n\Theta(\omega_0 - |\xi(\vec{k})|). \tag{3.17}$$

The coupled mean-field equations for the gaps take the form originally introduced for two-band superconductors [122]:

$$\Delta_n(\vec{k}) = -\frac{1}{\Omega}\sum_{m,\vec{k}'} V_{nm}(\vec{k},\vec{k}')\frac{\Delta_m(\vec{k}')}{2\sqrt{\xi^2_m(\vec{k}') + \Delta^2_m(\vec{k}')}}, \tag{3.18}$$

Ω being the surface area of the nanofilm.

The total density of the conduction electrons n_e is fixed at values typical for metals, $n_e = 10^{22}/cm^3$, corresponding to a non interacting Fermi energy in the bulk $E_F = 1.7$ eV, which will be our reference value for the chemical potential in the nanofilms in the limit of large thicknesses. At a mean field level at $T = 0$ K the density equation is given by

$$n_e = \frac{2}{\Omega}\sum_{n,\vec{k}}\frac{1}{2}\left[1 - \frac{\xi_n(\vec{k})}{\sqrt{\xi^2_n(\vec{k}) + \Delta_n(\vec{k})^2}}\right]. \tag{3.19}$$

The sums over $\vec{k}$ are replaced by two-dimensional integrals over momenta and then by integrals over the energy variable, after introducing the $2D$ density of states $N_{2D} = m/(2\pi)$. The integrals of (3.18) and (3.19) can be expressed in a closed form, as shown in Ref. [3].

Now we will evaluate also the spatial profile of the total superconducting gap $\Delta(z)$ and the total density of conduction electrons $n_e(z)$ along the direction transverse to the nanofilm. Within the Anderson approximation we have,

$$\Delta(z) = V^0 \sum_n |\Psi_n(z)|^2 \Delta_n \int \frac{dE N_{2D}}{2\sqrt{(E + E_n - \mu)^2 + \Delta_n^2}}, \tag{3.20}$$

$$n_e(z) = 2 \sum_n |\Psi_n(z)|^2 \int dE N_{2D} v_n^2(E), \tag{3.21}$$

where $\Psi_n(z) = \sqrt{2/L}\sin(n\pi z/L)$ is the single particle wave-function along the z direction corresponding to the energy level E_n, solution of the Schrödinger equation in the transverse direction with infinite wall potential. The extremes of the integral are the same of the coupled self-consistent gap and density equations, determined by the entering and exiting of each subband bottom E_n from the Debye energy window. In the density profile of (3.21), the contribution of the free electron density outside the Debye energy window (hence, with zero gaps) is also included.

In Fig. 3.5, we report the superconducting gap in the first subband as a function of the nanofilm thickness for different $3D$ couplings, from weak ($\lambda = 0.3$) to very strong coupling ($\lambda = 2.0$), at fixed energy cutoff of the pairing interaction ($\omega_0 = 300$ K). The gaps are normalized to their bulk value, obtained in the limit of large thickness ($k_F L >> 1$).

In Table 3.2 , we report the bulk values of the gap for different couplings, from the weak ($\lambda < 0.6$) to the strong ($\lambda > 1.0$) coupling regime. In the third column of Table 3.2, we show the amplification factor $A = \Delta_{max}/\Delta_{bulk}$ of the gap at the shape resonance, taken in the ultrathin regime at $L = 0.8$ nm. For weak coupling, the gap amplification is large, while it approaches values of order unity for stronger couplings. Therefore, weakly coupled superconductors are the best candidate to observe quantum size effects and shape resonances in the superconducting gaps (and in the critical temperature).

Note that increasing the thickness L the amplification A becomes less dependent on the coupling. Interestingly for experimental detection, even for the large thickness $L = 5$ nm, the amplification of the gap is approximately 1.25, which is a measurable effect in all practical cases.

In Fig. 3.6, we show the superconducting gaps in the first subband and in the last subband contributing to the pairing as a function of the nanofilm thickness tuned around a shape resonance ($N_{res} = 10$) for different values of the energy cutoff ω_0, at fixed coupling strength

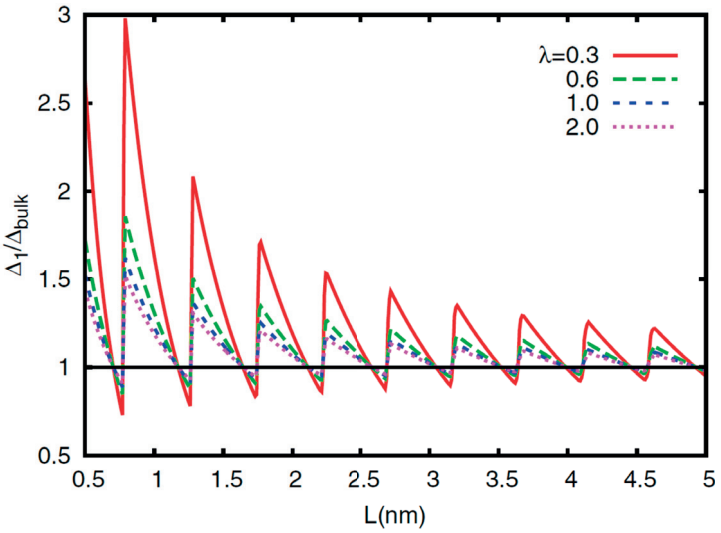

Figure 3.5: Superconducting gap in the first subband Δ_1 as a function of the film thickness L for different couplings. Δ_1 is normalized to the corresponding bulk values of the gap Δ_{bulk} determined for different couplings.

λ	$\frac{\Delta_{bulk}}{\omega_0}$	A
0.3	0.073	2.98
0.6	0.394	1.85
1.0	0.855	1.61
1.5	1.399	1.54
2.0	1.926	1.50

Table 3.2: Bulk values of the gap normalized to ω_0 and the amplification factors $A = \Delta_{max}/\Delta_{bulk}$ at $L = 0.8$ nm for the different couplings λ here considered

chosen in the intermediate coupling regime ($\lambda = 0.6$). As in Fig. 3.5, the gaps are normalized to their bulk value, obtained in the limit of large thickness ($k_F L >> 1$), see Table 3.2. As one can see, the multigap regime of the superconducting condensate is present only in the shape resonant region, and for the here-considered cases we have all the gaps equal ($\Delta_1 = \Delta_2 = ... = \Delta_9$), except the gap of the last subband (Δ_{10}). For $\omega_0 = 300$ K, the largest difference between these gaps is found at the anti-resonance, with a factor 1.05 of difference for the resonance $N_{res} = 10$ at $L = 4.56$ nm, and the width of the resonance having multigap character is found over width-span $\delta L = 0.07$ nm. Increasing the energy cutoff to $\omega_0 = 1500$ K, the width-span of the resonance showing multiple gaps increases to $\delta L = 0.37$ nm, which is now a range of thicknesses realizable in current nanofilm deposition

processes. It is therefore crucial to consider systems with large energy cutoffs and in the weak coupling regime to amplify in size and in width the multigap resonant character of the confined superconductors, in order to be able to access experimentally the interesting multigap regime, never observed in the single superconducting nanofilms.

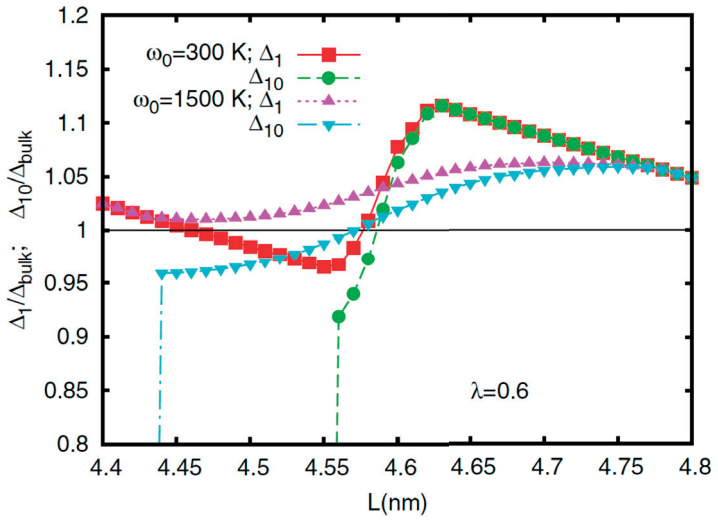

Figure 3.6: Δ_1 and Δ_{10} as function of thickness, close to a shape resonance, and normalized to Δ_{bulk}. The aim is to study the width of the shape resonance as a function of the cutoff energy and multigap structure of the condensate.

In Fig. 3.7, the chemical potential as a function of thickness for different couplings and two different cutoff energies is reported. The chemical potential μ is normalized with respect to the Fermi energy of the three dimensional (3D) bulk non interacting system E_F , value that is approached in the limit ($k_F L >> 1$). Since we work at fixed conduction electron density, the chemical potential is renormalized by the discrete structure of the electronic levels and by the superconducting gap opening. The main effect is the discreteness of the levels, while the gap opening, both in value and in energy extension ($2\omega_0$), determines differences only around the shape resonant region, differences which become sizable when ω_0 and the gaps increases in the strong coupling regime. We find that in the ultrathin limit $L < 3$ nm, the solution of the coupled gaps and density equations is important and it is not possible to work at fixed chemical potential to get the precise locations in L of the shape resonances.

Figure 3.8 shows the total gap profile $\Delta(z)$ along the direction transverse to the film (z), evaluated according to (3.20). For the case $\lambda = 0.6$ and $\omega_0 = 300$ K, we consider three cases: the thickness $L = 2.210$ nm at the $N = 4$ antiresonance, $L = 2.222$ nm very close to the shape resonance, and $L = 2.270$ nm outside and above the shape resonance. The results shown in Fig. 3.8 indicate an interesting behavior of the su-

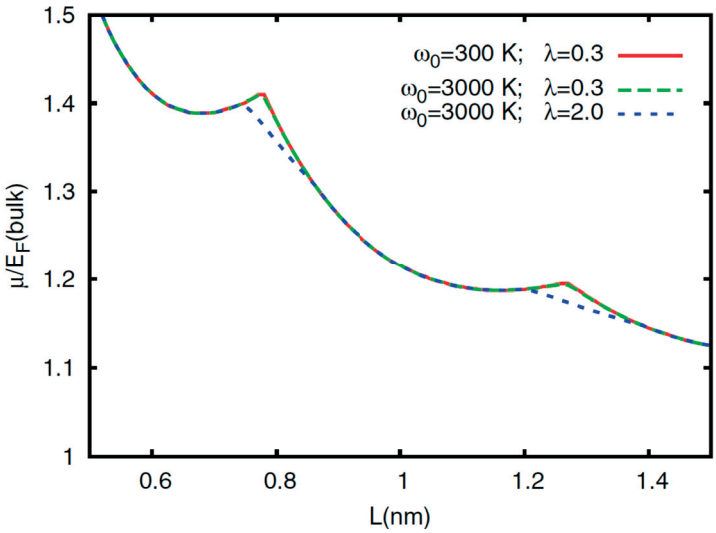

Figure 3.7: Chemical potential as a function of thickness for different couplings and different ω_0 at fixed density.

perconducting gap profile: $\Delta(z)$ outside resonance displays the Friedel oscillations, as already discussed in Ref. [3], together with the vanishing of the gap profile at the boundaries due to infinite-wall boundary conditions. The new interesting property reported here is a quite flat behavior of $\Delta(z)$ when the nanofilm thickness L is tuned very close to the shape resonance, see the case $L = 2.222$ nm in Fig. 3.8. We have also analyzed other shape resonances for larger L, finding an even flatter behavior at resonance, owing to the larger number of harmonics entering in the calculation of $\Delta(z)$. Regarding the electron density profile $n_e(z)$ of (3.21), we have found a very flat dependence of $n_e(z)$ at the center of the nanofilm, with tiny oscillations as a function of z (less than 10 % of the maximal density). Therefore, close to shape resonances the superconducting ground state of the nanofilms in the quantum-size regime appears to be quite uniform, with the exception of the boundaries (for more realistic boundary conditions, see [133], together with sizable amplifications of the gaps, and hence it points toward an optimized shape-resonant superconductivity.

In this Section we have shown that near the shape resonances the ground state strongly depend on the microscopic details of the pairing interaction. The amplification of the superconducting gap is the largest in the ultrathin limit and in the weak-coupling regime of pairing. The same amplification is progressively reduced when the coupling is increased toward strong coupling. The width of the shape resonance is instead governed by the energy cutoff of the pairing interaction: the range of thicknesses of the nanofilms in which superconductivity is shape-resonant increases for increasing energy cutoff, allowing the formation of a multicondensate and multigap superconducting phase in the shape-resonant region. Interestingly, the gap profile along the

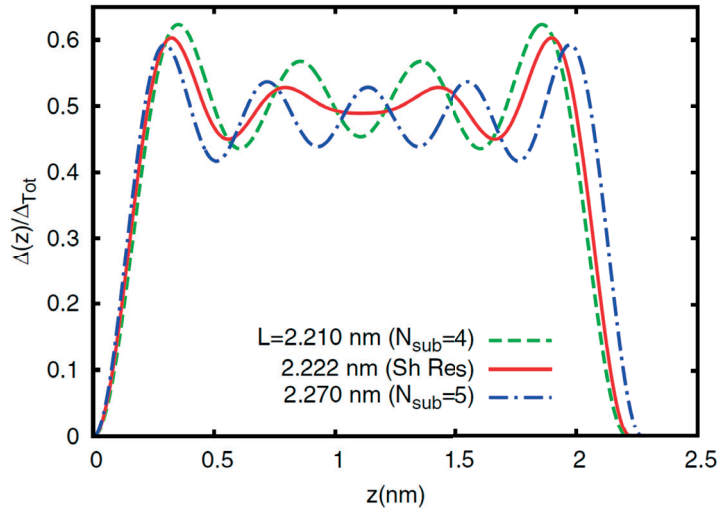

Figure 3.8: Superconducting gap profile along the transverse direction z for $\lambda = 0.6$ and $\omega_0 = 300$ K. $\Delta(z)$ is normalized by Δ_{Tot}, the integral over z of the gap profile itself. Three different thicknesses are considered, before, at, and after the $N_{sub} = (4, 5)$ shape resonance.

transverse direction of the nanofilm indicates a uniform and robust superconducting state at resonances. The multigap properties at resonance may be detected by next generation nano-ARPES [12, 106] or nano-STM measurements [21], which are in construction to investigate structural and electronic complexity in high-Tc superconductors. Therefore, we conclude that the optimal shape resonant superconductors can be realized starting from intermediate to weak-coupling bulk superconductors having large energy cutoffs, as in FeSe monolayers or doped graphene systems, reducing one or more dimensions to the nano or atomic scale. The self-consistent system of equations governing the shape resonances for the multiple gaps and the chemical potential in superconducting nanofilms have been investigated recently both at an analytical and numerical level in Refs. [132, 133], with their focus on the role of different boundary conditions of the nanofilms and the continuity of the shape resonances as a function of thickness.

3.2 MULTICOMPONENT GINZBURG-LANDAU THEORIES

As we saw in Section 3.1, superconductors with different bands can present multiple gap openings in the density of states. These different bands can be incorporated within the Gor'kov Green function formalism as presented in Eq.(3.3). In this context, a question naturally arises: What is the Ginzburg-Landau equation coming from a multigap superconductor? To answer this question we must review the microscopic derivation of the GL equation from the BCS-Hamiltonian using

the Green function formalism introduced in Section 2.3.2. This microscopic derivation not only reproduces qualitatively the GL equations (2.68) and (2.69) but also introduces some factors that are material dependent, e.g. the density of states and the electrical charge $2e$. It is the purpose of the present Section to derive the Ginzburg-Landau equation for a N-band system which contains only intraband pairing and show how in such a system we have only a single order parameter.

3.2.1 *Multicomponent Ginzburg-Landau equation*

Following the seminal derivation of the GL equations by Gor'kov [53, 54], Tilley extended the derivation for the case of two-band superconductors [126]. Later the same has been done for three, four and more components. A review of the Gor'kov derivation for multiband superconductor can be found in [96]. In presence of IBP only, the Hamiltonian (3.3) is diagonal over the band index[1]. This means that derivation for each component is obtained independently for each band and therefore we need to repeat the steps presented in Section 2.3.3 for each band separately. Once the calculation is done, the gaps equations for a N-band system become:

$$\begin{pmatrix} \Delta_1 \\ \Delta_2 \\ \vdots \\ \Delta_N \end{pmatrix} = \begin{pmatrix} g_{11} & g_{12} & \cdots & g_{1N} \\ g_{21} & g_{22} & \cdots & g_{2N} \\ \vdots & \vdots & \cdots & \vdots \\ g_{N1} & g_{N2} & \cdots & g_{NN} \end{pmatrix} \begin{pmatrix} R_1[\Delta_1] \\ R_2[\Delta_2] \\ \vdots \\ R_N[\Delta_N] \end{pmatrix}. \tag{3.22}$$

The above Eq.(3.22) is equivalent to Eq.(2.111) of the derivation for the single component case where now the band index is denoted by the Latin letters $i, j, \ldots$. The full expressions for $R_i[\Delta_i]$ is given by

$$R_i[\Delta_i] = \mathcal{A}_i\Delta_i + a_i\tau\Delta_i - b_i|\Delta_i|^2\Delta_i + K_i\vec{D}^2\Delta_i, \tag{3.23}$$

$$\mathcal{A}_i = N_i(0)\ln\left(\frac{2e^\gamma\Omega}{\pi T_c}\right), \quad a_i = N_i(0), \tag{3.24}$$

$$b_i = N_i(0)\frac{7\zeta(3)}{8\pi^2T_c^2}, \quad K_i = N_i(0)\frac{v_i^2}{6}\frac{7\zeta(3)}{8\pi^2T_c^2}, \tag{3.25}$$

where $\vec{D} = \hbar/i\vec{\nabla} - 2e/c\vec{A}$ is the covariant derivative and

$N_i(0)$	band dependent density of states,
γ	Euler constant,
Ω	average energy scale of the effective interaction,
v_i	band-dependent Fermi velocity,
$\zeta(x)$	Riemann zeta function.

1 This is not longer true in presence of CBP as we will see in the next Chapter.

It is important to note that in Eq. (3.22) we have omitted the τ expansion for clarity. Nonetheless, the τ expansion can be restore by adopting the same procedure described in the previous Chapter in Eq. (2.84), which for the multiband case now reads as follows:

$$\Delta_i \to \tau^{1/2}\Delta_i \quad \vec{x} \to \tau^{-1/2}\vec{x}, \quad \vec{\nabla} \to \tau^{1/2}\vec{\nabla}, \tag{3.26}$$

Now, to elucidate better the interplay between the different GL-components, lets consider the two-component case. From Eq. (3.22) when $N = 2$ we obtain:

$$\begin{pmatrix} \Delta_1 \\ \Delta_2 \end{pmatrix} = \begin{pmatrix} g_{11} & g_{12} \\ g_{21} & g_{22} \end{pmatrix} \begin{pmatrix} R_1[\Delta_1] \\ R_2[\Delta_2] \end{pmatrix}. \tag{3.27}$$

The above Eq. (3.27) is the version derived by Tilley [126]. Multiplying its first row by g_{22} and using the second row, we obtain:

$$(g_{11}g_{22} - g_{12}g_{21})R_1\Delta_1 - g_{22}\Delta_1 + g_{12}\Delta_2 = 0. \tag{3.28}$$

In the above equation we identify the determinant of the 2×2 interaction matrix g_{ij} as $\det g = g_{11}g_{22} - g_{12}g_{21}$. An analogous equation can be obtained for Δ_2, thus the system of equations (3.27) can be written as

$$-K_1\vec{D}^2\Delta_1 - \alpha_1\Delta_1 + b_1|\Delta_1|^2\Delta_1 + \gamma_{12}\Delta_2 = 0, \tag{3.29}$$
$$-K_2\vec{D}^2\Delta_2 - \alpha_2\Delta_2 + b_2|\Delta_2|^2\Delta_2 + \gamma_{21}\Delta_1 = 0, \tag{3.30}$$

where the new coefficients are:

$$\gamma_{ij} = -\frac{g_{ij}}{\det g}, \quad \alpha_1 = \mathcal{A}_1 - \frac{g_{22}}{\det g} + a_1\tau, \quad \alpha_2 = \mathcal{A}_2 - \frac{g_{11}}{\det g} + a_2\tau. \tag{3.31}$$

The set of Eqs. (3.29) and (3.30) corresponds to the two-component Ginzburg-Landau equation whose free energy is given by:

$$\sum_{i=1,2}\left[K_i|\vec{D}\Delta_i|^2 - \alpha_i|\Delta_i|^2 + b_i|\Delta_i|^4\right] + \gamma_{12}(\Delta_1^*\Delta_2 + \Delta_1\Delta_2^*) + \frac{\vec{h}^2}{8\pi}, \tag{3.32}$$

where $\vec{h} = \vec{\nabla} \times \vec{A}$. From Eq.(3.32), we can take the variational principle with respect to the vector potential $\vec{A}$ and obtain Ampere's law for a two band superconductor.

After the formulation of the two-component Ginzburg-Landau equation in 1964, hundreds if not thousands of articles were published related to this topic. Even an intermediate state, so called 1.5-superconductivity was proposed [6, 7]. This state is originated by the mismatch of GL characteristic lengths between the two GL components. This means that one component behaves as type I and the other as type II[2].

In 2011 the community of researchers working with multicomponent GL theories went through a huge step back regarding the validity of the multicomponent GL equations [67]. The problem was the introduction of higher order terms beyond the Gor'kov domain. As we mentioned in Section 2.3.2, the coupling between the different GL components is the cause of this flaw.

To understand what went wrong, lets consider the equation for T_c. Expanding each gap according to Eq. (3.26) in Eq. (3.22) and collecting the terms proportional to $\tau^{1/2}$, we get:

$$\begin{pmatrix} g_{11}\mathcal{A}_1 - 1 & g_{12}\mathcal{A}_2 & \dots & g_{1N}\mathcal{A}_N \\ g_{21}\mathcal{A}_1 & g_{22}\mathcal{A}_2 - 1 & \dots & g_{2N}\mathcal{A}_N \\ \vdots & \vdots & \dots & \vdots \\ g_{N1}\mathcal{A}_1 & g_{N2}\mathcal{A}_2 & \dots & g_{NN}\mathcal{A}_N - 1 \end{pmatrix} \begin{pmatrix} \Delta_1 \\ \Delta_2 \\ \vdots \\ \Delta_N \end{pmatrix} = 0. \quad (3.33)$$

From the determinant of the matrix (3.33) and using Eq. (3.24), we obtain a polynomial whose largest root will give us the expression for critical temperature, *Tc*. Considering that the multicomponent GL equation is an expansion around $T = T_c$, we can substitute Eq.(3.33) into Eq.(3.22). Therefore the multicomponent GL equation becomes:

$$\begin{pmatrix} g_{11} & g_{12} & \dots & g_{1N} \\ g_{21} & g_{22} & \dots & g_{2N} \\ \vdots & \vdots & \dots & \vdots \\ g_{N1} & g_{N2} & \dots & g_{NN} \end{pmatrix} \begin{pmatrix} a_1\tau\Delta_i - b_1|\Delta_1|^2\Delta_1 + K_1\vec{D}^2\Delta_1 \\ a_2\tau\Delta_i - b_2|\Delta_2|^2\Delta_2 + K_2\vec{D}^2\Delta_2 \\ \vdots \\ a_N\tau\Delta_N - b_N|\Delta_N|^2\Delta_N + K_N\vec{D}^2\Delta_N \end{pmatrix} = 0. \quad (3.34)$$

If the coupling matrix g_{ij} is not singular, then Josephson couplings given by Eq. (3.31) do not appear in the GL domain or canonical Gor'kov derivation. Then system of Eqs. (3.34) remains coupled only via the vector potential $\vec{A}$. However, in zero field we have:

$$\Delta_{i0}^2 = \frac{a_i\tau}{\beta_i}, \quad \rightarrow \frac{\Delta_{i0}^2}{\Delta_{j0}^2} = \frac{a_i\beta_j}{a_j\beta_i}. \quad (3.35)$$

2 The name 1.5-superconductivity states that the densities of states describing each component are exactly equal, which is too restrictive. Therefore, it is better to refer to it in general terms as an intermediate state.

Eq. (3.35) shows that the ratio between two different components of the GL equation is temperature independent within the canonical Gor'kov derivation. Therefore the different GL components must vary on the same length scale and cannot present different coherence lengths. This breaks the foundation not only of 1.5-superconductivity but also any multicomponent GL theory.

3.2.2 *Reconstruction of the order parameter*

We know from the above Section 3.2.1 that there should be only one length scale ξ_{GL} in the multicomponent GL equation, so which one of the N length scales is the correct one? ξ_1, ξ_2, ... or ξ_N? To identify the correct GL length we need to reconstruct the OP taking into account the contribution of the different components of the GL equations [96, 131].

The reconstructive procedure begins by expanding the gaps as a function of temperature using Eq. (2.93) and then systematically solving the different equations given by the factors proportional to $\tau^{1/2}$ and $\tau^{3/2}$ respectively. The terms proportional to $\tau^{1/2}$ will give us Eq.(3.33) whose largest eigenvalue will correspond to the determinant of the matrix in Eq.(3.33),

$$\mathcal{L} = \begin{pmatrix} g_{11}\mathcal{A}_1 - 1 & g_{12}\mathcal{A}_2 & \dots & g_{1N}\mathcal{A}_N \\ g_{21}\mathcal{A}_1 & g_{22}\mathcal{A}_2 - 1 & \dots & g_{2N}\mathcal{A}_N \\ \vdots & \vdots & \dots & \vdots \\ g_{N1}\mathcal{A}_1 & g_{N2}\mathcal{A}_2 & \dots & g_{NN}\mathcal{A}_N - 1 \end{pmatrix} \rightarrow \det \mathcal{L} = 0. \quad (3.36)$$

The solution of $\det \mathcal{L} = 0$ with the largest eigenvalue will give us T_c. Furthermore, from the each eigenvalue we can construct an orthogonal basis $\vec{\eta}_i$, where $i = 1, ..., N$. The eigenvector associated to T_c can be written as

$$\begin{pmatrix} \Delta_1^{(0)}(\vec{r}) \\ \Delta_2^{(0)}(\vec{r}) \\ \vdots \\ \Delta_N^{(0)}(\vec{r}) \end{pmatrix} = \psi(\vec{r}) \begin{pmatrix} 1 \\ c_{21} \\ \vdots \\ c_{N1} \end{pmatrix}, \quad (3.37)$$

where $\Delta_i^{(0)}$ corresponds to the leading order of the gap expansion in terms of τ and the coefficients c_{Ni} are constants which are obtained by solving Eq.(3.33). We note that Eq. (3.37) corroborates the assertion by Kogan and Schmalian that within the GL domain all components are strictly proportional to one another $\Delta_i \propto \Delta_j$ [67], see Eq. (3.35). Therefore the position dependence of all components is given by $\psi(\vec{r})$.

Now, the terms proportional to $\tau^{3/2}$ will give us the following equation

$$\mathcal{L}\vec{\Delta}^{(1)} + \vec{W}[\vec{\Delta}^{(0)}] = 0, \quad \vec{W} = \begin{pmatrix} W_1 \\ W_2 \\ \vdots \\ W_N \end{pmatrix} \tag{3.38}$$

where $\vec{\Delta}^{(1)}$ corresponds to the next to the leading order of the gap expansion in terms of τ. The expressions for $\vec{\Delta}^{(1)}$ and W_i are

$$\vec{\Delta}^{(1)T} = (\Delta_1^{(1)}, \Delta_2^{(1)}, \dots, \Delta_N^{(1)}), \tag{3.39}$$

$$W_i = a_i\Delta_i^{(0)} - b_i|\Delta_i^{(0)}|^2\Delta_i^{(0)} + K_i\vec{D}^2\Delta_i^{(0)}. \tag{3.40}$$

We note that Eq. (3.38) mixes contributions from different orders in the τ-expansion of the OP. Fortunately this new contribution is linear and can be disregarded by a properly chosen basis. Therefore, we proceed as follows:

1. We obtain the mutually orthogonal basis $\{\vec{\eta}_i\}$, which includes the eigenvector with zero eigenvalue, i.e. the eigenvector of T_c given by Eq. (3.37).
2. Expand the next to the leading order OP in the new basis $\{\vec{\eta}_i\}$:
$$\Delta^{(1)}(\vec{r}) = \phi_1(\vec{r})\vec{\eta}_1 + \phi_2(\vec{r})\vec{\eta}_2 + \cdots + \phi_N(\vec{r})\vec{\eta}_N. \tag{3.41}$$
3. Substitute Eqs.(3.37) and (3.41) into Eq.(3.38), note that $\phi_1(\vec{r})$ will not appear:
$$\phi_2\mathcal{L}\vec{\eta}_2 + \phi_3\mathcal{L}\vec{\eta}_3 + \cdots + \phi_N\mathcal{L}\vec{\eta}_N + \vec{W}[\psi\eta_1] = 0. \tag{3.42}$$
4. Project Eq.(3.42) onto $\vec{\eta}_1$, which will give us the standard form of the GL equation
$$\left(-K\vec{D}^2 - a + b|\psi(\vec{r})|^2\right)\psi(\vec{r}) = 0, \tag{3.43}$$
where the coefficients are given by
$$K = K_1 + c_{21}^2K_2 + c_{31}^2K_3 + \cdots + c_{N1}^2K_N, \tag{3.44}$$
$$a = a_1 + c_{21}^2a_2 + c_{31}^2a_3 + \cdots + c_{N1}^2a_N, \tag{3.45}$$
$$b = b_1 + c_{21}^4b_2 + c_{31}^4b_3 + \cdots + c_{N1}^4b_N. \tag{3.46}$$

The above steps describe the reconstruction of the order parameter of a multicomponent GL theory, whose equation is given by (3.43). The coherence length of this OP is then given by

$$\xi_{GL} = \frac{K}{a\tau}, \tag{3.47}$$

where K and a contain the contributions of all bands and are given by Eqs. (3.44) and (3.45) respectively.

It is important to underline that the microscopic order parameters given by the gap openings Δ_i are not longer equal to the GL order parameter $\psi(\vec{r})$. However they are related by Eq. (3.37).

In this Chapter we have reviewed the standard properties and emergent phenomena in multigap superconductors. In particular Higgs and Leggett modes which accompany the $s^{+-} \leftrightarrow s^{++}$ transitions, are the most distinctive features of these systems. On the other hand we have underline the problems regarding the foundation of multi-component superconductors within the Gor'kov domain. In the next two Chapters we will introduce from first principles the possibility of Cooper pairs belonging to different bands. Then we will study its emergent phenomena in multigap systems with both IBP and CBP and discuss its implications in MgB_2 and (BaK)Fe_2As_2. Consecutively we will review the foundation of multi-component GL theories when crosspairing is included.

Part II

SUPERCONDUCTIVITY WITH INTRABAND AND CROSS-BAND PAIRING

4

MICROSCOPIC THEORY OF CROSSPAIRING

Multiband superconductivity is known to promote novel quantum phenomena of great fundamental importance and versatility [86]. Recent examples are optically excited collective modes in multiband MgB_2 [48] and the emergent phenomena at the BCS-BEC crossover in FeSe [60]. Further scientific appeal of multiband superconductivity stems from its pronounced tunability. External pressure, lattice strain effects, gating, chemical doping, photo-induction, quantum confinement and surface effects are all able to move and change the band dispersions and the position of the chemical potential with respect to Lifshitz transitions [25, 26, 73, 74, 104], where superconducting properties can radically change.

To date, multiband electronic structure is proven to be of crucial importance in rather versatile superconducting systems, such as MgB_2 [92], iron-based compounds [16, 31, 61, 139], superconducting nanostructures [116], 2D electron gases at interfaces [88, 129, 134], metal-organic superconductors [142], etc. In such multiband superconductors, the pairing interaction can promote a Cooper pair formation within a single band or between electrons in different bands. The former is called intraband pairing an the latter is termed “cross-band pairing" or simply “crosspairing". This pairing is to be distinguished from the Josephson-like pair transfer between the intraband condensates, which is usually taken as their sole coupling in multiband superconductors. CBP and IBP are intuitively competitive, therefore it is necessary to understand their interplay qualitatively and quantitatively, together with associated changes in physical properties and observables. Such understanding is far from established, as crosspairing and its competition with IBP were mostly neglected in the studies to date. In superfluid systems with at least two fermionic species, the partially overlapping bands at the Fermi level are prone to crosspairing, as discussed in Refs. [56, 75]. In superconductors, the hybridization of multiple bands close to the Fermi level is favorable for cross-band pair formation. This occurs in the iron-based superconductors (FeSCs) which present strongly hybridized orbitals [89, 91], cuprates with the hybridization of $d_{x^2-y^2}$ and d_{z^2} orbitals [81, 123], and also in the heavy-fermion compounds, where crosspairing between electrons with f and d orbital character has been considered [32]. Even without hybridization, the plain proximity of multiple bands can facilitate crosspairing, as is constraint to bound states whose total momentum is zero. For example is two bands are close to each other crosspairing becomes energetically favorable, see Fig. 4.1.

4.1 CONDITIONS FOR CROSS-BAND PAIRING FORMATION

There are two situations that can facilitate crosspairing:

1. **Band Proximity.** Cooper pairs with zero momentum forbids CBP of electrons if the interband distance $c_1 - c_2$ is larger than 2Ω, where Ω is the average energy scale of the effective interaction, e.g. the Debye frequency for phonon mediated superconductors and c_1, c_2 are the initial gap energies of band 1 and band 2, see Fig. 4.1.

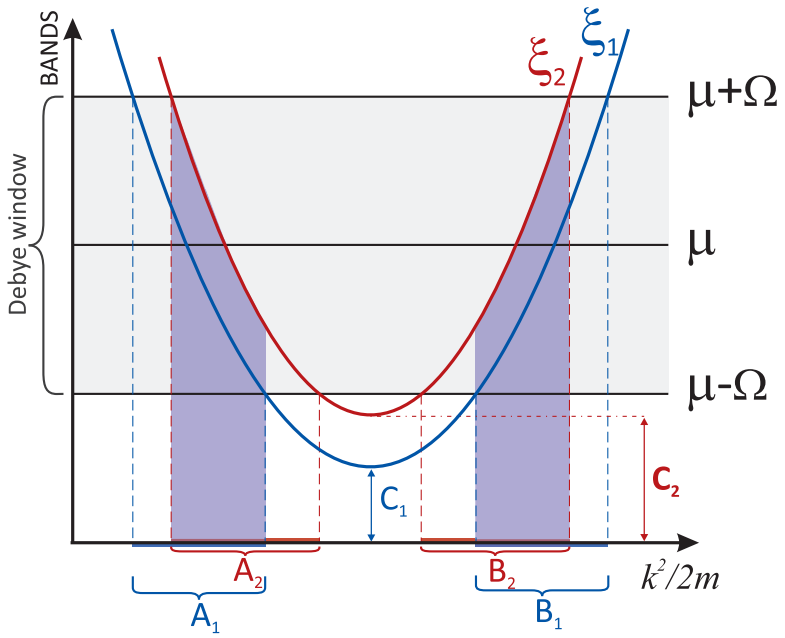

Figure 4.1: Two parabolic bands ξ_1 (blue) and ξ_2 (red) with the same curvature and separated by a distance $c_2 - c_1 < 2\Omega$. The (purple) shadow is projected on the momentum states where CBP is feasible and is given by $(A_1 \cap A_2) \cup (B_1 \cap B_2)$.

2. **Band hybridization.** One naturally introduces crosspairing in a multiorbital Hamiltonian with hybridization. For example, consider the mean field Hamiltonian of the effective two-orbital tight-binding model [90],

$$H_{MF} = \begin{pmatrix} \xi_{xx} & \xi_{xy} & \Delta_1 & 0 \\ \xi_{xy} & \xi_{yy} & 0 & \Delta_2 \\ \Delta_1 & 0 & -\xi_{xx} & -\xi_{xy} \\ 0 & \Delta_2 & -\xi_{xy} & -\xi_{yy} \end{pmatrix}, \tag{4.1}$$

where its orbital basis is $(d^\dagger_{\vec{k},x,\uparrow}, d^\dagger_{\vec{k},y,\uparrow}, d_{-\vec{k},x,\downarrow}, d_{-\vec{k},y,\downarrow})$.

The mixed kinetic terms from the Hamiltonian (4.1) come from the hybridization between the d_{xz} and d_{yz} orbitals of Fe. Those terms can become diagonal by an appropriate unitary transformation $H'_{MF} = U^{-1} H_{MF} U$,

$$H'_{MF} = \begin{pmatrix} \epsilon_1 & 0 & V_{12} & V_1 \\ 0 & \epsilon_2 & V_2 & V_{12} \\ V_{12} & V_2 & -\epsilon_2 & 0 \\ V_1 & V_{12} & 0 & -\epsilon_1 \end{pmatrix}, \tag{4.2}$$

the above Hamiltonian is written in the band basis, $(c^\dagger_{\vec{k},1,\uparrow}, c^\dagger_{\vec{k},2,\uparrow}, c_{-\vec{k},2,\downarrow}, c_{-\vec{k},1,\downarrow})$ where V_1 and V_2 are the intraband pair amplitudes and V_{12} is the cross-band pair amplitude.

4.2 N-BAND HAMILTONIAN WITH CROSSPAIRING

The simplest inclusion of cross-band pairs will make the mean-field Hamiltonian non diagonal with respect to the band index:

$$H = \sum_{i\sigma} \int d^3\vec{x} \psi^\dagger_{i\sigma} T_i \psi_{i\sigma} + \sum_{ij} \int d^3\vec{x} \left[\psi^\dagger_{i\uparrow} \psi^\dagger_{j\downarrow} \Delta_{ij} + c.c \right], \tag{4.3}$$

where $i, j = 1, 2, \ldots, N$, represents the band index of the N-band system and $\sigma = \uparrow, \downarrow$ the spin. The kinetic energy of the electrons is $T_i = -\hbar^2 \nabla^2 / 2m_i - \mu + c_i$, with chemical potential μ and initial band energy c_i. The pair amplitudes are given by

$$\Delta_{ij}(\vec{x}) = -\sum_{kl} g_{ij,kl} \left\langle \psi_{k\downarrow}(\vec{x}) \psi_{l\uparrow}(\vec{x}) \right\rangle, \tag{4.4}$$

the above expression for Δ_{ij} is usually referred as the gap for systems with only intraband pairing or systems with only cross-band pairing, however in the following Chapters of this thesis we should refer to it as pair amplitudes or order parameters to avoid confusion with the gap opening in the density of states. As we will see later these two concepts do not longer coincide when one includes intraband pairing and cross-band pairing simultaneously.

The number of pair amplitudes is $2N$ for N even and $2N - 1$ for N odd and the number of matrix element $g_{ij,kl}$ is $(3N)^2/4$ for N even and $(3N-1)^2/4$ for N odd, see App. A.1. However, we will assume that the Hamiltonian Eq. (4.3) presents crosspairing only every two bands (Δ_{12}, Δ_{34},...). For example, for the 4−band system we have that $g_{13,13} = g_{14,14} = g_{23,23} = g_{24,24} = 0$.

The spectra of electrons in presence of only IBP are BCS-like:

$$\varepsilon_i^2 = \xi_i^2 + |\Delta_{ii}|^2, \quad \xi_i = \frac{\vec{k}^2}{2m_i} - \mu + c_i. \tag{4.5}$$

The wave-vector structure of the interaction matrix elements is approximated by a separable potential, in which the interaction among the electrons is active only for an energy window around the Fermi surface, modeled with step-like functions, which induces a step-like behavior in the pair amplitudes:

$$\Delta_{ij}(\vec{k}) = \Theta(\Omega - |\xi_i(\vec{k})|)\Theta(\Omega - |\xi_j(\vec{k})|)|\Delta_{ij}|e^{i\varphi_{ij}}. \tag{4.6}$$

Now we use Gor'kov Green function formalism to obtain the pair amplitude equations for a two-band system. Details of this calculation can be found in the Appx. A.1.

The energy spectra and the pair amplitude equations are phase sensitive in presence of both IBP and CBP.

$$\Delta_{ij} = \sum_{kl} g_{ij,kl} \int \frac{d^3\vec{k}}{(2\pi)^3} \Delta_{kl} \left\{ \chi^{+}_{kl}(\theta) f[E_{+}(\theta)] + \chi^{-}_{kl}(\theta) f[E_{-}(\theta)] \right\}, \tag{4.7}$$

$$f[E] = \frac{\tanh\left(\frac{\beta E}{2}\right)}{2E}, \qquad \chi^{\pm}_{kl}(\theta) = 1 \pm \frac{1}{b(\theta)}\chi_{kl}(\theta), \tag{4.8}$$

where $\theta = 2\varphi_{12} - \varphi_{11} - \varphi_{22}$.

The expressions for $\chi_{kl}(\theta)$ and $b(\theta)$ are

$$\chi_{11} = \varepsilon_1^2 - \varepsilon_2^2 + 2|\Delta_{12}| \left(1 + \frac{|\Delta_{22}|}{|\Delta_{11}|} e^{i\theta}\right), \tag{4.9}$$

$$\chi_{22} = \varepsilon_2^2 - \varepsilon_1^2 + 2|\Delta_{12}| \left(1 + \frac{|\Delta_{11}|}{|\Delta_{22}|} e^{i\theta}\right), \tag{4.10}$$

$$\chi_{12} = (\xi_1 - \xi_2)^2 + |\Delta_{11}|^2 + |\Delta_{22}|^2 + 2|\Delta_{11}||\Delta_{22}|e^{-i\theta}, \tag{4.11}$$

$$b(\theta) = \sqrt{\left(\varepsilon_1^2 - \varepsilon_2^2\right)^2 + 4\left|\Delta_{12}\right|^2 \Re\chi_{12}(\theta)}. \tag{4.12}$$

The system of equations given by (4.7) generalize the gap equations of system with only IBP to systems with both IBP and CBP. Those equations were originally derived by Korchorbe and Palistrant in [68] and later by Arkady in [116]. However in none of those publications were reported the phase dependence of the pair amplitude equations which is a new result of the present thesis.

The crosspairing pair amplitude Δ_{12} hybridizes the energy spectra of the two BCS-like excitation branches:

$$E_{\pm}(\theta) = \sqrt{\frac{1}{2}\left(\varepsilon_1^2 + \varepsilon_2^2 + 2\left|\Delta_{12}\right|^2 \pm b(\theta)\right)}, \tag{4.13}$$

from the above equation if one takes the limit $\Delta_{12} = 0$, we recover the spectra of the electrons given by (4.5) which are the BCS-like spectra in presence of only intraband pairing.

We emphasize here that angle θ will introduce new degrees of freedom not present in systems with only IBP or CBP. Now, in presence of both IBP and CBP the relative phase between condensates can change from 0 to π depending if the scattering between electrons between

different bands is attractive or repulsive. This phase dependence is different from the Josephson-like coupling which is given by the interband coupling, e.g. in a two band system is proportional to λ_{12}. However in presence of crosspairing this new phase dependence will not only affect the pair amplitude equations but also the energy spectra of the electrons and the gap openings in the density of states (DOS).

The gap openings can be obtained from the spectra (4.13) as follows:

$$\Delta_{\pm}(\theta) = E_{\pm}(\theta)|_{\xi_{1,2}=0}. \tag{4.14}$$

These are the two gaps $\Delta_{\pm}(\theta)$ present in the DOS, however these gaps no longer correspond to the energy needed to break intraband Cooper pairs, (as is with purely IBP). Instead, they describe the energy needed to break both IBP and CBP. Therefore, the pairing amplitudes (i.e. the order parameters Δ_{11}, Δ_{22} and Δ_{12}) *do not correspond* to the measurable gaps openings in the density of states.

4.3 ANALYTIC SOLUTIONS

We are able to obtain analytical solutions at $T = 0$ K, for a two-band system with overlapping bands and zero Josephson-like couplings. This means that $\xi_1 = \xi_2$ and $\Delta_{11} = \Delta_{22}$. Therefore, at $T = 0$ K and overlapping bands the system given by Eq (4.7) is reduced to only two equations:

$$\Delta_{11} = g_{1111} \int \frac{d^3\overrightarrow{k}}{(2\pi)^3} \Delta_{11} \left(\frac{1 + \frac{|\Delta_{12}|}{|\Delta_{11}|}\delta(\theta)}{4E_+} + \frac{1 - \frac{|\Delta_{12}|}{|\Delta_{11}|}\delta(\theta)}{4E_-} \right), \tag{4.15}$$

$$\Delta_{12} = g_{1212} \int \frac{d^3\overrightarrow{k}}{(2\pi)^3} \Delta_{12} \left(\frac{1 + \frac{|\Delta_{11}|}{|\Delta_{12}|}\delta(\theta)}{4E_+} + \frac{1 - \frac{|\Delta_{11}|}{|\Delta_{12}|}\delta(\theta)}{4E_-} \right), \tag{4.16}$$

where the coupling matrix $g_{ij,kl}$ is defined after Eq.(4.4). In this case, the energy spectra and excitation gaps are,

$$E_{\pm}(\theta) = \sqrt{\xi_1^2 + \Delta_{\pm}^2(\theta)}, \tag{4.17}$$

$$\Delta_{\pm}(\theta) = \sqrt{|\Delta_{11}|^2 + |\Delta_{12}|^2 \pm |\Delta_{11}||\Delta_{12}|\sqrt{2(1 + cos\theta)}}. \tag{4.18}$$

We note, that the energy spectra $E_{\pm}$ and effective gaps $\Delta_{\pm}$ are phase dependent. Now, for $\theta = 0$, the presence of crosspairing makes Δ_+ larger while Δ_- gets smaller, i.e. induces a gap splitting. Interestingly, a gapless state is obtained when the intraband pair formation and cross-band pair formation are energetically equally favorable, thus $\Delta_{12} = \Delta_{11}$. On the other hand, for $\theta = \pi$, we have total degeneracy

In a two-band system the gap splitting and the gapless state signature the presence of crosspairing.

because $\Delta_+ = \Delta_- = \sqrt{|\Delta_{11}|^2 + |\Delta_{12}|^2}$.

Before solving Eqs. (4.15) and (4.16), we introduce the effective coupling as follows:

$$\lambda_{ij,kl} = g_{ij,kl} N_{kl}(0), \tag{4.19}$$

where the density of states $N_{12}(0) = N_{11}(0) + N_{22}(0)$. This definition comes naturally from the sum over the band indices, e.g. $\lambda_{11,12} = g_{11,12}N_{22}(0) + g_{11,21}N_{11}(0)$, using the symmetry relations for $g_{ij,kl} = g_{ji,lk}$ which implies that $g_{11,12} = g_{11,21}$, then we have that $\lambda_{11,12} = g_{11,12}(N_{11}(0) + N_{22}(0)) = g_{11,12}N_{12}(0)$.

Using the step-like behavior for the pair amplitudes, Eq. (4.6) and the effective couplings, Eq. (4.19), then Eqs. (4.15) and (4.16) become

$$\frac{1}{\lambda_{11,11}} = \int_{-\Omega}^{\Omega} d\epsilon \left[\frac{1 + \frac{|\Delta_{12}|}{|\Delta_{11}|}\delta(\theta)}{4E_+}\right] + \int_{-\Omega}^{\Omega} d\epsilon \left[\frac{1 - \frac{|\Delta_{12}|}{|\Delta_{11}|}\delta(\theta)}{4E_-}\right], \tag{4.20}$$

$$\frac{1}{\lambda_{12,12}} = \int_{-\Omega}^{\Omega} d\epsilon \left[\frac{1 + \frac{|\Delta_{11}|}{|\Delta_{12}|}\delta(\theta)}{4E_+}\right] + \int_{-\Omega}^{\Omega} d\epsilon \left[\frac{1 - \frac{|\Delta_{11}|}{|\Delta_{12}|}\delta(\theta)}{4E_-}\right], \tag{4.21}$$

where $\epsilon = \vec{k}^2/2m$.

4.3.1 *Analytic solution for $\theta = 0$*

Integrating Eqs.(4.20) and (4.21),

$$\frac{\left(\frac{|\Delta_{11}|}{\lambda_{11,11}} + \frac{|\Delta_{12}|}{\lambda_{12,12}}\right)}{(|\Delta_{11}| + |\Delta_{12}|)} = \log\left(\frac{\sqrt{\Omega^2 + (|\Delta_{11}| + |\Delta_{12}|)^2} + \Omega}{(|\Delta_{11}| + |\Delta_{12}|)}\right), \tag{4.22}$$

$$\frac{\left(\frac{|\Delta_{11}|}{\lambda_{11,11}} - \frac{|\Delta_{12}|}{\lambda_{12,12}}\right)}{(|\Delta_{11}| - |\Delta_{12}|)} = \log\left(\frac{\sqrt{\Omega^2 + (|\Delta_{11}| - |\Delta_{12}|)^2} + \Omega}{\sqrt{(|\Delta_{11}| - |\Delta_{12}|)^2}}\right). \tag{4.23}$$

We can simplify the above equations further if $\Omega >> \sqrt{(|\Delta_{11}| \pm |\Delta_{12}|)^2}$, then

$$\Delta_+ = |\Delta_{11}| + |\Delta_{12}| = 2\Omega e^{-\frac{1}{(|\Delta_{11}|+|\Delta_{12}|)}\left(\frac{|\Delta_{11}|}{\lambda_{11,11}} + \frac{|\Delta_{12}|}{\lambda_{12,12}}\right)}, \tag{4.24}$$

$$\Delta_- = ||\Delta_{11}| - |\Delta_{12}|| = 2\Omega e^{-\frac{1}{(|\Delta_{11}|-|\Delta_{12}|)}\left(\frac{|\Delta_{11}|}{\lambda_{11,11}} - \frac{|\Delta_{12}|}{\lambda_{12,12}}\right)}. \tag{4.25}$$

Eqs. (4.24) and (4.25) correspond to the opening gaps Δ_+ and Δ_- expected to be observed in the DOS. As mentioned earlier a gapless state emerges when $|\Delta_{11}| = |\Delta_{12}|$. The single-gap solution is recover whenever $|\Delta|_{11} = |\Delta_{22}| = 0$ or $\Delta_{12} = 0$.

4.3.2 *Analytic solution for $\theta = \pi$*

In this case there is only one analytic solution which corresponds to the total degenerated case:

$$\frac{1}{\lambda_{11,11}} = \frac{1}{\lambda_{12,12}} = \log\left(\frac{\sqrt{\Omega^2 + |\Delta_{11}|^2 + |\Delta_{12}|^2} + \Omega}{\sqrt{|\Delta_{11}|^2 + |\Delta_{12}|^2}}\right). \tag{4.26}$$

Again if $\Omega >> \sqrt{|\Delta_{11}|^2 + |\Delta_{12}|^2}$, then

$$\sqrt{|\Delta_{11}|^2 + |\Delta_{12}|^2} = 2\Omega \exp^{-\frac{1}{\lambda_{11,11}}} = 2\Omega \exp^{-\frac{1}{\lambda_{12,12}}}. \tag{4.27}$$

From (4.27), we recover the single-gap solution if either $\Delta_{12} = 0$ or $\Delta_{11} = 0$. Although the solution for $\theta = \pi$ seems very restrictive, it becomes robust when one allows scattering among the different pair amplitudes by introducing non-zero Josephson-like couplings ($\lambda_{ii,ij} \neq 0$).

4.4 NUMERICAL SOLUTIONS

For clarity we will focus on solutions for the two-band system. In this situation, we expect the intraband pair amplitudes $\{\Delta_{11}, \Delta_{22}\}$ and cross-band pair amplitudes $\{\Delta_{12}, \Delta_{21}\}$ to be competitive due to the constant density of states $N_{11}(0)$ and $N_{22}(0)$. For example, if n_1 and n_2 is the number of electrons that can form Cooper pairs belonging to band 1 and 2 respectively, then the number of intraband and cross-band Cooper pairs is constraint to the finite values of n_1 and n_2. In other words, for any intraband Cooper pair we expect to have one less cross-band Cooper pair and vice versa.

The effective couplings for a two-band system in presence of cross-pairing is given by 3×3 matrix:

$$\lambda_{ij,kl} = \begin{pmatrix} \lambda_{11,11} & \lambda_{11,22} & \lambda_{11,\{12\}} \\ \lambda_{22,11} & \lambda_{22,22} & \lambda_{22,\{12\}} \\ \lambda_{\{12\},11} & \lambda_{\{12\},22} & \lambda_{\{12\},\{12\}} \end{pmatrix}, \tag{4.28}$$

where the upper left 2×2 inner matrix corresponds to the well established SMW case [122], and the third row and column include the crosspairing (where $\{12\}$ indicates symmetrization under given indices, so that e.g. $\lambda_{\{12\},\{12\}} = \lambda_{12,12} + \lambda_{21,21}$). In the effective coupling matrix, the attraction between electrons is given by its diagonal elements, i.e. $\lambda_{11,11}$ is the effective attraction of electrons belonging to band 1, $\lambda_{22,22}$ is the effective attraction of electrons belonging to band 2 and $\lambda_{12,12}$ is the effective attraction of electrons one which

belongs to band 1 and the other to band 2. The off-diagonal elements in (4.28) describe the Josephson-like coupling among the intraband and cross-band Cooper pairs. For example $\lambda_{11,22}$, describes the Cooper pair transfer between band 1 and 2. The elements of the form $\lambda_{ii,ij}$ describe not the rigid Cooper pair transfer but the quasiparticle scattering between band i and band j. All Josephson-like couplings connect the different order parameters $\{\Delta_{11}, \Delta_{22}, \Delta_{12}\}$ which induces a single T_c in our system.

The conventional method to solve the pair amplitude equation or gap equation for the one-band case is the iterative-self-consistent method. Even when we have multiple bands with only IBP, modification of the iterative-self-consistent method can be applied which in general converge to a unique solution. However, when we have both IBP and CBP, then the intrinsic competition between these two types of pairing promotes three non trivial solutions: (a) only intraband pairing solution (IPS), (b) only cross-band pairing solution (CPS) and (c) coexistent solution with both IBP and CBP. Therefore, with three latent solutions the long used iterative-self-consistent method fails on obtaining a single solution which is dictated by the initial condition. To avoid this issue and respect the initial condition we adopt the Newton-Raphson method to solve the matrix system of equations (4.7), which keeps track on the same solution by following its derivative. To perform the integrals we use the Gaussian quadrature method. In this thesis we developed a new numerical procedure whose details are given in App. C.

For the rest of the Chapter we will show the numerical results obtained by this numerical procedure.

4.4.1 *Zero Josephson-like coupling*

First we recall that the off-diagonal elements of the interaction matrix $\lambda_{ij,kl}$ given by Eq. (4.28) are referred as Josephson-like couplings. However, to understand better the role of crosspairing in a two-band system we make equal to zero all Josephson-like couplings in the matrix (4.28). This limit with only IBP describes two decoupled bands and therefore presents two critical temperatures. However in presence of both IBP and CBP the system of equations given by (4.7) remains coupled due to the induced hybridization between bands by crosspairing, $\Delta_{12} \neq 0$.

Without any particular superconductor in mind, we consider the following parameters $\Omega = 45$ meV, $\mu = 300$ meV and effective couplings,

$$\lambda_{ij,kl} = \begin{pmatrix} 0.5 & 0 & 0 \\ 0 & 0.4 & 0 \\ 0 & 0 & \lambda_{\{12\},\{12\}} \end{pmatrix}. \tag{4.29}$$

The solution for coincident bands at zero temperature is given in Fig. 4.2.

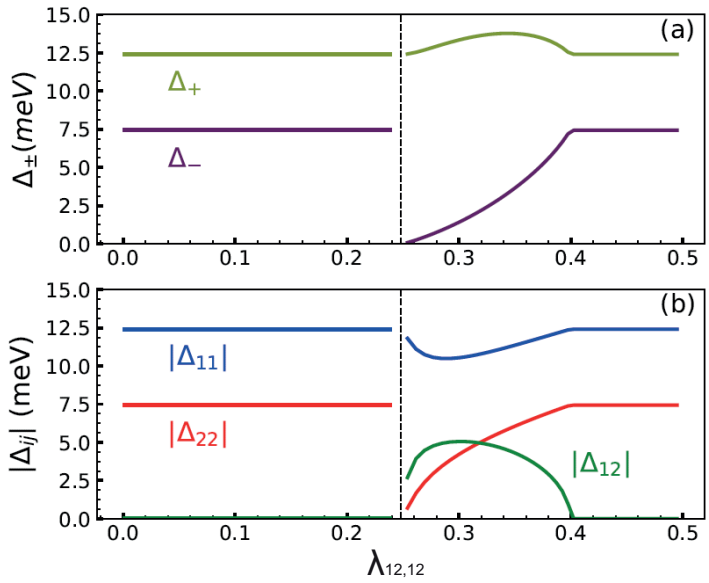

Figure 4.2: Coexistence of IBP and CBP at zero temperature. (a) Excitation gaps $\Delta_\pm$. (b) Magnitude of the pair amplitudes for $\theta = 0$. The black dotted line indicates the transition where crosspairing begins to coexist with intraband pairing ($\lambda_{12,12} \approx 0.24$).

First, we emphasize that the gap openings in the DOS is not longer given by order parameters Δ_{11}, Δ_{22} and Δ_{12} but rather by the excitation gaps $\Delta_\pm$ given in Eq. (4.14) and shown in Fig. 4.2a. Furthermore, the onset of coexistence between IBP and CBP is accompanied by a gapless state, $\Delta_- = 0$ when $\lambda_{12,12} \approx 0.24$. Coexistent solutions for weak coupling, $\lambda_{12,12} < 0.24$, are not possible in this range because all electrons have formed intraband Cooper pairs and no one is left for crosspairing. This means that to initiate crosspairing we need to break some intraband Cooper pairs. This is shown by the decrease of Δ_{11} and Δ_{22}, see Fig. 4.2b. As we increase $\lambda_{12,12}$, the cross-band pair amplitude fails to overcome the intraband pair amplitudes due to the yet dominant value of Δ_{11}. The abrupt transition to the coexistent solution with IBP and CBP indicates that the system is unstable at the gapless state.

The gapless state and the phase change in the pair amplitudes indicates the onset of cross-band Cooper pairs.

The coexistence of IBP and CBP begins when $\lambda_{12,12} \approx 0.24$ which gives a value of $\lambda_{\{12\},\{12\}} = 0.48$ which is approximately the average of the intraband couplings $\lambda_{11,11}$ and $\lambda_{22,22}$ given by the matrix 4.29.

The gapless state obtained in Fig. 4.2a ($\Delta_- = 0$ for $\lambda_{12,12} = 0.24$), resembles the new class of interior gap superfluids, see Fig. 4.3b. There are two conditions for the formation of an interior gap: (a) First, we need at least two fermionic species, like the quarks up, down and strange in QCD or ultracold atoms with different atoms. (b) Second, their Fermi surfaces should slightly differ, like the two electronic spin

states ↑ and ↓ or the hyperfine states of cold ^{40}K and ^{6}Li. Under this conditions the kinetic energy can promote particles of one fermionic species to the exterior of the Fermi sphere. This migration of particles in the momentum states will create a "breach" of particle of one fermionic species, which is where its name came from. The ground state of a interior gap superfluid will present both superfluid and normal Fermi components.

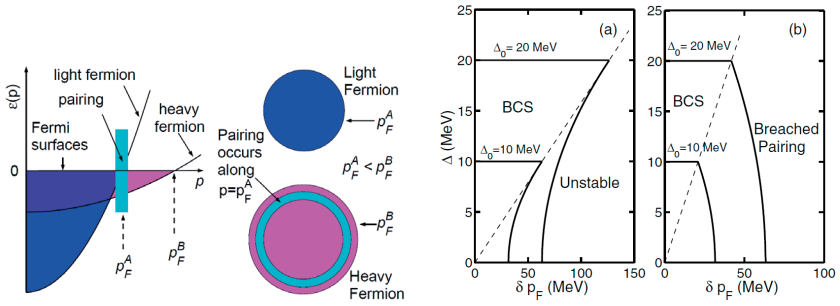

(a) Prototype situation for a interior gap superfluid at weak coupling. The pairing between different species can be favorable by promoting some particles of the heavier species to the exterior Fermi sphere. Thus carving an interior "breach" of the species B near momentum $p = p_F^A$ From Ref. [75]

(b) Solutions of the gap equation as function of the Fermi momentum mismatch δp_F for different coupling constants parameterized by Δ_0. (a) Fixed chemical potential and (b) fixed total density. The dashed line marks the transition between the BCS and breached pairing phases. From Ref. [56]

Figure 4.3: Gapless state as predicted in superfluidity.

Now we will present the temperature dependence of the pair amplitudes Δ_{ij} and gaps $\Delta_\pm$ for the same set of effective couplings given by Eq. (4.29) with $\lambda_{12,12} = 0.3$. We choose $\lambda_{12,12} = 0.3$ to show the effect of increasing temperature on the three pair amplitudes (Δ_{11}, Δ_{22} and Δ_{12}) and their derived gaps, (Δ_+ and Δ_-).

The presence of crosspairing induces a non-BCS profile of the gaps as function of temperature.

Fig. 4.4b shows three critical temperatures, $T = T_c^{11} \approx 80$ K ($\Delta_{11} = 0$), $T = T_c^{22} \approx 50$ K ($\Delta_{22} = 0$) and $T = T_c^{12} = 42$ K ($\Delta_{12} = 0$). The presence of crosspairing ($\Delta_{12} \neq 0$) induces a non BCS behavior of the gaps versus temperature, because Δ_- increases with temperature until T_c^{12}. This means that increment of Δ_- with temperature cannot be explained by the conventional BCS theory. Above T_c^{12} the crosspairing amplitude becomes zero ($\Delta_{12} = 0$) and the gaps dependence with temperature recovers its conventional BCS behavior as function of temperature. In this regime the gaps Δ_+ and Δ_- coincide with the non zero pair amplitudes Δ_{11} and Δ_{22} respectively.

Up to now multiband superconductors with no electron scattering among the different bands have not been found, although a superconductor with two superconducting transition has been hypothesized for $U_{1-x}Th_xBe_{13}$. Therefore one can assume that most superconductors have non-zero values for the off-diagonal elements of the interaction

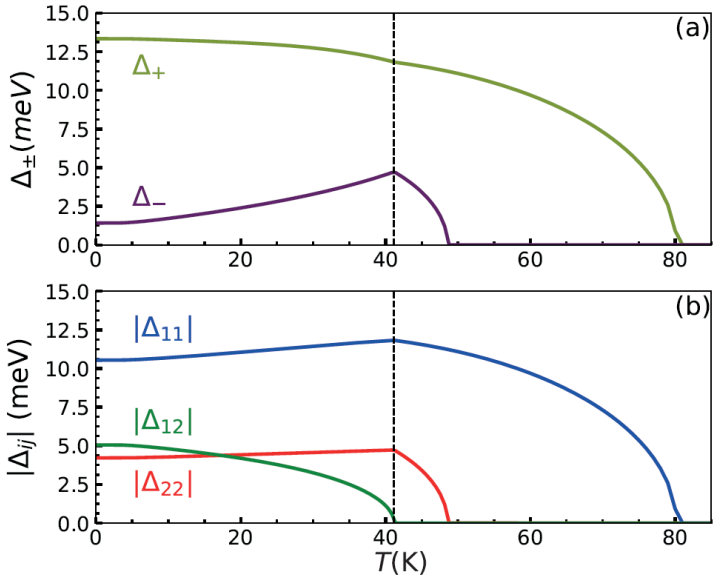

Figure 4.4: Coexistence of IBP and CBP at finite temperature for $\lambda_{12,12} = 0.3$. (a) Excitation gaps $\Delta_\pm$. (b) Magnitude of the pair amplitudes for $\theta = 0$. The black dotted line indicates the critical temperature for the crosspairing order parameter Δ_{12}.

matrix $g_{ij,kl} \neq 0$. Therefore in the next Section we will present solutions where the Josephson-like couplings are non zero.

4.4.2 *Finite Josephson-like coupling*

The novelty in this Section is the presence of couplings between the intraband pair amplitudes (Δ_{11}, Δ_{22}) and the cross-band pair amplitude (Δ_{12}). The effective coupling in this situation is given by terms of the form $\lambda_{ii,ij}$ ($\lambda_{11,12}$, $\lambda_{12,11}$, $\lambda_{12,22}$, $\lambda_{22,12}$). Here, we will present solutions at finite Josephson-like when $\lambda_{ii,ij}$ is weak (0.005), medium (0.01) and strong (0.1).

As we mentioned in the previous Section, the different pair amplitudes open a gap in different parts of the Fermi surface which are inevitably coupled by the electron-electron scattering. In multiband superconductors with only IBP this coupling is guaranteed by the presence of the pair exchange interactions, $\lambda_{ii,jj} \neq 0$, which can be interpreted as the transfer of Cooper pairs from band i to band j. Furthermore, this interband coupling will establish the presence of a unique T_c which is a reasonable assumption for most superconducting compounds [**stewart2019**]. Therefore, motivated by the uniqueness of T_c, we will introduce Josephson-like couplings between the intraband pair amplitudes $\{\Delta_{ii}, \Delta_{jj}, \dots\}$ with the cross-band pair amplitudes $\{\Delta_{ij}, \Delta_{kl}, \dots\}$. This would imply in the presence of effective couplings of the form $\lambda_{ii,ij}$, which cannot longer be interpreted as the Cooper

Pair breaking scenarios favor the coupling between intraband pair amplitudes and cross-band pair amplitudes.

pair transfer between two bands but should rather be interpreted in terms of electron-electron scattering. This type of scattering can be promoted by any pair breaking scenario which would allow the intraband pairs once broken to cross-band pair and vice-versa. Therefore, in presence of a pair breaking scenario we expect the solutions with both IBP and CBP to coexist even at weak coupling.

To elucidate the role of crosspairing for finite Josephson-like coupling ($\lambda_{ii,ij} \neq 0$, $\lambda_{ii,jj} \neq 0$), we use the following parameters: $\Omega = 45$ meV, $\mu = 300$ meV and effective couplings

$$\lambda_{ij,kl} = \begin{pmatrix} 0.5 & 0.1 & 0.01 \\ 0.1 & 0.4 & 0.01 \\ 0.01 & 0.01 & \lambda_{\{12\},\{12\}} \end{pmatrix}. \tag{4.30}$$

The above matrix, Eq. (4.30) describes a system whose intraband pair amplitudes are strongly coupled, $\lambda_{11,22} = 0.1$ while the coupling with the crosspairing pair amplitude is weak, $\lambda_{11,12} = \lambda_{22,12} = 0.01$.

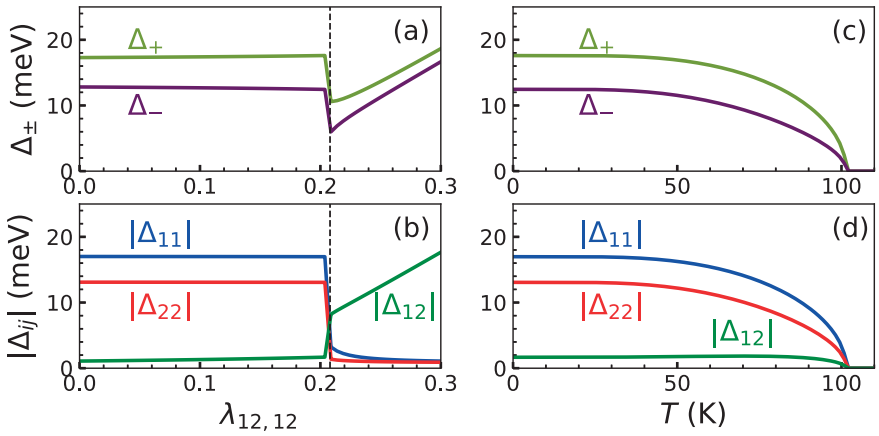

Figure 4.5: Coexistence of IBP and CBP for finite Josephson-like couplings, $\lambda_{11,22} = 0.1$ and $\lambda_{11,12} = \lambda_{22,12} = 0.01$. Solutions at zero temperature (a,b) and finite temperature (c,d). The excitation gaps are shown in (a,c) with their respective pair amplitudes (b,d). For the solution at finite temperature we fix $\lambda_{12,12} = 0.2$ ($\lambda_{\{12\},\{12\}} = 0.4$). The dotted lines in (a,c) indicates the transition from intraband pairing dominated regime to a cross-band pairing dominated regime.

From Fig. 4.5, we observe that the role of the Josephson-like couplings do not only induce a single T_c in our system but extend the coexistence between the IPS and CPS to a new domain where the attraction between two electrons belonging to different bands can be infinitesimally small, $\lambda_{12,12} \to 0$. Interestingly, we observe a clear competition between IBP and CBP which presents a discontinuity at $\lambda_{12,12} = \lambda_c \approx 0.21$, Figs. 4.5(a,b). This characteristic value marks the

maximal competition between the intraband and the crossband pairing channels and separates our solution in two regimes: the IDR for $\lambda_{12,12} < \lambda_c$, and a CDR for $\lambda_{12,12} > \lambda_c$. In the CDR, both gaps, $\Delta_\pm$, increase at the same rate, similarly to the one-band scenario. Therefore, the CDR describes a two-gap system which is characterized by a sole order parameter Δ_{12}, while the intraband pair amplitudes Δ_{11} and Δ_{22} participate only passively, due to proximity effect [49, 50].

Now we analyze the situation where all Josephson-like couplings are equal $\lambda_{ij,kl} = 0.1$. This particular value implies that the Cooper pair transfer is strongly equal to the coupling between intraband pair amplitudes and cross-band pair amplitudes, e.g. ($\lambda_{ii,12} = \lambda_{11,22}$). The coupling matrix becomes,

$$\lambda_{ij,kl} = \begin{pmatrix} 0.5 & 0.1 & 0.1 \\ 0.1 & 0.4 & 0.1 \\ 0.1 & 0.1 & \lambda_{\{12\},\{12\}} \end{pmatrix}. \tag{4.31}$$

In Fig. 4.6, we observe that the role of the Josephson-like couplings $\lambda_{11,12}$ and $\lambda_{22,12}$ has a different effect than $\lambda_{11,22}$. The former, makes the crosspairing pair amplitude stronger which increases the larger gap Δ_+ and decreases the smaller gap Δ_-. This behavior is in opposition of $\lambda_{11,22}$ which has the effect of increasing both gaps Δ_+ and Δ_-. Interestingly, the transition to the CDR starts at $\lambda_{12,12} \approx 0.17$ which is accompanied by a gapless state.

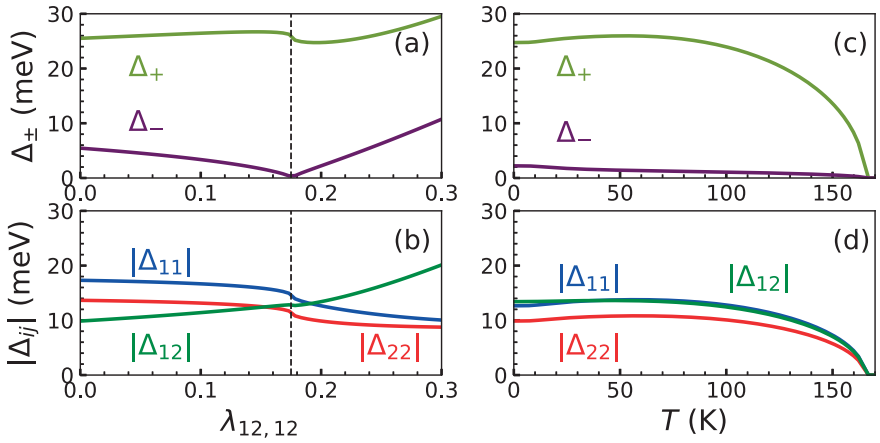

Figure 4.6: Coexistence of IBP and CBP for finite Josephson-like couplings, $\lambda_{11,22} = 0.1 = \lambda_{11,12} = \lambda_{22,12}$. Solutions are presented at zero temperature (a,b) and finite temperature (c,d). The excitation gaps are shown in (a,c) with their respective pair amplitudes (b,d). For the solution at finite temperature we fix $\lambda_{12,12} = 0.2$ ($\lambda_{\{12\},\{12\}} = 0.4$). This value is taken just before crosspairing is dominant. The dotted lines in (a,c) indicates the transition from IDR to a CDR.

Figs. 4.5, 4.6 describe the effect of the Josephson like coupling from weak to strong coupling. The effect of changing $\lambda_{ii,12}$ from 0.01 to 0.1 has a net effect of changing the critical temperature from 100 K to 165 K. Furthermore, both figures 4.5 and 4.6, present a discontinuity at the transition from the IDR to the CDR which is more pronounced at weak coupling. Now, it would be interesting to find some values of the Josephson-like couplings where this discontinuity disappears. In order to do so, lets consider the following matrix of effective couplings:

$$\lambda_{ij,kl} = \begin{pmatrix} 0.5 & 0.01 & 0.005 \\ 0.01 & 0.4 & 0.005 \\ 0.005 & 0.005 & \lambda_{\{12\},\{12\}} \end{pmatrix}. \tag{4.32}$$

The above matrix (4.32), describes a system which is weakly coupled and where cross-band Cooper pairs are present mostly due to proximity for $\lambda_{12,12} < 0.2$, see Fig. 4.7. This solution is obtained when one takes as a initial condition $\Delta_{11} = \Delta_{22} = 0.5$ meV, $\Delta_{12} = 17$ meV, $\theta = 0$ and sweeps the parameter $\lambda_{12,12}$ from 0.3 to 0.01. Remarkably we observe that θ changes phase from 0 to π at the transition from the CDR to the IDR. This indicates that the solution given in Fig. 4.7 is meta-stable because when one approaches the limit $\Delta_{12} \to 0$, the solution with only IBP and $\theta = 0$ should be recovered.

The above solution can become stable when one introduces repulsive scattering among the electrons. As we know from the previous Chapter, negative values of Josephson-like couplings describe repulsive scattering and promote phase changes in the pair amplitudes. In this sense we can state that repulsive scattering between different superconducting condensates induces a continuous transition from the IDR to the CDR and vice-versa. This repulsive scattering between electrons belonging to different condensates have been reported in many superconductors. For example, in the family of FeSCs one can have two cases where a π-phase difference between two pair amplitudes is present (s^{+-} symmetry). The first is the conventional s^{+-} case, which contemplates a π-phase difference between electron-like and hole-like pair amplitudes [84]. The second case is the orbital antiphase s^{+-}, where one has a π-phase difference between bands of the same type (electron-like or hole-like), as reported in the optimally doped (BaK)Fe_2As_2 ($T_c = 36$ K) [77, 138, 141]. Other phase changing mechanisms are driven by impurity scatterings which are particularly important across the Lifshitz transitions [127, 128].

Repulsive scattering between different superconducting condensates induces a continuous transition from the IDR to the CDR

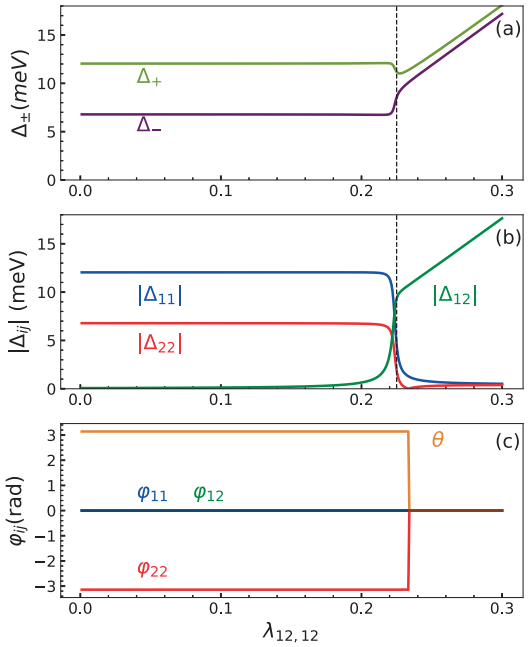

Figure 4.7: Coexistence of IBP and CBP at zero temperature. (a) Excitation gaps $\Delta_\pm$. (b) Magnitude of the pair amplitudes and their respective phases (c). The black dotted line indicates the transition from the CDR to the IDR at $\lambda_{12,12} \approx 0.225$. The brown line in (c) represents θ.

To end this Section, we will present a case where a phase change is induced by temperature. Let us consider $\mu = 500$ meV, $\Omega = 75$ meV and

$$\lambda_{ij,kl} = \begin{pmatrix} 0.28 & -0.005 & 0.01 \\ -0.005 & 0.27 & 0.01 \\ 0.01 & 0.01 & 0.13 \end{pmatrix}. \tag{4.33}$$

The solution of the system described by the matrix (4.33) is shown in Fig. 4.8. There we can observe a non-BCS behavior of the excitation gaps $\Delta_\pm$ as a function of temperature. Fig. 4.8b presents only the imaginary part of the pair amplitudes because the real parts are negligible. The dotted lines in Figs. 4.8(a,b) mark the $s^{+-} \leftrightarrow s^{++}$ transition at $T = 19.8$ K. This transition is an indicator of a phase frustrated state among the pair amplitudes which in this case is induced by the condition $\lambda_{11,22}\lambda_{11,12} < 0$. Phase frustrations are known in three-band systems [20, 97, 120] and can lead to skyrmionic vortex states [40, 41, 95], but are not possible in a two-band systems without crosspairing.

The phase frustrated state is not possible in two-band systems unless crosspairing is present.

We conclude this Section by underlying the competitive nature between IBP and CBP which is general characteristic in superconductors with both IBP and CBP. This type of competition has been reported

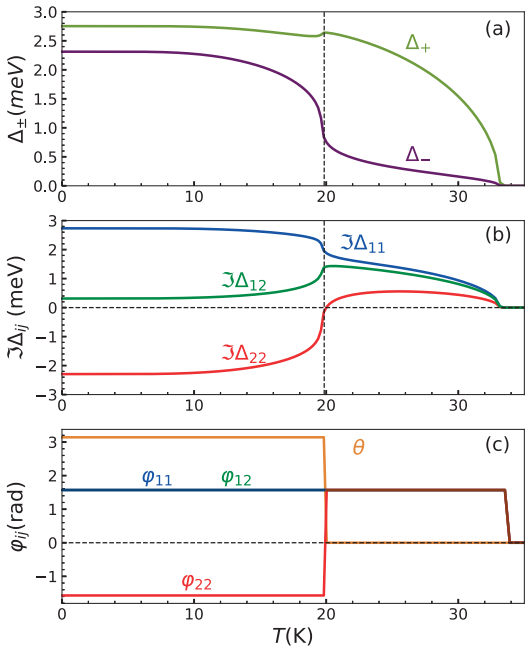

Figure 4.8: Coexistence of IBP and CBP at finite temperature. (a) Excitation gaps $\Delta_\pm$. (b) Imaginary part of the pair amplitudes and their respective phases (c). The black dotted line indicates when we have an $s^{+-} \leftrightarrow s^{++}$ transition. The brown line in (c) represents θ.

also in one-dimensional superconducting nanowires [107] and electron doped BiS_2 [55].

4.4.3 *The Gapless state*

As we mentioned in the previous Section, the most pronounced feature of the presence of crosspairing in two-band superconductors is the tendency towards a gapless state for the smaller gap. This state marks the maximum level of competition between the IBP and CBP and delimits the IDR and CDR. Interestingly the transition between these two regimes (IDR and CDR) is either continuous or discontinuous depending if the scattering between electrons belonging to different condensates is attractive or repulsive.

In this Section we will study the conditions for the formation of the gapless state by calculating the spectral wave function and its related density of states. A zero of the spectral wave function for a particular combination of parameters $\lambda_{ij,kl}$ signals the presence of a gapless state.

To help our search for a numerical solution of the gapless state we analyze it analytically. We begin by writing down the normal Green function in presence of both IBP and CBP for a two-band system (its full derivation can be found in Appx. A.2).

$$G_{ij\omega} = \frac{(i\hbar\omega+\xi_2)(i\hbar\omega+\xi_1)}{(\hbar^2\omega^2+E_+^2)(\hbar^2\omega^2+E_-^2)} \times$$
$$\times \begin{pmatrix} i\hbar\omega - \xi_2 - \frac{|\Delta_{12}|^2}{i\hbar\omega+\xi_1} - \frac{|\Delta_{22}|^2}{i\hbar\omega+\xi_2} & \frac{\Delta_{11}\Delta_{12}^*}{i\hbar\omega+\xi_1} + \frac{\Delta_{12}\Delta_{22}^*}{i\hbar\omega+\xi_2} \\ \frac{\Delta_{12}\Delta_{11}^*}{i\hbar\omega+\xi_1} + \frac{\Delta_{22}\Delta_{12}^*}{i\hbar\omega+\xi_2} & i\hbar\omega - \xi_1 - \frac{|\Delta_{11}|^2}{i\hbar\omega+\xi_1} - \frac{|\Delta_{12}|^2}{i\hbar\omega+\xi_2} \end{pmatrix}. \quad (4.34)$$

Interestingly the normal Green function (4.34) presents off-diagonal elements only due to crosspairing. This will introduce new terms for the spectral wave function, however as we will see later these terms do not contribute to the total particle density.

Before we calculate the spectral wave function, we note that the elements of the normal Green function are symmetric under the exchange of the band indices, $1 \leftrightarrow 2$. Therefore in what follows we will present the relevant quantities regarding $G_{11\omega}$ and $G_{12\omega}$ only.

The spectral wave function is defined by

$$S_{ij\omega}(\vec{k}) = -\frac{1}{\pi}\Im G_{ij\omega}(\vec{k})(i\omega \to \omega + i\epsilon), \quad \epsilon = 0^+. \quad (4.35)$$

Substituting (4.34) into (4.35), we obtain

$$S_{11\omega}(\vec{k}) = (v_{k11}^2 A - v_{k12}^2 C)\delta(E_+ + \omega) + (u_{k11}^2 A - u_{k12}^2 C)\delta(E_+ - \omega) +$$
$$+(v_{k21}^2 B + v_{k22}^2 C)\delta(E_- + \omega) + (u_{k21}^2 B - u_{k22}^2 C)\delta(E_- - \omega) \quad (4.36)$$
$$S_{12\omega}(\vec{k}) = (v_{k12}^2 P + v_{k11}^2 R)\delta(E_+ + \omega) + (u_{k12}^2 P + u_{k11}^2 R)\delta(E_+ - \omega) +$$
$$-(v_{k22}^2 P + v_{k21}^2 R)\delta(E_- + \omega) - (u_{k22}^2 P - u_{k21}^2 R)\delta(E_- - \omega), \quad (4.37)$$

where $A = (E_+^2 - \varepsilon_2^2)/b$, $B = (E_-^2 - \varepsilon_2^2)/b$, $C = |\Delta_{12}|^2/b$, $P = |\Delta_{11}||\Delta_{12}|\cos(\varphi_{12} - \varphi_{11})/b$, $R = |\Delta_{22}||\Delta_{12}|\cos(\varphi_{12} - \varphi_{22})/b$ and the spectral weight for holes and electrons are given by the 2×2 matrices u_{kij}^2 and v_{kij}^2 respectively

$$u_{kij}^2 = \begin{pmatrix} \frac{1}{2} + \frac{\xi_1}{2E_+} & \frac{1}{2} + \frac{\xi_2}{2E_+} \\ \frac{1}{2} + \frac{\xi_1}{2E_-} & \frac{1}{2} + \frac{\xi_2}{2E_-} \end{pmatrix}, \quad v_{kij}^2 = \begin{pmatrix} \frac{1}{2} - \frac{\xi_1}{2E_+} & \frac{1}{2} - \frac{\xi_2}{2E_+} \\ \frac{1}{2} - \frac{\xi_1}{2E_-} & \frac{1}{2} - \frac{\xi_2}{2E_-} \end{pmatrix}, \quad (4.38)$$

where the sub-index kij of u_{kij}^2 and v_{kij}^2 represent the momentum k and its respective matrix element ij.

At this point it is instructive to check the correctness of our result by taking the limit $\Delta_{12} = 0$. We verify that one obtains the standard result for the spectral weight for holes and electrons in presence of only IBP. Taking the limit $\Delta_{12} = 0$ into Eqs. (4.36) and (4.37), we get

$$S_{11\omega}(\vec{k}) = v_{k1}^2\delta(\varepsilon_1 + \omega) + u_{k1}^2\delta(\varepsilon_1 - \omega), \quad (4.39)$$
$$S_{12\omega}(\vec{k}) = 0, \quad (4.40)$$

where $\varepsilon_1 = \sqrt{\xi_1^2 + |\Delta_{11}|^2}$ and the spectral weights for hole and electrons have BCS-like form: $u_{k1}^2 = 1/2(1 + \xi_1/\varepsilon_1)$, $v_{k1}^2 = 1/2(1 - \xi_1/\varepsilon_1)$.

As it is well known the integration of the spectral wave function (4.35) with respect to the energy ω constitute the sum rule for a two-band system in presence of crosspairing. Indeed our formalism is checked to be correct since:

$$\int_{-\infty}^{+\infty} d\omega S_{ij\omega}(\vec{k}) = \begin{pmatrix} 1 & 0 \\ 0 & 1 \end{pmatrix}. \tag{4.41}$$

From the above expression (4.41) we conclude that the off-diagonal terms of the spectral function do not contribute to the total particle density.

The DOS is defined by

$$N_{ij}(\omega) = \int \frac{d^3k}{(2\pi)^3} S_{ij\omega}. \tag{4.42}$$

To calculate the DOS, we first solve the pair amplitude equations (4.7) and then we introduce the obtained solutions Δ_{ij} into Eq. (4.42) which finally we integrate numerically with respect to $\vec{k}$. For example, in case of a presence of gapless state for E_-, then its associated spectral weight function $S_{22\omega}$ is equal to zero. Nonetheless $S_{11\omega}$ and $S_{12\omega}$ are not zero. Furthermore, according to Eq. (4.42) at the gapless state $N_{22}(\omega) = 0$ and $N_{11}(\omega) \neq 0$, $N_{12}(\omega) \neq 0$.

Now, we have everything to our disposal to verify the presence of the gapless state, but first we will illustrate the shape of the DOS for the crossover from the IDR to the CDR when $\mu = 200$ meV, $\Omega = 30$ meV and

$$\lambda_{ij,kl} = \begin{pmatrix} 0.4 & 0.05 & 0.05 \\ 0.05 & 0.3 & 0.05 \\ 0.05 & 0.05 & \lambda_{12,12} \end{pmatrix}. \tag{4.43}$$

In Figs. 4.9a and 4.9b, we show the excitation gaps and all three pairing amplitudes at 4.2 K (an experimental standard). As the crosspairing coupling $\lambda_{12,12}$ is increased, the two excitation gaps Δ_+ and Δ_- split further as discussed before. The value of $\lambda_{12,12} = \lambda_c$ was obtained numerically (roughly half the average of $\lambda_{11,11}$ and $\lambda_{22,22}$) and marks the maximal competition between the intraband and the crossband pairing channels and separates the two regimes: the intraband-dominated regime (IDR) for $\lambda_{12,12} < \lambda_c$, and a crosspairing-dominated regime (CDR) for $\lambda_{12,12} > \lambda_c$. Fig. 4.9c shows that superconducting critical temperature T_c increases with $\lambda_{12,12}$ faster than expected considering the range of values of $\lambda_{12,12}$ alone. In the miniplots above

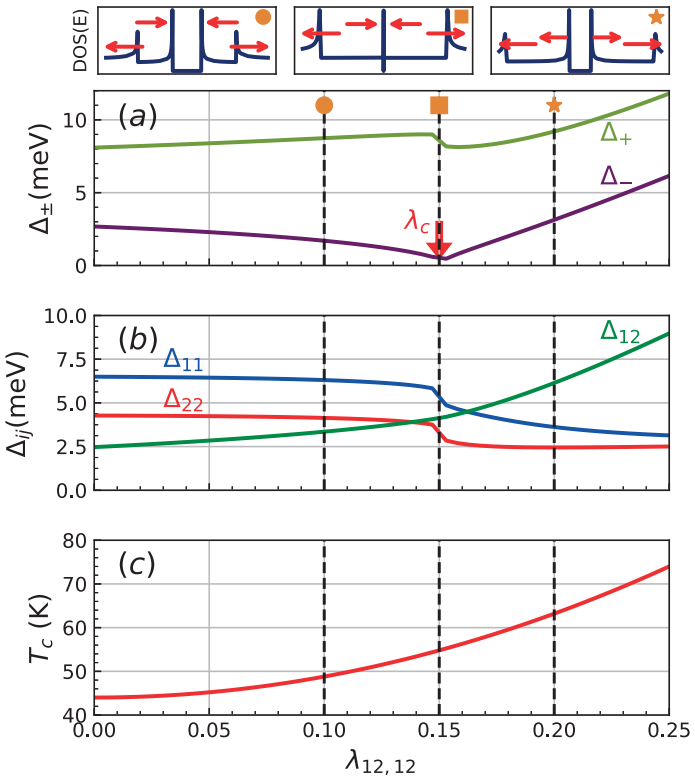

Figure 4.9: Effect of crosspairing for the same phase. Excitation gaps (a) with their corresponding pair amplitudes (b) as function of $\lambda_{12,12}$ at $T = 4.2$ K. The three miniplots above (a) show the density of states for $\lambda_{12,12} = 0.1$, 0.15, and 0.2, illustrating the behavior in the intraband-dominated regime, gapless state, and the cross-pairing dominated regime, respectively. (c) Mean-field critical temperature versus $\lambda_{12,12}$.

Fig. 4.9a, we show the density of states obtained from Eq. (4.42) (as a measurable quantity in STM/STS) for the IDR, CDR as well as for the crossover point $\lambda_{12,12} = \lambda_c$. At this point our analytical approach is helpful to confirm that we have a gapless state for the case of total degeneracy ($\Delta_{11} = \Delta_{22} = \Delta_{12}$), where $S_{22\omega}$ vanishes. Note that in the latter situation the Δ_- (inner coherence peak) approaches zero, and become exactly zero for a favorable combination of parameters. Now, we analyze the spectral wave functions (4.36, 4.37) and confirm that at least we have a gapless state for the case of total degeneracy as we have already have seen from the analytical solutions, see Eqs. (4.24) and (4.25). We have not been able to find other combination of parameters that could make zero the weaker gap Δ_-. Nonetheless we cannot discard its possibility.

The three miniplots shown above Fig. 4.9a, present four coherence peaks. The energy separation between the outer coherence peaks (the two more distant to each other) is equal to $2\Delta_+$ and the energy

separation between the inner coherence peaks (the more close to each other) is equal to $2\Delta_-$. As indicated by the red arrows, across the IDR the inner coherence peaks move closer to each other while the outer coherence peaks split further apart. At the critical value of $\lambda_{12,12} = \lambda_c$, we do not have gapless state because $\Delta_- \neq 0$. Interestingly the inner coherence peaks due to its proximity look like a single coherence peak. At the CDR the inner and outer coherence peaks move both outwards.

The DOS for $\lambda_{12,12} = \lambda_c$ (closest point to the gapless state) resembles the scanning tunneling microscopy (STM) measurements in superconductors doped with magnetic impurities [51] or the Majorana zero-energy bound states [135, 137]. In the next Section, we will illustrate the effects of the inclusion of crosspairing in MgB_2 and $Ba_{0.6}K_{0.4}Fe_2As_2$.

4.5 SIGNATURES OF CROSSPAIRING IN MAGNESIUM DIBORIDE AND IRON ARSENIDE

One of the most well established two-gap superconductors is MgB_2. The fermiology of this compound presents two 2D σ bands localized within the boron layers and two π bands which are delocalized and manifest 3D properties, see Fig. 4.10.

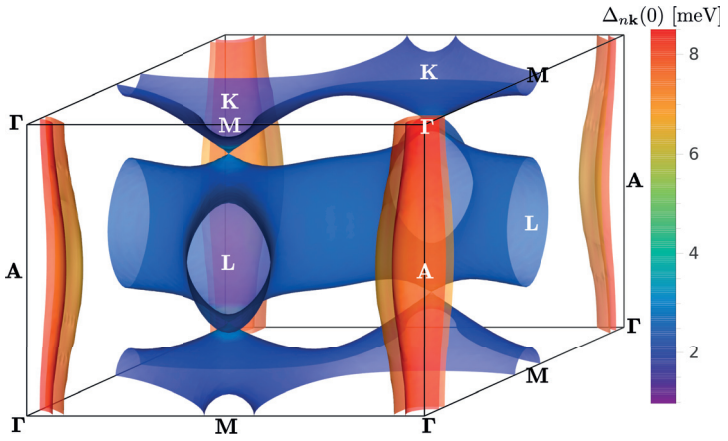

Figure 4.10: The superconducting energy gaps of MgB_2 (expressed in meV) on the Fermi surface for $T = 10$ K. Dark orange and light orange come from the bonding $p_{x,y}$ bands, the top and bottom tubular networks (hole-like) from the bonding p_z bands, and the middle tubular network (electron-like) from the antibonding p_z band. From Ref [103].

Although MgB_2 has four gaps, its mean-field description contemplates only two gaps. One gap comes from the merging of two σ bands and the other by the the electron-like π band, this simplification permits to treat MgB_2 effectively as a two-gap superconductor. Nonetheless, in this Section we will relax this assumption and consider the two σ bands independent. Moreover, based on the feasibility of

crosspairing due to band proximity, we will explore the implications of cross-band pairing in MgB_2 between the two σ-bands.

Our starting point is to observe the band structure and determine how close are the two σ bands in the vicinity of the Fermi level. Unfortunately, angle-resolved photoemission spectroscopy (ARPES) measurements do not have enough resolution to determine the inter-band distance between the two σ bands at the Γ point of the Brillouine zone [119]. Therefore we will use the bands structure obtained from density functional theory (DFT) calculations to observe specifically the σ bands at the Γ point. Interestingly the band structure of MgB_2 in the ultrathin limit presents several bands with small interband distance among them close to the Fermi level. This motivates the presence of cross-band pairing in the atomically-thin limit or even when one has 6-monolayers of MgB_2 [11], see Fig. 4.11.

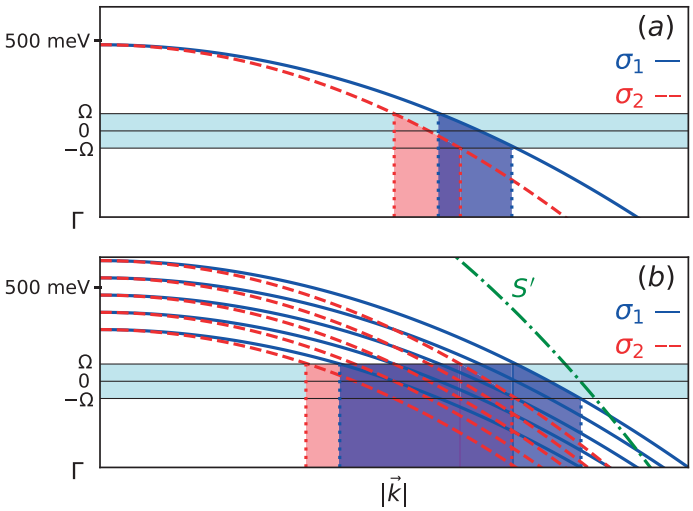

Figure 4.11: The relevance of crosspairing is illustrated based on the band structure of (a) bulk MgB_2 [103] and (b) 6-monolayer MgB_2 [11]. Only sigma bands close to the Γ point of the Brillouine zone are shown, with chemical potential $\mu = 500$ meV and energy scale of the pairing $\Omega = 75$ meV. In (b), each interior monolayer contributes a pair of hole-like bands σ_1 and σ_2, and the surface band is denoted by S'. The (purple) overlapping shadows project the momentum states where cross-band pairing between opposite momenta states among the σ bands is feasible.

To describe this system we will consider MgB_2 as three gap superconductor, two σ bands and one π band. When we have crosspairing only between the two σ bands the pair amplitude equations are obtained from Appx. A.1,

$$\Delta_{ij} = \sum_{kl=1,2} g_{ij,kl} \int \frac{d^3\vec{k}}{(2\pi)^3} \Delta_{kl} \left\{ \chi^+_{kl} f[E_+] + \chi^-_{kl} f[E_-] \right\} + \\ + g_{ij,33} \int \frac{d^3\vec{k}}{(2\pi)^3} \Delta_{33} f(E_3), \tag{4.44}$$

where $\Delta_{ij} \equiv \{\Delta_{11}, \Delta_{22}, \Delta_{12}, \Delta_{33}\}$, with 1, 2 denoting the two σ bands and 3 the π band. The expression for $f(E_\pm)$ is obtained from Eq. (4.7) and $E_3 = \sqrt{\xi_3^2 + |\Delta_{33}|^2}$ is the BCS-like spectra of the π band. The distance of two σ-bands in the vicinity of the Fermi level is approximately 75 meV (see Fig. 4.11a). Taking the parameters $\mu =$ 500 meV and $\Omega = 75$ meV from Refs. [70, 103], we consider the crosspairing between the σ-bands, with the coupling matrix

$$\lambda_{ij,kl} = \begin{pmatrix} 0.275 & 0.032 & \lambda_{ij,12} & 0.032 \\ 0.032 & 0.274 & \lambda_{ij,12} & 0.032 \\ \lambda_{12,ij} & \lambda_{12,ij} & 0.1 & 0.01 \\ 0.01 & 0.01 & 0.01 & 0.22 \end{pmatrix}. \tag{4.45}$$

Here $\lambda_{ij,33}$ is the coupling to the π band, and the third column and row correspond to the coupling to the crosspairing channel, with $\lambda_{ij,12}$ as a free (small) parameter. Other coupling constants are taken from literature, and yield the experimentally measured gaps of MgB_2 (≈ 7 and 3 meV) in absence of crosspairing ($\lambda_{ij,12} = 0$, see Fig. 4.12). Even a small $\lambda_{ij,12} = 0.01$ yields a 2 meV split of the two σ gaps and a 1 K increase in T_c. This gives confidence that crosspairing effects, even if seemingly small, can lead to significant modifications of the gap spectrum without changing significantly T_c. That in turn calls for revisiting of theoretical approaches, e.g. to include crosspairing in anisotropic Eliashberg calculations even for materials that seemed previously well described [5, 24], as well as revisiting the available experimental data (bearing in mind the non-equivalence between $\Delta_\pm$ and the pairing amplitudes in presence of crosspairing). Conducting more refined ARPES measurements (e.g. in case of crystalline MgB_2, on two σ-bands separately) can provide the required resolution to observe the gap splitting predicted by crosspairing.

Last but not least, we discuss the phase-frustrated solutions of Eq. (4.7), with non-zero angle θ. As we mentioned before, see Fig. 4.7, superconductors with non trivial phase symmetry include the FeSCs where one can have two types of s^{+-} symmetry. The case of interest is the orbital antiphase s^{+-}, with a π-phase difference between bands of the same type (electron-like or hole-like), as reported in the optimally doped (BaK)Fe_2As_2 ($T_c = 36$ K) [77, 138, 141]. This compound presents two hole-like bands (α, β) stemming from two nested Fermi sheets at Γ-point, and two electron-like bands (γ, δ) stemming from two

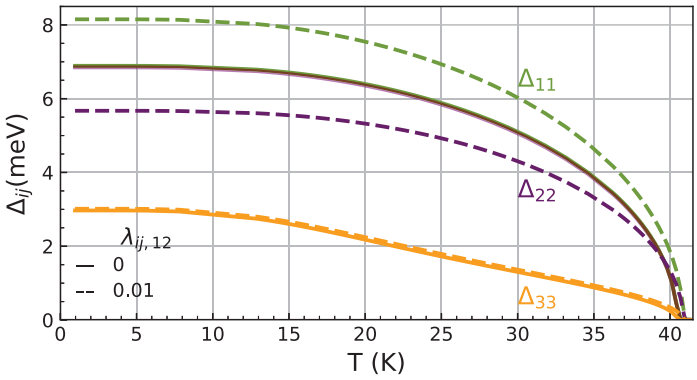

Figure 4.12: Superconducting gaps of bulk MgB_2 as a function of temperature, for intraband pairing only (solid lines), and in the presence of weak crosspairing (dashed lines).

nested Fermi sheets at the M-point, see Fig. 4.13. The proximity of both pairs of bands to the Fermi level and the smallness of their interband distance justifies the assumption of crosspairing between bands α and β or γ and δ. To identify the emergent effects, we will consider the effect of crosspairing only between α and β (assume similar consequences for crosspairing between γ and δ).

We take the interband distance between α and β as 10 meV and the Fermi level at $\mu = 50$ meV, see Fig. 4.13. To obtain the gaps ($\Delta_\pm$) as measured in low-temperature experiments ($\approx$ 12.4 and 6.2 meV extrapolated to $T = 0$, [31]), we take for the coupling matrix:

$$\lambda_{ij,kl} = \begin{pmatrix} 0.51 & \lambda_{11,22} & \lambda_{11,12} \\ 0.5\lambda_{11,22} & 0.39 & \lambda_{11,12} \\ 0.5\lambda_{11,12} & 0.5\lambda_{11,12} & 0.25 \end{pmatrix}. \tag{4.46}$$

Here $\lambda_{11,22}$ is taken negative, which is the standard way to obtain the sign change in the band-dependent order parameters (as reported in $Ba_{0.6}K_{0.4}Fe_2As_2$ [108]). We introduce a small repulsion $\lambda_{11,22} = -0.005$, which induces a phase shift between the two intraband pair amplitudes Δ_{11} and Δ_{22}, therefore $\varphi_{11} - \varphi_{22} = \pi$.

In such a case, the coupling of the crosspairing pair amplitude with the intraband pair amplitudes (for $\lambda_{ij,12} > 0$) will introduce frustration on the phase of the crosspairing order parameter φ_{12}. Phase frustration of similar sort is known in three-band systems [20, 97, 120] and can lead to skyrmionic vortex states [40, 41, 95], but is not possible in a two-band system unless crosspairing is present. In the present case, we reveal additional new physics, as crosspairing induces $s^{+-} \to s^{++}$ transition as a function of temperature, as shown in Fig. 4.14(a,b) for exemplified parameters of $(BaK)Fe_2As_2$.

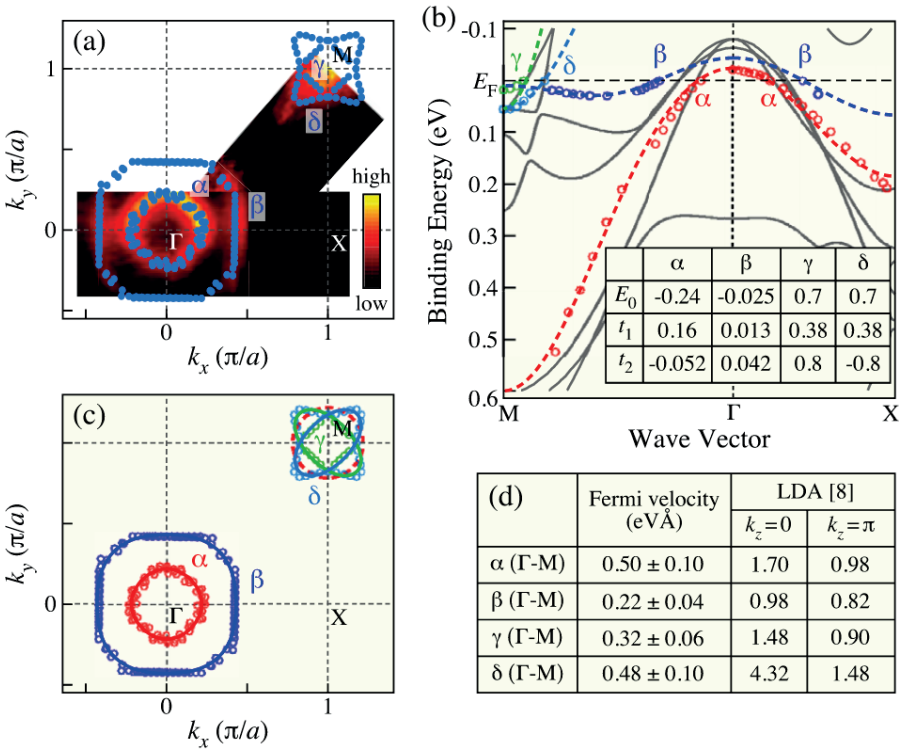

	α	β	γ	δ
E_0	-0.24	-0.025	0.7	0.7
t_1	0.16	0.013	0.38	0.38
t_2	-0.052	0.042	0.8	-0.8

(d)	Fermi velocity (eVÅ)	LDA [8]	
		k_z=0	k_z=π
α (Γ-M)	0.50 ± 0.10	1.70	0.98
β (Γ-M)	0.22 ± 0.04	0.98	0.82
γ (Γ-M)	0.32 ± 0.06	1.48	0.90
δ (Γ-M)	0.48 ± 0.10	4.32	1.48

Figure 4.13: (a) Fermi surfaces in the 2D Brillouine zone. (b) Measured band dispersion (circles) along $\Gamma - M$ and $\Gamma - X$, compared with the local density approximated bands normalized by a factor of 2 (solid lines), and tight-binding fits (dashed lines). The inset table lists parameter of tight-binding bands. (c) Measured Fermi surface (circles) and fitted tight-binding curves (solid lines). (d) Table of measured and calculated Fermi velocities along $\Gamma - M$. From Ref. [30].

In the example shown in Fig. 4.14(a,b), after the transition, the pair amplitudes recover the same phase ($\theta = 0$) until the expected BCS critical temperature of ≈ 80 K. In experiment however [31], the measured gaps abruptly cease at $T_c \approx 40$ K, for reasons that are not understood to date. Without claiming to rigorously describe the non BCS behavior of the gaps versus temperature, we notice that our calculation of the gaps vs. temperature can closely reproduce the experimentally measured data (as shown in Fig. 4.14c), assuming that the s^{+-} orbital antiphase is protected by symmetry or the transition to s^{++} state is disallowed.

In this Chapter we have introduced crosspairing from first principles in the BCS-mean-field Hamiltonian. Furthermore, we assume that the Cooper pair instability holds for a small attraction among electrons with opposite spin and momentum. This restricts the formation of cross-band Cooper pairs to hybridized bands or close bands in the vicinity of the Fermi level. The pair amplitude solutions showed an increment of the gap splitting between the the initial gaps with only IBP

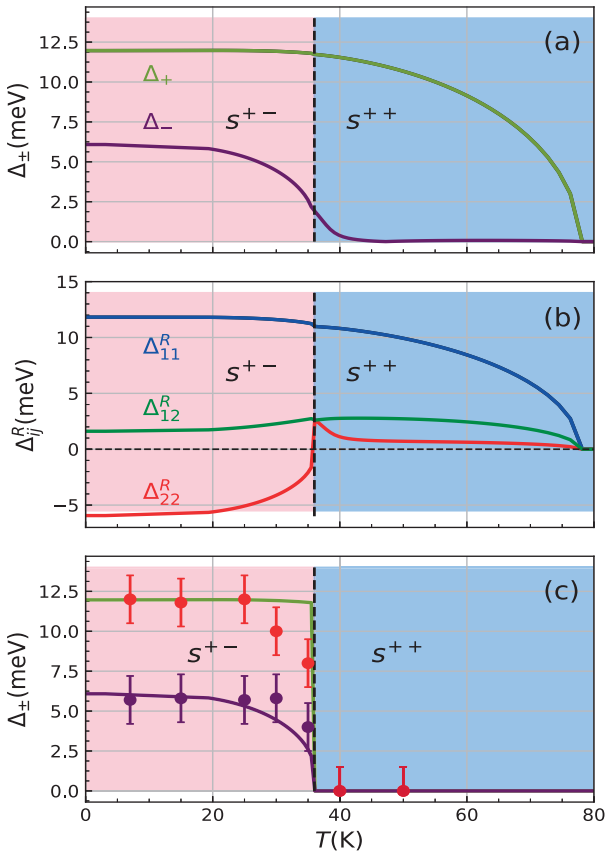

Figure 4.14: (a) Excitation gaps $\Delta_\pm$, and (b) real part of the pair amplitudes Δ^R_{ij} as a function of temperature, for parameters of (α, β) bands in (BaK)Fe_2As_2, with nominal s^{+-} antiphase and in presence of crosspairing. For parameters given in the text, $s^{+-} \to s^{++}$ transition is found at 36 K, corresponding to the critical temperature of the measured gaps at the Γ-point of $Ba_{0.6}K_{0.4}Fe_2As_2$ [31]. Panel (c) superimposes the theoretical data of (a) on experimental data of Ref. [31], highlighting their agreement in case s^{+-} antiphase is protected.

with a tendency to decrease the weaker gap Δ_- to zero (gapless state). The competition between IBP and CBP induces phase frustration where one has two possible solutions: (a) one with $\theta = 0$ and another (b) with $\theta = \pi$. In the next Chapter, we will address this issue by studying the free-energy of the mean-field Hamiltonian (4.3). To obtain the free energy we will derive first the GL equations when one has intraband and cross-band pair amplitudes. Once we have the GL equations, we will use the variational principle to obtain its correspondent free energy. The minimum of the free energy will determine unequivocally which of the above mentioned solutions ($\theta = 0$ or $\theta = \pi$) is more stable.

5

GINZBURG LANDAU THEORY WITH CROSSPAIRING

Superconductors with multiple gaps are a common scenario in the current most studied compounds. The origin of the different gaps is usually linked to the presence of different bands and can present non homogeneous electronic structures. For example, MgB_2 is a well characterized two-gap superconductor which presents 2D and 3D bands [119]; the four-gap $Ba_{1-x}K_xFe_2As_2$ superconductor which presents two hole-like and two electron-like nested pockets [31]; Pb which was first described as a single-gap superconductor presents two gaps due to the disjoint nature of the electron-phonon energy [37]; UPt_3 which presents different phonon modes that promote the formation of singlet and triplet Cooper pairs [64]; or the whole class of $p-$wave superconductors whose symmetry can only be described in a multi-gap scenario. All these examples motivated the inclusion of two [126] or multiple [97] components within the GL formalism. A multicomponent GL theory with only IBP has each component associated with a different gap opening in the DOS.

The derivation of the GL equations is done by expanding the order parameter in powers of $\tau^{1/2}$. In the expansion the terms proportional to $\tau^{1/2}$ give us an expression for the critical temperature, while the terms proportional to $\tau^{3/2}$ give us the GL equation. Here we will refer this particular expansion in $\tau^{1/2}$ and $\tau^{3/2}$ as the Gor'kov domain. We showed in Sec. 3.2.2 that a multicomponent GL theory with only IBP is reduced to a single-component GL theory with a sole coherence length, see Eq. (3.47). Immediately after the presentation of this issue [67], several publications managed to restore the multicomponent nature of the GL theory (extended GL theory) [114, 130, 131]. However, all those efforts require the inclusion of a higher order ($\tau^{5/2}$) in the expansion of the OP around T_c. This means that within the Gor'kov domain and in presence of only IBP the multi-component nature of the GL theory is lost.

The purpose of the present Chapter is to study a multicomponent GL theory in presence of both IBP and CBP. In order to do this we will derive microscopically the GL equations within the Gor'kov domain and proceed with the conventional reconstruction of the OP. Then we will study the normal-superconducting interface and the vortex lattice. At the end we will discuss its experimental signatures in MgB_2 and FeSCs.

5.1 DERIVATION OF THE GINZBURG-LANDAU EQUATIONS

We will derive the GL equations in presence of crosspairing for a two-band system using the method developed by Vagov, Shanenko, et al. [131]. The Hamiltonian in consideration and the pair amplitude definition are given by Eqs. (4.3) and (4.4) respectively. From this system one can write the Gor'kov equations in the form of the Dyson equation for the matrix propagator $\mathcal{G}_{ij\omega}$,

$$\mathcal{G}_{ij\omega} = \mathcal{G}^{(0)}_{ij\omega} + \mathcal{G}^{(0)}_{ik\omega}\tilde{\Delta}_{kl}\mathcal{G}_{lj\omega}, \tag{5.1}$$

with

$$\mathcal{G}_{ij\omega} = \begin{pmatrix} G_{ij\omega} & F_{ij\omega} \\ \bar{F}_{ij\omega} & \bar{G}_{ij\omega} \end{pmatrix}, \quad \mathcal{G}^{(0)}_{ij\omega} = \begin{pmatrix} G^{(0)}_{ij\omega} & 0 \\ 0 & \bar{G}^{(0)}_{ij\omega} \end{pmatrix}, \tag{5.2}$$

$$\tilde{\Delta}_{ij} = \begin{pmatrix} 0 & \Delta_{ij} \\ \Delta^*_{ij} & 0 \end{pmatrix}, \quad M_{ij} = \begin{pmatrix} M_{11} & M_{12} \\ M_{21} & M_{22} \end{pmatrix}, \tag{5.3}$$

where $G_{ij\omega}$, $F_{ij\omega}$, $\bar{G}_{ij\omega}$, $\bar{F}_{ij\omega}$, $G^{(0)}_{ij\omega}$, $\bar{G}^{(0)}_{ij\omega}$, Δ_{ij} and Δ^*_{ij} are matrices 2×2 whose general form is given by M_{ij}. Therefore $\mathcal{G}_{ij\omega}$ and $\mathcal{G}^{(0)}_{ij\omega}$ are 4×4 matrices. One can write Eq.(5.1) in an integral form as follows:

$$F_{ij\omega}(\vec{r},\vec{r}') = \int d^3y G^{(0)}_{ik\omega}(\vec{r},\vec{y})\Delta_{kl}(\vec{y})\bar{G}_{lj\omega}(\vec{y},\vec{r}') \tag{5.4}$$

$$\bar{G}_{ij\omega}(\vec{r},\vec{r}') = \bar{G}^{(0)}_{ij\omega}(\vec{r},\vec{r}') + \int d^3y \bar{G}^{(0)}_{ik\omega}(\vec{r},\vec{y})\Delta_{kl}(\vec{y})F_{lj\omega}(\vec{y},\vec{r}'). \tag{5.5}$$

The systematic expansion in small deviation from the critical temperature is controlled by the parameter $\tau = 1 - T/T_c$. This parameter allows us to introduce the following scaling for the order parameter and the coordinates,

$$\Delta_{ij} = \tau^{1/2}\bar{\Delta}_{ij}, \quad \vec{r} = \tau^{-1/2}\bar{\vec{r}}. \tag{5.6}$$

We recall that the Gor'kov domain is defined by solving the system of equations (5.4) and (5.5) by an iterative method and consider only terms up to $\tau^{3/2}$ as done without crosspairing. Substituting Eq. (5.4) into Eq. (5.5) and its result back into Eq. (5.4) we obtain

$$\begin{aligned} F_{ij\omega}(\vec{r},\vec{r}') &= \int d^3y G^{(0)}_{ik\omega}(\vec{r},\vec{y})\Delta_{kl}(\vec{y})\bar{G}^{(0)}_{lj\omega}(\vec{y},\vec{r}') + \int d^3y_1 d^3y_2 \times \\ &\times \; d^3y_3 G^{(0)}_{ik\omega}(\vec{r},\vec{y}_1)\Delta_{kl}(\vec{y}_1)\bar{G}^{(0)}_{lm\omega}(\vec{y}_1,\vec{y}_2)\Delta^*_{mn}(\vec{y}_2) \times \\ &\times \; G^{(0)}_{no\omega}(\vec{y}_2,\vec{y}_3)\Delta_{op}(\vec{y}_3)\bar{G}^{(0)}_{pj\omega}(\vec{y}_3,\vec{r}'). \end{aligned} \tag{5.7}$$

The order parameter can be obtained from the above equation as follows:

$$\Delta_{ij} = \lim_{\vec{r}'\to\vec{r}} \left[-\frac{1}{\beta} \sum_{kl} g_{ij,kl} \sum_{\omega} F_{kl\omega}(\vec{r},\vec{r}') \right] = \tau^{1/2}\bar{\Delta}_{ij}^{(0)} + \tau^{3/2}\bar{\Delta}_{ij}^{(1)}, \quad (5.8)$$

where $\beta = 1/(k_B T)$ with $k_B = 1$ and we have further expanded the order parameter to be consistent with the Gor'kov derivation[1]. Using the expression to obtain the order parameter (5.8) in the expansion of the anomalous Green function (5.7), we obtain

$$\Delta_{ij}(\vec{r}) = -\frac{1}{\beta} \sum_{kl} g_{ij,kl} \sum_{\omega} I_{kl}^{(A)} - \frac{1}{\beta} \sum_{kl} g_{ij,kl} \sum_{\omega} I_{kl}^{(B)}, \quad (5.9)$$

$$I_{kl}^{(A)} = \int d^3y G_{km\omega}^{(0)}(\vec{r},\vec{y}) \Delta_{mn}(\vec{y}) \bar{G}_{nl\omega}^{(0)}(\vec{y},\vec{r}), \quad (5.10)$$

$$I_{kl}^{(B)} = \int d^3y_1 d^3y_2 d^3y_3 G_{km\omega}^{(0)}(\vec{r},\vec{y}_1) \Delta_{mn}(\vec{y}_1) \bar{G}_{no\omega}^{(0)}(\vec{y}_1,\vec{y}_2) \times$$
$$\times \Delta_{op}^*(\vec{y}_2) G_{pq\omega}^{(0)}(\vec{y}_2,\vec{y}_3) \Delta_{qr}(\vec{y}_3) \bar{G}_{rl\omega}^{(0)}(\vec{y}_3,\vec{r}). \quad (5.11)$$

We note that our system is symmetric under the exchange of the band index $1 \leftrightarrow 2$. Therefore it is sufficient to write down the GL equations for $\Delta_{11}(\vec{r})$ and $\Delta_{12}(\vec{r})$. The details of the sum over Matsubara frequencies and the integration in Eq. (5.9) are given in the Appx. (B).

$$\begin{aligned}
\Delta_{ij} &= \sum_{kl} g_{ij,kl} \left(\mathcal{A}_{kl} + a_{kl}\tau + K_{kl}\vec{D}^2 \right) \Delta_{kl} + \\
&- g_{ij,11} \left(b_{11}|\Delta_{11}|^2\Delta_{11} + 2b_{12}|\Delta_{12}|^2\Delta_{11} + b_{12}\Delta_{12}^2\Delta_{22}^* \right) + \\
&- g_{ij,22} \left(b_{22}|\Delta_{22}|^2\Delta_{22} + 2b_{12}|\Delta_{12}|^2\Delta_{22} + b_{12}\Delta_{12}^2\Delta_{11}^* \right) + \\
&- 2g_{ij,12} \left(b_{12}|\Delta_{12}|^2\Delta_{12} + b_{12}|\Delta_{11}|^2\Delta_{12} + b_{12}|\Delta_{22}|^2\Delta_{12} + \right. \\
&+ \left. b_{12}\Delta_{11}\Delta_{22}\Delta_{12}^* \right), \quad (5.12)
\end{aligned}$$

with

$$\mathcal{A}_{ij} = N_{ij}(0) \ln\left(\frac{2e^\gamma}{\pi T_c}\right), \quad a_{ij} = N_{ij}(0), \quad (5.13)$$

$$K_{ij} = N_{ij}(0) \frac{v_{F_{ij}}^2}{6} \frac{7\zeta(3)}{8(\pi T_c)^2}, \quad b_{ij} = N_{ij}(0) \frac{7\zeta(3)}{8(\pi T_c)^2}, \quad (5.14)$$

$$N_{12}(0) = \frac{1}{2}\left[N_{11}(0) + N_{22}(0)\right], \quad v_{F_{12}}^2 = \frac{1}{2}(v_{F_{11}}^2 + v_{F_{22}}^2), \quad (5.15)$$

where $\zeta(x)$ is the Riemann zeta function, γ is the Euler constant, $N_{ii}(0)$ is the density of states relative to band i and v_{Fii} is the Fermi velocity relative to band i. At this point, it is important to remark that the above

1 In principle the above expression should contain all orders in the τ-expansion, however the Gor'kov domain only contains two terms $\tau^{1/2}$ and $\tau^{3/2}$. Extended GL formulations include terms up to $\tau^{5/2}$.

coefficients given by Eqs. (5.13) and (5.14) are obtained when the two bands in consideration overlap, see Appx. (B). In general, the presence of a finite interband distance will affect the GL coefficients. Nonetheless, we will proceed with the two-band system with overlapping bands and later heuristically assume that the variation in the coefficients can be represented by variation of the normalization factors in the GL equations.

The number of components of a two-band system in presence of IBP and CBP is three, because $\Delta_{12} = \Delta_{21}$. Therefore we can write the GL equations using $3-$component order parameter $(\Delta_{11}, \Delta_{22}, \Delta_{12})$.

Now we introduce Eq. (5.8) into (5.12) and group all terms proportional to $\tau^{1/2}$,

$$\begin{pmatrix} g_{11,11}\mathcal{A}_{11} - 1 & g_{11,22}\mathcal{A}_{22} & g_{11,12}\mathcal{A}_{12} \\ g_{22,11}\mathcal{A}_{11} & g_{22,22}\mathcal{A}_{22} - 1 & g_{22,12}\mathcal{A}_{12} \\ g_{12,11}\mathcal{A}_{11} & g_{12,22}\mathcal{A}_{22} & g_{12,12}\mathcal{A}_{12} - 1 \end{pmatrix} \begin{pmatrix} \bar{\Delta}_{11}^{(0)} \\ \bar{\Delta}_{22}^{(0)} \\ \bar{\Delta}_{12}^{(0)} \end{pmatrix} = 0. \quad (5.16)$$

As usual from the determinant of the above matrix one can obtain the expression for the critical temperature, T_c.

The GL equation is obtained by collecting the terms proportional to $\tau^{3/2}$ in Eq. (5.12),

$$M_{ij} \begin{pmatrix} \bar{\Delta}_{11}^{(1)} \\ \bar{\Delta}_{22}^{(1)} \\ \bar{\Delta}_{12}^{(1)} \end{pmatrix} + \begin{pmatrix} g_{11,11} & g_{11,22} & g_{11,12} \\ g_{22,11} & g_{22,22} & g_{22,12} \\ g_{12,11} & g_{12,22} & g_{12,12} \end{pmatrix} \begin{pmatrix} \Omega_{11}[\bar{\Delta}_{11}^{(0)}] \\ \Omega_{22}[\bar{\Delta}_{22}^{(0)}] \\ \Omega_{12}[\bar{\Delta}_{12}^{(0)}] \end{pmatrix} = 0, \quad (5.17)$$

where M_{ij} is the same matrix given by l.h.s in Eq. (5.16), $\Omega_{ij}[\bar{\Delta}_{ij}^{(0)}]$ is given by the terms proportional to $\tau^{3/2}$ in the r.h.s of Eq. (5.12). Now, we assume that the term proportional to $\bar{\Delta}_{ij}^{(1)}$ of Eq. (5.17) when multiplied by the inverse of $g_{ij,kl}$ vanishes or that it satisfies the equation for T_c given by (5.16). Then Eq. (5.17) becomes

$$\begin{pmatrix} \Omega_{11}[\bar{\Delta}_{11}^{(0)}] \\ \Omega_{22}[\bar{\Delta}_{22}^{(0)}] \\ \Omega_{12}[\bar{\Delta}_{12}^{(0)}] \end{pmatrix} = 0, \quad (5.18)$$

where we assumed that $g_{ij,kl}$ is non singular. In what follows we will drop the bar notation and upper index (0), $\bar{\Delta}_{ij}^{(0)} \to \Delta_{ij}$. The full expressions for $\Omega_{ij}[\Delta_{ij}]$ are given by

$$
\begin{aligned}
\Omega_{11}[\Delta_{11}] &= \left[a_{11}\tau + K_{11}\vec{D}^2 - b_{11}|\Delta_{11}|^2 - 2b_{12}|\Delta_{12}|^2 - b_{12}\frac{\Delta_{12}^2\Delta_{22}^*}{\Delta_{11}}\right]\Delta_{11} \\
\Omega_{22}[\Delta_{22}] &= \left[a_{22}\tau + K_{22}\vec{D}^2 - b_{22}|\Delta_{22}|^2 - 2b_{12}|\Delta_{12}|^2 - b_{12}\frac{\Delta_{12}^2\Delta_{11}^*}{\Delta_{22}}\right]\Delta_{22} \\
\Omega_{12}[\Delta_{12}] &= \Big[2a_{12}\tau + 2K_{12}\vec{D}^2 - 2b_{12}|\Delta_{12}|^2 - 2b_{12}|\Delta_{11}|^2 - 2b_{12}|\Delta_{22}|^2 + \\
&- 2b_{12}\frac{\Delta_{11}\Delta_{22}\Delta_{12}^*}{\Delta_{12}}\Big]\Delta_{12}.
\end{aligned}
$$

From the above equations, we can identify the GL operators in presence of only IBP, L_{11}, L_{22} and in presence of only crosspairing L_{12}:

$$\left[L_{11} - 2b_{12}|\Delta_{12}|^2 - b_{12}\frac{\Delta_{12}^2\Delta_{22}^*}{\Delta_{11}}\right]\Delta_{11} = 0, \tag{5.19}$$

$$\left[L_{22} - 2b_{12}|\Delta_{12}|^2 - b_{12}\frac{\Delta_{12}^2\Delta_{11}^*}{\Delta_{22}}\right]\Delta_{22} = 0, \tag{5.20}$$

$$\left[L_{12} - b_{12}|\Delta_{11}|^2 - b_{12}|\Delta_{22}|^2 - b_{12}\frac{\Delta_{11}\Delta_{22}\Delta_{12}^*}{\Delta_{12}}\right]\Delta_{12} = 0, \tag{5.21}$$

where $L_{ij} = K_{ij}\vec{D}^2/2 + a_{ij}\tau - b_{ij}|\Delta_{ij}|^2$ are the conventional GL operators.

Remarkably the system of equations (5.19-5.21) remains coupled only due to the presence of cross-band pairing ($\Delta_{12} \neq 0$). Furthermore the coupling between the condensates contains a non-trivial phase dependence which is different from the Josephson coupling due to the presence of the crosspairing phase φ_{12}.

At this point is useful to test the validity of our system of equations by taking the limit with only IBP, $\Delta_{12} = 0$, and the limit with only CBP, $\Delta_{11} = \Delta_{22} = 0$. Interestingly for both cases we recover the single-component GL equation.

A two-band superconductor with both IBP and CBP constitute effectively a three-component GL system.

Now using the variational principle we write the free energy density that contains the system of equations (5.19-5.21),

$$
\begin{aligned}
f &= K_{11}|\vec{D}\Delta_{11}|^2 - a_{11}\tau|\Delta_{11}|^2 + \frac{b_{11}}{2}|\Delta_{11}|^4 + 2b_{12}|\Delta_{12}|^2|\Delta_{11}|^2 + \\
&+ K_{22}|\vec{D}\Delta_{22}|^2 - a_{22}\tau|\Delta_{22}|^2 + \frac{b_{22}}{2}|\Delta_{22}|^4 + 2b_{12}|\Delta_{12}|^2|\Delta_{22}|^2 + \\
&+ 2K_{12}|\vec{D}\Delta_{12}|^2 - 2a_{12}\tau|\Delta_{12}|^2 + b_{12}|\Delta_{12}|^4 + b_{12}\Delta_{12}^2\Delta_{22}^*\Delta_{11}^* \\
&+ b_{12}\Delta_{11}\Delta_{22}\Delta_{12}^{*2} + \frac{\vec{h}^2}{8\pi}.
\end{aligned} \tag{5.22}
$$

We note that although the GL equations (5.19-5.21) are phase dependent, the reality of the free energy is preserved. This can be seen from the sum of the phase-dependent terms of Eq. (5.22). Interestingly, we observe the emergence of the angle $\theta = 2\varphi_{12} - \varphi_{11} - \varphi_{22}$

which was also present in the microscopic pair amplitude equations (4.7). This angle introduces new degrees of freedom similarly to the Josephson coupling. However, we recall that Josephson couplings in the conventional GL theories cannot be incorporated when one has only intraband pairing. Remarkably, when one has both IBP and CBP we have phase interaction between the different components which are well defined within the Gor'kov domain (see introduction of the present Chapter). This surprising result constitutes one of the main contributions of the present thesis.

The free energy (5.22) reaches a minimum for $\theta = \pi$ as a consequence of the positive coefficient b_{12}, see Eq. (5.14). We show in the previous Chapter that the mere competition between IBP and CBP can induce a phase shift of π between condensates, see Fig. 4.7. Now from the GL equations (5.19-5.21) and its related free energy (5.22), we conclude that the origin of the π-phase shift in θ is a requirement to reach the minimum of the free energy.

In the next Section we will attempt to reconstruct the order parameter to elucidate if our system of equations can be reduced to a single-component GL equation with only one coherence length.

5.2 RECONSTRUCTION OF THE GINZBURG-LANDAU ORDER PARAMETER

We will perform the reconstruction of the order parameter following the same method from Ref. [130, 131]. For our case, the reconstruction of the order parameter consist in the reduction of the three GL Eqs. (5.19-5.21) to a single GL equation with only one component. First we introduce the γ_{ij} as the inverse of the coupling matrix $g_{ij,kl}$:

$$\gamma_{ij} = \begin{pmatrix} g_{11,11} & g_{11,22} & g_{11,12} \\ g_{22,11} & g_{22,22} & g_{22,12} \\ g_{12,11} & g_{12,22} & g_{12,12} \end{pmatrix}^{-1} = \begin{pmatrix} \gamma_{11} & \gamma_{12} & \gamma_{13} \\ \gamma_{21} & \gamma_{22} & \gamma_{23} \\ \gamma_{31} & \gamma_{32} & \gamma_{33} \end{pmatrix}. \tag{5.23}$$

Using the above matrix (5.23), we can write Eq. (5.16) as follows:

$$\begin{pmatrix} \gamma_{11} - \mathcal{A}_{11} & \gamma_{12} & \gamma_{13} \\ \gamma_{21} & \gamma_{22} - \mathcal{A}_{22} & \gamma_{23} \\ \gamma_{31} & \gamma_{32} & \gamma_{33} - \mathcal{A}_{12} \end{pmatrix} \begin{pmatrix} \bar{\Delta}_{11}^{(0)} \\ \bar{\Delta}_{22}^{(0)} \\ \bar{\Delta}_{12}^{(0)} \end{pmatrix} = 0. \tag{5.24}$$

Now we begin the reconstruction of the order parameter by obtaining the eigenvector whose eigenvalue is zero from equation (5.16),

$$\vec{\Delta}^{(0)}(\vec{r}) = \begin{pmatrix} 1 \\ \frac{\gamma_{21}\gamma_{13} - \gamma_{23}S_{11}}{\gamma_{23}\gamma_{12} - S_{22}\gamma_{13}} e^{i(\varphi_{22} - \varphi_{11})} \\ \frac{S_{11}\gamma_{23}\gamma_{32} + S_{22}\gamma_{13}\gamma_{31} - 2\gamma_{12}\gamma_{23}\gamma_{31}}{S_{33}(\gamma_{12}\gamma_{23} - S_{22}\gamma_{13})} e^{i(\varphi_{12} - \varphi_{11})} \end{pmatrix} \psi(\vec{r}), \tag{5.25}$$

where $S_{11} = \gamma_{11} - \mathcal{A}_{11}$, $S_{22} = \gamma_{22} - \mathcal{A}_{22}$ and $S_{33} = \gamma_{33} - \mathcal{A}_{12}$.

The proportionality of the multiple components given by Eq. (5.25) is a physical constraint because all pair amplitudes become simultaneously zero at T_c. This proportionality holds also for the GL equations in presence of only IBP which ultimately makes our system to present a single coherence length. However, we observe that our eigenvector (5.25) presents a relative phase which can induce a negative sign whenever $\varphi_{22} - \varphi_{11} = \pi$ or $\varphi_{12} - \varphi_{11} = \pi$.

The eigenvector with zero eigenvalue is obtained from the expression $\vec{\eta}_1\psi(\vec{r})$ in Eq. (5.25). To form an orthogonal basis we obtain the second eigenvector by taking the scalar product, $\vec{\eta}_1.\vec{\eta}_2 = 0$ and the third one by taking the vectorial product, $\vec{\eta}_3 = \vec{\eta}_1 \times \vec{\eta}_2$.

We proceed with the reconstruction of the OP in the GL equation as follows:

$$\begin{pmatrix} \gamma_{11} - \mathcal{A}_{11} & \gamma_{12} & \gamma_{13} \\ \gamma_{21} & \gamma_{22} - \mathcal{A}_{22} & \gamma_{23} \\ \gamma_{31} & \gamma_{32} & \gamma_{33} - \mathcal{A}_{12} \end{pmatrix} \begin{pmatrix} \Delta_{11}^{(1)} \\ \Delta_{22}^{(1)} \\ \Delta_{12}^{(1)} \end{pmatrix} = \begin{pmatrix} R_{11}[\Delta_{11}^{(0)}] \\ R_{22}[\Delta_{22}^{(0)}] \\ R_{12}[\Delta_{12}^{(0)}] \end{pmatrix}, \quad (5.26)$$

where we have dropped the bar notation, $\bar{\Delta}_{ij}^{(k)} \to \Delta_{ij}^{(k)}$.

The term $\tau^{3/2}$ of the Gor'kov expansion mixes the different orders of the order parameter, $\Delta_{ij}^{(0)}$ and $\Delta_{ij}^{(1)}$. Interestingly the relation between different orders is linear and can be decouple if we chose an appropiate basis for $\Delta_{ij}^{(1)}$,

$$\begin{pmatrix} \Delta_{11}^{(1)} \\ \Delta_{22}^{(1)} \\ \Delta_{12}^{(1)} \end{pmatrix} = \chi_1(\vec{r})\vec{\eta}_1 + \chi_2(\vec{r})\vec{\eta}_2 + \chi_3(\vec{r})\vec{\eta}_3. \quad (5.27)$$

Substituting (5.27) into (5.26) and projecting its result to $\vec{\eta}_1^{\dagger}$,

$$0 = \begin{pmatrix} \eta_{1(1)}^* & \eta_{1(2)}^* & \eta_{1(3)}^* \end{pmatrix} \begin{pmatrix} \Xi_1 & 0 & 0 \\ 0 & \Xi_2 & 0 \\ 0 & 0 & \Xi_3 \end{pmatrix} \begin{pmatrix} \Delta_{11}^{(0)} \\ \Delta_{22}^{(0)} \\ \Delta_{12}^{(0)} \end{pmatrix}, \quad (5.28)$$

with

$$\Xi_1 = L_{11} - 2b_{12}|\Delta_{12}^{(0)}|^2 - b_{12}\frac{|\Delta_{12}^{(0)}|^2|\Delta_{22}^{(0)}|}{|\Delta_{11}^{(0)}|}e^{i\theta} \quad (5.29)$$

$$\Xi_2 = L_{22} - 2b_{12}|\Delta_{12}^{(0)}|^2 - b_{12}\frac{|\Delta_{12}^{(0)}|^2|\Delta_{11}^{(0)}|}{|\Delta_{22}^{(0)}|}e^{i\theta} \quad (5.30)$$

$$\frac{\Xi_3}{2} = L_{12} - b_{12}|\Delta_{11}^{(0)}|^2 - b_{12}|\Delta_{22}^{(0)}|^2 - b_{12}\frac{|\Delta_{11}^{(0)}||\Delta_{22}^{(0)}||\Delta_{12}^{(0)}|}{|\Delta_{12}^{(0)}|}e^{-i\theta}, \quad (5.31)$$

where $\theta = 2\varphi_{12} - \varphi_{11} - \varphi_{22}$.

We finish the reconstructive procedure by substituting (5.25) into (5.28),

$$\left[\mathcal{K}\vec{D}^2 + \alpha\tau - \beta(\theta)|\psi(\vec{r})|^2\right]\psi(\vec{r}) = 0, \tag{5.32}$$

with

$$\mathcal{K} = K_{11} + \eta_b^2 K_{22} + 2\eta_c^2 K_{12}, \tag{5.33}$$

$$\alpha = a_{11} + \eta_b^2 a_{22} + 2\eta_c^2 a_{12}, \tag{5.34}$$

$$\beta(\theta) = b_{11} + \eta_b^4 b_{22} + 2\eta_c^4 b_{12}\left[1 + 2\frac{(1+\eta_b^2+\eta_b\cos\theta)}{\eta_c^2}\right], \tag{5.35}$$

where $(\eta_a, \eta_b, \eta_c) = \vec{\eta}_1^T$ are given by Eq. (5.25).

It is important to remember that the reconstructed GL equation (5.32) is equivalent to the multicomponent system of equations (5.19-5.20) only when the phases of the different components φ_{11}, φ_{22} and φ_{12} are constant. This can be seen from Eq. (5.35), where normalization of $\beta(\theta)$ is ill-defined due to the phase dependence from the other components. Nonetheless, we will proceed the analysis assuming θ as an auxiliary variable (non-dynamical variable). The minimization of the free energy will constraint the values of θ to two cases: $\theta = \pi$ for $\eta_{1(2)} > 0$ or $\theta = 0$ for $\eta_{1(2)} < 0$.

Now the GL equation is reduced to a single component where β is now phase-dependent. From the GL equation in presence of IBP and CBP, Eq. (5.32) and using Eqs. (2.52) and (2.59), we obtain the superfluid density and London penetration depth:

$$n_s(\theta) \propto \sqrt{\frac{\alpha}{\beta(\theta)}}, \quad \lambda_L(\theta) = \sqrt{\frac{m^* c^2 \beta(\theta)}{4\pi e^{*2}\alpha}}, \tag{5.36}$$

where m^* and e^* are the effective mass and electric charge when one solves the London equation together with Eq. (5.32).

To end this Section, we will speculate the connection of our results with the experimental data. The phase dependence of the London penetration depth (5.36) implies that the phase transition $s^{+-} \leftrightarrow s^{++}$ should be accompanied by a change in λ_L or in the superfluid density. Particularly, the phase transition $s^{+-} \rightarrow s^{++}$ can be induced by disorder in superconductors with a pristine s^{+-} state [93]. In a two-band superconductor, the physical origin of this transition is caused by the strong scattering between the two bands induced by disorder. This means that the mean lifetime that an electron stays in a single band approaches zero until one obtains effectively a dirty-one-band superconductor. Suitable candidates that present this transition are

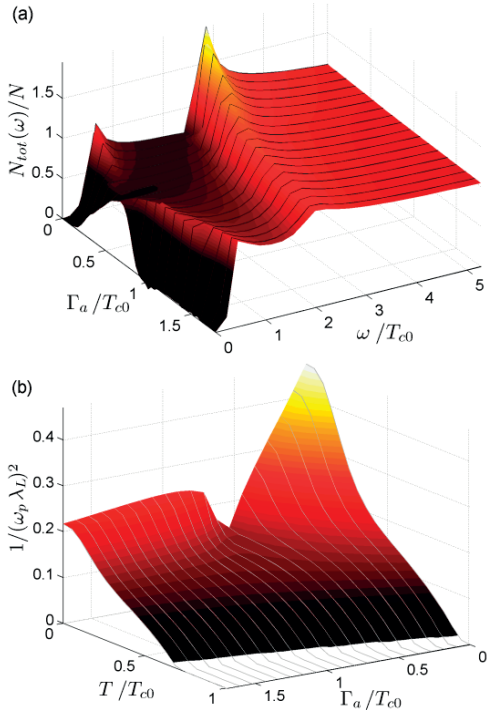

Figure 5.1: (a) Density of states $N_{tot}(\omega)/N$ vs. the scattering rate Γ_a/T_{c0} and ω/T_{c0}. (b) Total superdluidity density $1/(\omega_p\lambda_L)^2$ vs. Γ_a/T_{c0} and T/T_{c0} where ω_p is the total plasma frequency and λ_L. From Ref. [35]

the FeSCs were disordered can be induced by proton irradiation [35], see Fig. 5.1.

The reported results shown in Fig. 5.1 from Ref. [35] were obtained using the linearized Eliashberg equations and the T-matrix approximation for the the average impurity self-energy. Furthermore the GL formulation of a dirty two-band s^{+-} superconductors although agree with the conclusion that disorder disfavors the s^{+-} state [93], is not able to predict the phase dependence of the London penetration depth and superfluid density. Here we point out that if one includes IBP and CBP within the Abrikosov-Gor'kov framework, then one has the necessary degrees of freedom to describe the phase change in the London penetration depth and superfluid density induced by disorder. Experimentally the signatures of $s^{+-} \rightarrow s^{++}$ were found in single crystals $Ba(Fe_{1-x}Rh_x)As_2$ [45, 112], Fig. 5.2.

Strikingly in Fig. 5.2a we observe a small enhancement of T_c with increasing disorder. This effect is similar to the transition from IDR to the CDR see Fig. 4.7. Therefore, it is possible that as disorder increases, the mean lifetime that the electrons stays in one band gets smaller favoring cross-band pairing. If disorder can trigger the transition from the IDR to the CDR then we know from the previous Chapter (see Fig. 4.5) that it is also possible in absence of the $s^{+-} \rightarrow s^{++}$ phase

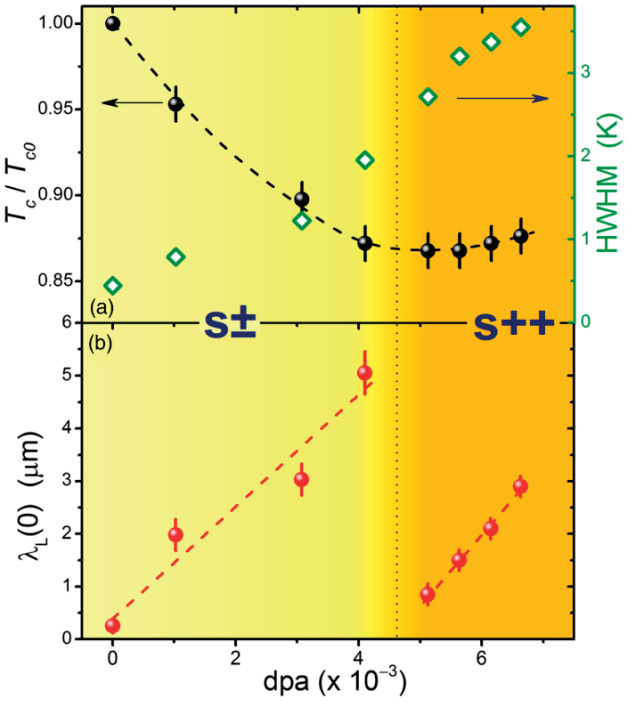

Figure 5.2: (a) Critical temperature of the irradiated crystal normalized to its value for the pristine crystal vs. disorder. (b) Low-temperature values of the London penetration depth. Here disorder is represented by the average displacement per atom dpa and the different background color are used to qualitatively distinguish between the s^{+-} and s^{++} phases. From Ref. [45]

transition. This would imply in a continuous decrease of the London penetration depth according to (5.36). Experiments in the thin film $Ba(Fe_{0.9}Co_{0.1})As_2$ [112], reported a tendency towards a gapless state for the weaker gap (in-gap) without discontinuity in the London penetration depth.

Disorder can drive the transition from the IDR to the CDR.

5.3 INTERFACE ENERGY

In this section we will calculate the surface energy E_S for the normal-superconductive interface at the thermodynamic critical field H_c. The interplay between the diamagnetic energy which is positive and the condensation energy which is negative will determine whether the superconductor is of type-I ($E_S > 0$) or type-II ($E_S < 0$).

Now, close to T_c and far from the normal-superconducting interface, we can neglect the variations of the order parameters as they become homogeneous in the bulk. The homogeneous order parameters are obtained from (5.25),

$$\Delta_{11}^{(0)} = \eta_a \tau^{1/2}, \quad \Delta_{22}^{(0)} = \eta_b \tau^{1/2}, \quad \Delta_{12}^{(0)} = \eta_c \tau^{1/2}. \tag{5.37}$$

From Fig. 2.4, we can see that the critical field equals the free energy when the order parameters are homogeneous. If we substitute (5.37) into (5.22) we can write the critical field as

$$\frac{H_c^2}{4\pi} = b_{11} + \eta_b^4 + 2\eta_c^4 b_{12}\left[1 + \frac{2}{\eta_c^2}(1 + \eta_b^2 + \eta_b \cos\theta)\right]. \tag{5.38}$$

When one considers the normal-superconductive interface in two-band superconductors without CBP, then it is possible to define the single-band penetration depth as $\lambda_{L,i}^{-2} = 4\pi e^2 |\Delta_{ii}^{(0)}|^2/(m_i c^2)$ [44]. Furthermore due to the additive property of the superfluid density relative to each band ($n_{total} = n_1 + n_2$, $n_i \propto 1/\lambda_{L,i}^{-2}$), then one can write the effective London penetration depth as $\lambda_L^{-2} = \lambda_{L,1}^{-2} + \lambda_{L,2}^{-2}$. However, we should have in mind that when one considers IBP and CBP in a two-band system, then the additive property of the band-dependent superfluid density is not longer valid. The presence of crosspairing, ($\Delta_{12} \neq 0$), introduces a new term in the total superfluid density which now must account not only for the density of Cooper pairs relative to band 1 and 2 but also for the density of cross-band Cooper pairs. This implies that we cannot extract the effective London penetration depth directly from Eq. (5.38). Nonetheless, in what follows we will analyze the normal-superconducting interface of the reconstructed GL equation where the London penetration depth will be given by Eq. (5.36).

We proceed by considering the interface between a normal state and a superconducting state defined by the plane $z = 0$, see Fig. 5.3,

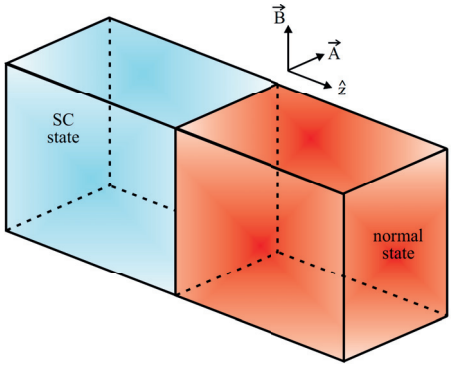

Figure 5.3: Schematic representation of the interface between the normal and the superconducting states. Figure extracted from Ref. [44]

In the above figure, Fig. 5.3, the external magnetic field is chosen to be the critical one along x-axis $H_x = H_x(z)$ with vector potential $A_y = -A(z)$, so $\vec{\nabla} \times \vec{A} = \vec{H}$. For systems with an external magnetic field is more convenient to work with the Gibbs free energy, then using

Eq. (2.76) we write the Gibbs energy G relative to the reconstructed GL equation (5.32),

$$G = \mathcal{K}|\vec{D}\psi(\vec{r})|^2 - \alpha\tau|\psi(\vec{r})|^2 + \frac{1}{2}\beta(\theta)|\psi(\vec{r})|^4 + \frac{(\vec{h}-\vec{H}_c)^2}{8\pi}. \quad (5.39)$$

We make the Gibbs energy (5.39) dimensionless by performing the following scaling in the variables,

$$\bar{G} = \frac{G}{\frac{H_c^2}{4\pi}}, \quad |\bar{\psi}|^2 = \frac{|\psi|^2}{\frac{\alpha\tau}{\beta(\theta)}}, \quad \bar{h} = \frac{\vec{h}}{\sqrt{2}H_c}, \quad s = \frac{z}{\lambda_L}, \quad (5.40)$$

where the coordinates where scaled in units of the London penetration depth λ_L.

We are interested in the spatial profile of the surface energy in the z-axis, then using Eq.(2.63), the above scaling (5.40) and integrating along the z-axis then the surface energy becomes

$$\gamma = \lambda \int ds \left[\frac{1}{2}\left|\left(\kappa^{-1}i\partial_s - \kappa\bar{A}\right)\bar{\psi}\right|^2 - |\bar{\psi}|^2 + \frac{1}{2}|\bar{\psi}|^4 + \left(\bar{h} - \frac{1}{\sqrt{2}}\right)^2\right], \quad (5.41)$$

where we used the expression of the critical field as function of the coherence length, $H_c = c/(2e\xi^2)$ and we have defined the coherence length and GL parameter as follows

$$\xi_{GL} = \sqrt{\frac{\mathcal{K}}{\alpha}}, \quad \kappa(\theta) = \frac{\lambda_L(\theta)}{\xi_{GL}}. \quad (5.42)$$

The angle dependence of the penetration depth $\lambda(\theta)$ and the GL parameter $\kappa = \kappa(\theta)$, implies that the classification of superconductors in type-I and type-II depends on the position $\vec{r}$. This means that depending on the value of $\theta = \theta(\vec{r})$, then one can can have type-I superconductivity, type-II superconductivity or both. See Fig 5.4.

One could be eager to conclude that even in presence of IBP and CBP the three-component Ginzburg-Landau equations are reduced to a single-component with only one GL parameter κ, see Eq. (5.42). However as we mentioned before, the reconstruction of the order parameter and the classification of superconductors in type I or type II is valid only when the phases are global. The assumption of $\theta = f(\varphi_{12}, \varphi_{11}, \varphi_{22})$ as an auxiliary variable is valid only for non dynamic variables which is the case for φ_{12} and φ_{22} but not for φ_{11}. This limits the validity of the reconstruction of the order parameter and the analysis of the surface energy to the homogeneous case, i.e. when all phases are constant.

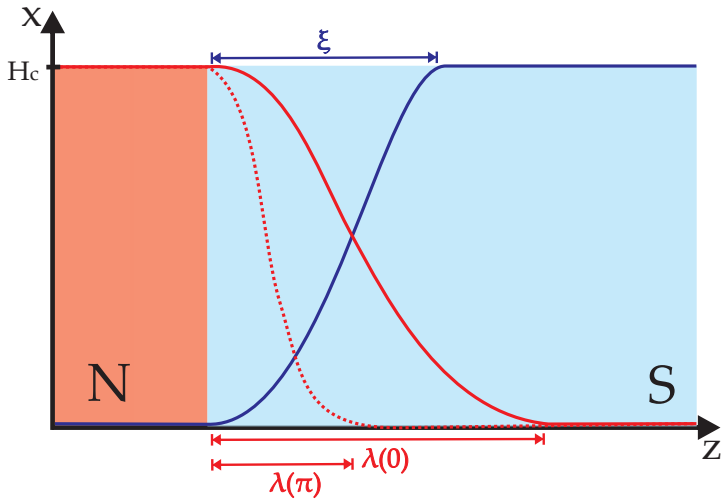

Figure 5.4: Hypothetical situation where the type-I/type-II classification dichotomy is present. The figure presents a transverse section along the xz-plane from the schematic representation 5.3. The spatial profile of the coherence length ξ is given by the solid blue line and the possible spatial profiles for the London penetration depth $\lambda(\theta)$ are given by the solid red line ($\theta = 0$) an the red dotted line ($\theta = \pi$).

It would be interesting to study the formation of Abrikosov vortices in presence of IBP and CBP using the three component GL equations (5.19-5.21). In the next Section, we will described the most pronounced features that signal the competition between intraband and cross-band Cooper pairs. Although not develop in this thesis would be interesting to study the inclusion of CBP in presence of other competitive orders such as the presence of charge-density waves or spin-density waves, which modify the periodic electronic structures of the solid [39], the presence of disorder in a two-gap superconductors which promotes the $s^{+-} \rightarrow s^{++}$ transition [35, 45].

5.4 VORTEX LATTICE

We start by writing the Gibbs free energy from Eq. (5.22) in dimensionless form,

$$\begin{aligned} F &= \frac{\vec{H}_c^2}{4\pi}\int dV\left[\frac{r_a^2}{2}|\vec{D}\Delta_{11}|^2 - r_a^2|\Delta_{11}|^2 + \frac{r_a^2}{2}|\Delta_{11}|^4 + 2r_a r_c|\Delta_{12}|^2|\Delta_{11}|^2 + \right. \\ &+ \frac{r_b^2}{2}|\vec{D}\Delta_{22}|^2 - r_b^2|\Delta_{22}|^2 + \frac{r_b^2}{2}|\Delta_{22}|^4 + 2r_b r_c|\Delta_{12}|^2|\Delta_{22}|^2 + \\ &+ r_c^2|\vec{D}\Delta_{12}|^2 - r_c^2 2|\Delta_{12}|^2 + r_c^2|\Delta_{12}|^4 + \sqrt{r_a r_b}r_c\Delta_{12}^2\Delta_{22}^*\Delta_{11}^* + \\ &+ \left.\sqrt{r_a r_b}r_c\Delta_{12}^{*2}\Delta_{22}\Delta_{11} + \kappa^2(\vec{h} - \vec{H}_0)^2, \right. \end{aligned} \tag{5.43}$$

here $H_c^2/(4\pi) = (a_{11}\tau)^2/b_{11}$, is the nominal critical field energy given by only Δ_{11}, see Eqs. (5.13-5.14). Each component Δ_{ij} is normalized with respect to $\sqrt{a_{ij}\tau/b_{ij}}$ where $r_a^2 = H_{c11}^2/H_c^2$, $r_b^2 = H_{c22}^2/H_c^2$ and $r_c^2 = H_{c12}^2/H_c^2$ are the relative ratios of the component-dependent critical field energies with respect to H_c^2. Furthermore $\vec{D} = \vec{\nabla}/i - \vec{A}$, $\vec{\nabla} \times \vec{A} = \vec{h}$, $\vec{H}_0$ is the applied magnetic field, κ is the GL parameter given by $\kappa = \lambda_L/\xi_{GL}$ where λ_L and ξ_{GL} are the London penetration depth and coherence length given by the presence of only Δ_{11}. Thus $\lambda_L = (c/e)\sqrt{b_{11}/8\pi\mathcal{K}_{11}a_{11}\tau}$ and $\xi_{GL} = \sqrt{\mathcal{K}_{11}/a_{11}}$. All distances are normalized by ξ_{GL} and the vector potential $\vec{A}$ by $c\hbar/(2e\xi_{GL})$. From the Gibbs free energy (5.43), we obtain the dimensionless GL equations

$$\left[r_a^2\bar{L}_{11} - 2r_a r_c|\Delta_{12}|^2 - \sqrt{r_a r_b}r_c\frac{\Delta_{12}^2\Delta_{22}^*}{\Delta_{11}}\right]\Delta_{11} = 0, \quad (5.44)$$

$$\left[r_b^2\bar{L}_{22} - 2r_b r_c|\Delta_{12}|^2 - \sqrt{r_a r_b}r_c\frac{\Delta_{12}^2\Delta_{11}^*}{\Delta_{22}}\right]\Delta_{22} = 0, \quad (5.45)$$

$$\left[r_c^2\bar{L}_{12} - r_c(r_a|\Delta_{11}|^2 + r_b|\Delta_{22}|^2) - \sqrt{r_a r_b}r_c\frac{\Delta_{11}\Delta_{22}\Delta_{12}^*}{\Delta_{12}}\right]\Delta_{12} = 0, \quad (5.46)$$

where $\bar{L}_{ij} = \vec{D}^2 + 1 - |\Delta_{ij}|^2$ is the dimensionless GL operator. The coefficients r_a, r_b and r_c will be the tuning parameters that control the crossover between the IDR and the CDR.

At this point we introduce the method of link variables to solve the system (5.44-5.46) in 2D. We apply the method as described in Ref. [87] and employ periodic boundary conditions. This method is based on the lattice gauge theory where the broken $U(1)$ symmetry is restored by the introduction of link variables. In addition we will insert a time relaxation term that will help us to determine the most adequate iteration step. The details of this method and its implementation for our system are given in the Appx. C.2. We note that Eq.s (5.44-5.46) are similar to equations (4.7) in the sense that we expect competition between the intraband components (Δ_{11}, Δ_{22}) and the cross-band component (Δ_{12}). Therefore we expect three non-trivial solutions: (a) only intraband components different than zero ($\Delta_{11} \neq 0$, $\Delta_{22} \neq 0$, $\Delta_{12} = 0$), (b) only crosspairing component different than zero ($\Delta_{11} = \Delta_{22} = 0$, $\Delta_{12} \neq 0$) and (c) all three components different than zero ($\Delta_{11} \neq 0$, $\Delta_{22} \neq 0$, $\Delta_{12} \neq 0$). For any case, we will assume that we have obtained a solution if after two consecutive iterations the maximum deviation of each component is lower than 10^{-7} ($\delta\Delta_{ij} < 10^{-7}$).

The figure on the right presents the scaled colorbars of the Cooper-pair density (a) and the phase of the GL component (b). All solutions presented in this thesis will follow the same scale. Therefore, blue and red will rep-

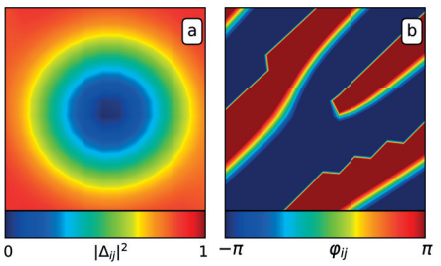

resent 0 and 1 for the minimum and maximum Cooper-pair density. It will also represent the phase change from $-\pi$ to π.

To elucidate better the interplay between the intraband and cross-band GL components we first calculate the solution for two identical overlapping bands. This means that the intraband and cross-band Cooper pairs are energetically equally favorable so in the free energy (5.43) the coefficients are $r_a = r_b = r_c = 1$. For this case, our system of three equation is reduced to only two, (5.44) and (5.46), which we solve by taking as initial condition, $\Delta_{11} = \Delta_{12} = 1$.

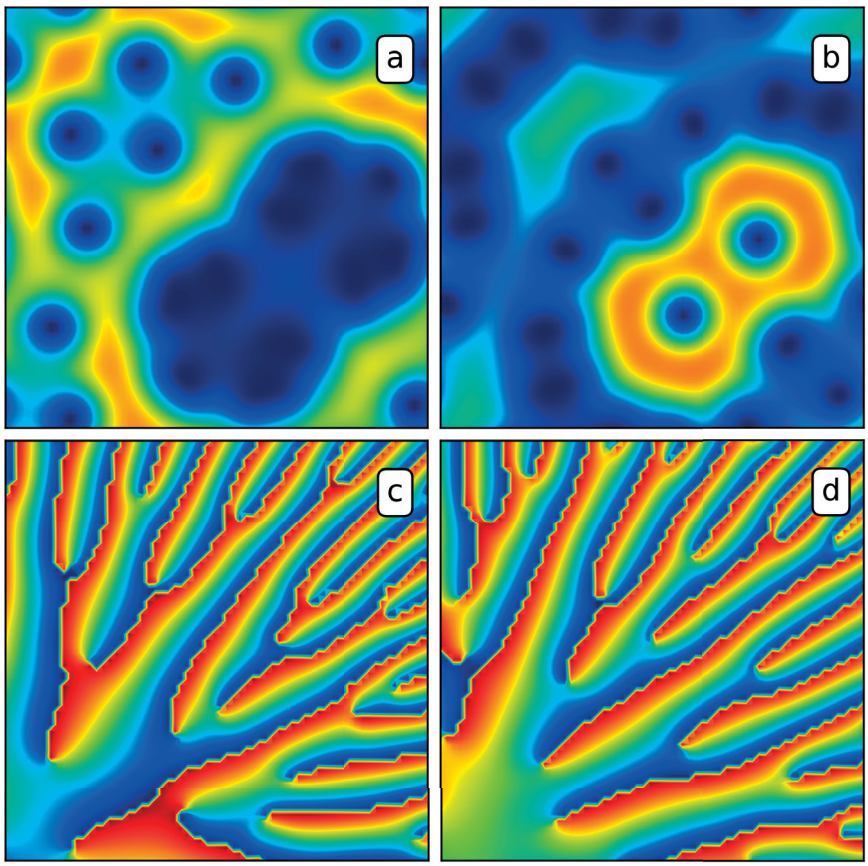

Figure 5.5: Superconducting square of lateral side 20ξ in a homogeneous magnetic field equal to $0.31H_c$. (a), (b) are the Cooper-pair density for the intraband $|\Delta_{11}|^2$ and cross-band $|\Delta_{12}|^2$ components respectively. Below each Cooper pair density we have their respective phases φ_{11}(c) and φ_{12} (d).

The competitive behavior between the intraband and cross-band GL components for a superconductor is depicted in Fig. 5.5. Interestingly we observe a tendency that whenever Δ_{11} is maximum, Δ_{12} is minimum and vice versa. This indicates a strong competitive interplay between the intraband and cross-band GL components. Note that in Fig. 5.5a we have the formation of a vortex cluster given by the big

blue region. In Fig. 5.5b we observe the formation of string of vortices that surround two vortices in the bottom right region. The vortex arrangements on Figs. 5.5(a,b) which are different from the Abrikosov lattice (triangular lattice), signal the presence of crosspairing. In case a similar simulation is done for $r_a > r_c$ and for $r_c > r_a$ we recover the Abrikosov lattice for the IDR and CDR respectively.

Although the above solution, Fig. 5.5 was obtained only for the case that IBP and CBP are both energetically equally favorable ($r_a = r_c$), the domain of coexistent with non trivial solutions can be enlarged. This can be achieved by considering a more realistic scenario where the two bands in consideration do not longer overlap, see Fig. 5.6.

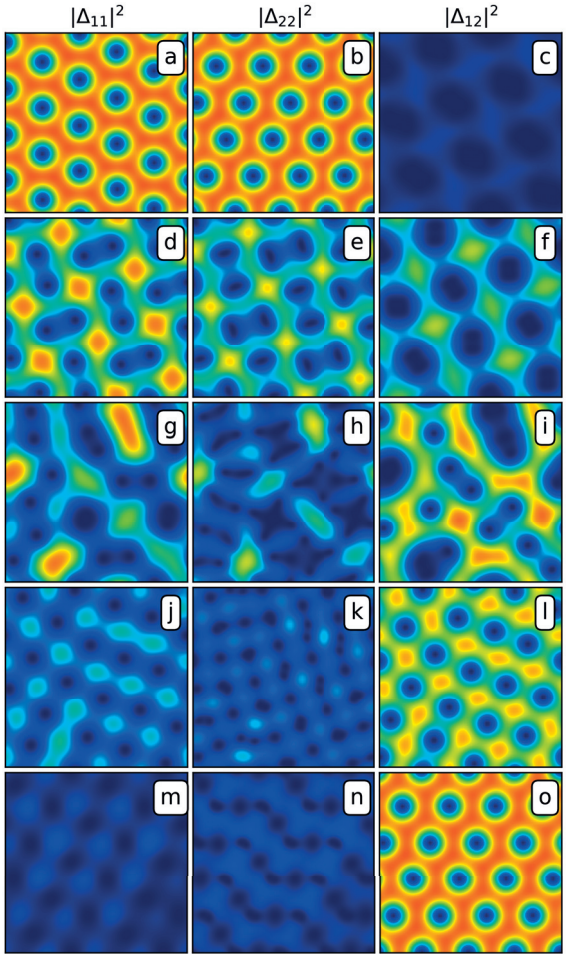

Figure 5.6: All solutions correspond to a superconducting square of lateral side 20ξ in a homogeneous magnetic field equal to $0.31\vec{H}_c$. For each row we fixed the normalization coefficients $\{r_a, r_b, r_c\}$: (a-c) $\{1, 0.43, 0.75\}$; (d-f) $\{1, 0.42, 0.75\}$; (g-i) $\{1, 0.3, 0.75\}$; (j-l) $\{1, 0.2, 0.75\}$; (m-o) $\{0.9, 0.1, 0.75\}$.

In Fig. 5.6, we present solutions for five different set of parameters $\{r_a, r_b, r_c\}$ with initial condition $\Delta_{11} = \Delta_{22} = \Delta_{12} = 1$. Those solutions

(intermediate states), describe a transition from the IDR to the CDR and were obtained by reducing the parameter r_b or r_a. Across the simulations we assumed that the following condition, $r_b < r_c < r_a$ holds. The intermediate states are characterized by the deformation of the Abrikosov lattice, in the form of a square lattice (Fig. 5.6(f,j,l)), elongated vortices (Fig. 5.6(e,f,l)), stripes (Fig. 5.6(g,i,k)) or clusters of vortices (Fig. 5.6(g,h,i)). The reestablishment of the Abrikosov lattice for the IDR or CDR is accompanied by the vanishment of Δ_{12} or $\{\Delta_{11}, \Delta_{22}\}$ respectively.

Usually the melting of the Abrikosov lattice is an indicative of a first order transition [62, 110, 111, 140]. In our case the free energy presents clear discontinuities when one approaches the crossover region as shown in Fig. 5.7.

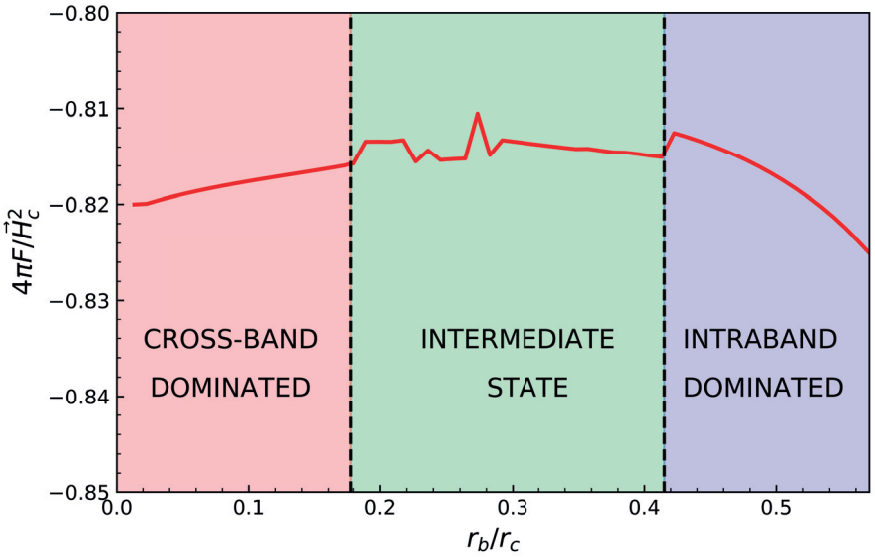

Figure 5.7: Normalized free energy vs ratio r_b/r_c where $ra = 1$. A first order transition is clearly observed at the the boundaries of the intermediate state with the CDR for $r_b/r_c = 0.178$ and with the IDR for $r_b/r_c = 0.418$.

Fig. 5.7 describes a first order transition which is accompanied by the melting of the Abrikosov lattice as follows from Fig. 5.6. Interestingly at the intermediate state we have other consecutive first order transitions which reveals a multi-phase nature of the superconducting state in presence of IBP and CBP.

Vortex configurations different from the triangular lattice has been reported in MgB_2 single crystals [27], superconducting/ferromagnetic hybrids [29], $BaFe_{2-x}Ni_xAs_2$ at low field [72], the order-disorder transition in $NbSe_2$ and the Turing like patterns as reported in $EuFe_2(As_{0.79}P_{0.21})_2$ [121]. In these materials, the origin of different vortex patterns is attributed to the competition between short-range repulsive and long-range attractive vortex-vortex interactions. Typically systems with

nonmonotonic repulsive-attractive interaction leads to the vortex core deformation which induce frustration and consequently the deformation of the Abriksov lattice [143]. For all practical cases the simulations and descriptions of unusual vortex configurations are only possible in presence of different lengths scales which is a fundamental premise of any multicomponent GL theory.

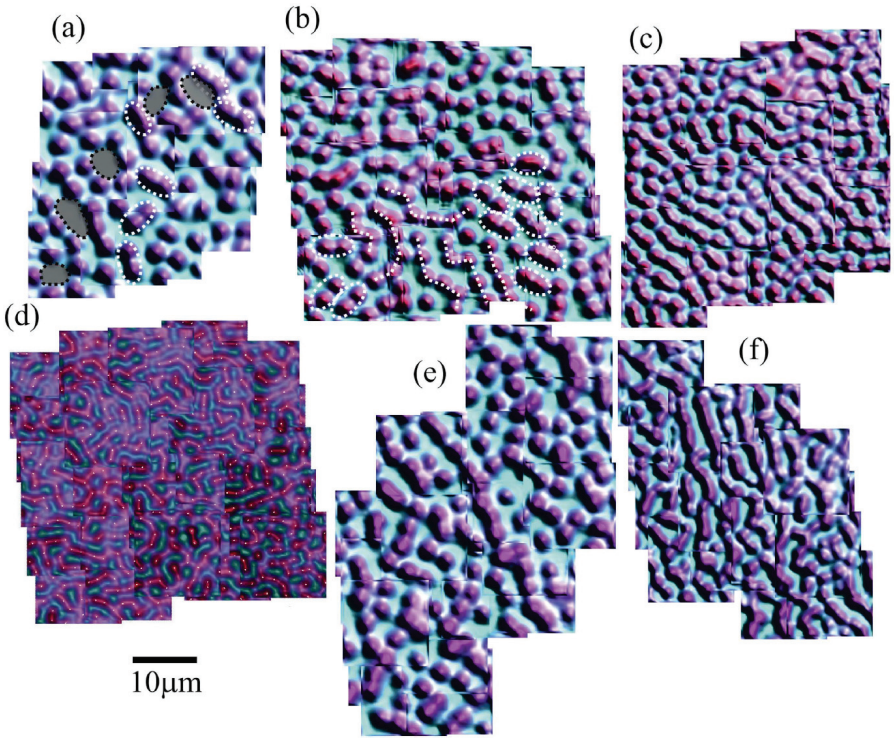

Figure 5.8: Scanning Hall probe images ($\approx 50 \times 50\ \mu m^2$) of the vortex distribution in a 160 nm thick superconducting MgB_2 film at T= 1.7 K and fields of (a) 1.25 G, (b) 1.7 G, (c) 2.8 G and (d) 5 G, and a 77 nm film at (e) 1.25 G and (f) 2.8 G. Typical examples of dimers and voids are indicated in (a), short chains in (b) while vortex locations in (d) are highlighted with white dots. From Ref. [27].

In this Chapter we have microscopically derived the GL equations using the Gor'kov approach for a two-band superconductor in presence of both IBP and CBP. In systems without crosspairing the reconstruction of the GL order parameter prohibits the definition of different length scales besides one London penetration depth and one coherence length. Remarkably the situation changes when one includes crosspairing due to mixing of the different components and its phase-dependent interaction. The reconstructive procedure for this case fails to globally lock all the phases of the different GL components. As a consequence one has a phase-dependent penetration depth $\lambda(\theta)$ which challenges the conventional classification of superconductors in type I or type II. This means that the long range order of the superconducting state cannot be described by the phase of a single component and one

needs to introduce other components. Moreover, we showed that a two-band system in presence of IBP and CBP is minimally described by a three-component GL theory. In this case, the smoking gun signatures of the interplay between superconductivity and magnetism are the intermediate states characterized by the deformation of the Abrikosov lattice in form of new patterns like, square lattices, stripes, labyrinths and vortex clusters.

6

CONCLUSIONS AND PERSPECTIVES

Emergent phenomena in multigap superconductors or multicomponent Ginzburg-Landau theories are defined as the new phenomena which cannot be attainable by a superconductor with a single gap or a single component. In this thesis we have studied the emergent phenomena in superconductors with multiple gaps and multicomponent Ginzburg-Landau theories in presence of intraband pairing and cross-band pairing. By cross-band pairing or simply crosspairing we refer to a Cooper pair formed by two electrons where each electron belongs to a different band. To distinguish the novel signatures and consequences of superconductors in presence of these two types of pairing, we have divided the conclusions in two parts:

Without crosspairing

A multigap superconductor or a multicomponent Ginzburg-Landau theory with zero interband coupling and without crosspairing presents no new phenomena besides the ones described by the conventionals BCS and Ginzburg-Landau theories. This is a natural conclusion because when different regions of a physical system do not interact with its surroundings, then each region becomes and independent system by itself. However, multigap superconductors with small interband coupling (scattering of electrons between different bands) present oscillations in the relative phase (Legget modes) and amplitude (Higgs modes) of the order parameters. Interestingly, in this thesis we have found that this effect is more pronounced at weak interband coupling. For example, in a two-band system when the interband coupling is positive the phase of both order parameters has the same sign. This defines an s^{++} phase, however when the interband coupling is negative, then we have a change of sign in one of the order parameters which defines an s^{+-} phase. As a consequence we have that the gap resonances accompanied by Legget and Higgs modes are more pronounced at the $s^{+-} \leftrightarrow s^{++}$ transition. On the other hand we have found that the Gor'kov derivation of the Ginzburg-Landau equations for multigap superconductors do not incorporate the Josephson couplings between the different components. Therefore effectively we have only one coherence length whose value is just renormalized by taking into account the contribution of all different bands. Hence, a multi-component Ginzburg-Landau theory with only intraband pairing can always be described by the conventional single-component Ginzburg-Landau equation.

With crosspairing

When one introduces crosspairing, even systems with zero interband coupling can present gap resonances accompanied with Leggett and Higgs modes. This occurs because cross-band pairing introduces phase interaction between the intraband pair amplitudes and the cross-band pair amplitude. In this thesis we have shown that in presence of crosspairing the energy spectra of the electrons, the gap openings in the density of states and the London penetration depth are phase-dependent. At the microscopic level, the interplay between intraband pairing and cross-band pairing have several unique effects. For one, cross-band pairing increases the splitting between intraband gaps, with a tendency to decrease the weaker gap towards an entirely novel "gapless" state. The signatures of this state will still be observable in measured quantities as the order parameters of the superconducting state, no longer directly correspond to the observable gaps. The crosspairing also introduces the possibility of a phase frustration between the pairing channels, leading to novel transitions as a function of temperature (such as $s^{+-} \to s^{++}$), and nontrivial response of the superconductor to an external magnetic field.

In this thesis we found that multicomponent Ginzburg-Landau theories within the Gor'kov domain (expansion of the order parameter up to $(1 - T/T_c)^{3/2}$) are only present when one considers intraband pairing and cross-band pairing simultaneously. The equation for T_c in this case also restricts the introduction of Josephson couplings between the different Ginzburg-Landau components, nonetheless the different order parameters remain coupled due to the induced hybridization by crosspairing. In this scenario, we have shown that a two-band system with intraband pairing and cross-band pairing is minimally described by a three-component Ginzburg-Landau theory. Interestingly the interplay of those components present an intrinsic competition similarly to the one found between intraband and cross-band Cooper-pair amplitudes. Moreover, we have obtained in this thesis new effects in presence of a constant magnetic field, where the competition between the different components drives effectively a nonmonotonic repulsive-attractive interaction among vortices which leads to the deformation of the Abrikosov lattice. This deformation presents itself as a first order transition at the boundaries of the intermediate state with the intraband dominated regime and cross-band dominated regime. The intermediate state presents multiple phases where the vortices arrange in different configurations like the square lattice, higher-flux vortices, elongated vortices, stripes, labyrinths and clusters. Therefore the new derivation of the Ginzburg-Landau theory with the inclusion of crosspairing introduces an exciting new venue where its signatures can experimentally be tested.

Perspectives

Our results call for revisiting the existing theories and experimental data for multiband superconductors with close bands or hybridized orbitals, bearing also in mind that the band dispersions and chemical potential can be tuned towards a parameter regime where the above mentioned signatures of crosspairing with and without an applied magnetic field can be detected. Remarkably, the signatures of crosspairing resemble the effects of magnetic impurity doping, applied magnetic field and disorder induced transitions which suggests that the presence of crosspairing in superconductors is more general that we initially thought. For example, the presence of magnetic impurities in MgB_2 induced by Mn substitution present a pronounced coherence peak in the density of states similarly to the gapless state tendency of the weaker gap. This signature in the density of states can also overlap with the long searched Majorana zero-energy bound states. Furthermore would be interesting to examine the competition between intraband pairing and crosspairing competition in the presence of spin-flip scattering, oddness in parity, and photo-induced phenomena. Also, the theoretical formulation of the two-gap GL theory in the dirty limit with nematicity looks very similar to the GL theory in presence of both intraband pairing and crosspairing and present the same vortex configuration (elongated vortices). Therefore, further investigation should be directed towards the origin of the elongated vortex formation in the FeSCs which can be an indicative of a nematic order, crosspairing or both. Even beyond superconductivity, crosspairing and its competition with intraband pairing remains insufficiently explored in molecular optics, multicomponent superfluidity, and quantum chromodynamics.

Part III

APPENDIX

A

ANOMALOUS AND NORMAL GREEN FUNCTIONS

This Appendix is divided in two Sections. The first one presents the derivation of the pair amplitude equations from the anomalous Green function. The second Section contains a detailed derivation of the spectral wave function and density of states from the normal Green function. For both Sections we use the Gor'kov Green function formalism.

A.1 NAMBU-GORKOV APPROACH FOR N-MULTIBAND HAMILTONIAN WITH CROSSPAIRING

In the Heisenberg picture of quantum mechanics the equations of motion of the Hamiltonian (4.3) are given by

$$-\hbar\partial_\tau \psi_{i\uparrow}\left(\vec{x}\tau\right) = T_i \psi_{i\uparrow}\left(\vec{x}\tau\right) + \sum_j \psi^\dagger_{j\downarrow}\left(\vec{x}\tau\right)\Delta_{ij}\left(\vec{x}\right), \tag{A.1}$$

$$-\hbar\partial_\tau \psi^\dagger_{i\downarrow}\left(\vec{x}\tau\right) = -T^*_i \bar{\psi}_{i\downarrow}\left(\vec{x}\tau\right) + \sum_i \Delta^*_{ij}\left(\vec{x}\right)\psi_{j\uparrow}\left(\vec{x}\tau\right). \tag{A.2}$$

Now we introduce the normal and anomalous Green functions:

$$G_{ij}\left(\vec{x}\tau,\vec{x}'\tau'\right) = -\frac{1}{\hbar}\left\langle T\psi_{i\uparrow}\left(\vec{x}\tau\right)\psi^\dagger_{j\uparrow}\left(\vec{x}'\tau'\right)\right\rangle, \tag{A.3}$$

$$\overline{F}_{ij}\left(\vec{x}\tau,\vec{x}'\tau'\right) = -\frac{1}{\hbar}\left\langle T\psi^\dagger_{i\downarrow}\left(\vec{x}\tau\right)\psi^\dagger_{j\uparrow}\left(\vec{x}'\tau'\right)\right\rangle, \tag{A.4}$$

$$\overline{G}_{ij}\left(\vec{x}\tau,\vec{x}'\tau'\right) = -\frac{1}{\hbar}\left\langle T\psi^\dagger_{i\downarrow}\left(\vec{x}\tau\right)\psi_{j\downarrow}\left(\vec{x}'\tau'\right)\right\rangle, \tag{A.5}$$

$$F_{ij}\left(\vec{x}\tau,\vec{x}'\tau'\right) = -\frac{1}{\hbar}\left\langle T\psi_{i\uparrow}\left(\vec{x}\tau\right)\psi_{j\downarrow}\left(\vec{x}'\tau'\right)\right\rangle, \tag{A.6}$$

using the Fourier transform of the periodic time τ:

$$\mathcal{O}_{nm}\left(\vec{x}\tau,\vec{x}'\tau'\right) = \frac{1}{\beta\hbar}\sum_\omega e^{-i\omega(\tau-\tau')}\mathcal{O}_{nm,\omega}\left(\vec{x},\vec{x}'\right), \tag{A.7}$$

with the equations of motion (A.1) and (A.2), then we can write the evolution of the Green functions as follows:

$$i\hbar\omega G_{ij,\omega} = \delta_{ij} + T_i G_{ij,\omega} + \sum_k \Delta_{ik}\overline{F}_{kj,\omega} \tag{A.8}$$

$$i\hbar\omega \overline{F}_{ij} = -T_i^* \overline{F}_{ij,\omega} + \sum_k \Delta_{ik}^* G_{kj}, \tag{A.9}$$

$$i\hbar\omega \overline{G}_{ij,\omega} = \delta_{ij} - T_i^* G_{ij,\omega} + \sum_k \Delta_{ik}^* \overline{F}_{kj}, \tag{A.10}$$

$$i\hbar\omega F_{ij,\omega} = T_i F_{ij,\omega} + \sum_k \Delta_{ik}\overline{G}_{kj,\omega}. \tag{A.11}$$

Assuming spatial isotropy, we introduce the Fourier transform of the spatial coordinates:

$$\mathcal{O}_{nm,\omega}\left(\vec{x},\vec{x}'\right) = \mathcal{O}_{nm,\omega}\left(\vec{x}-\vec{x}'\right), \tag{A.12}$$

$$\mathcal{O}_{nm,\omega}\left(\vec{k}\right) = \int d^3\vec{x} e^{-i\vec{k}.(\vec{x}-\vec{x}')}\mathcal{O}_{nm,\omega}\left(\vec{x}-\vec{x}'\right). \tag{A.13}$$

Now, for a N-band superconductor we introduce the kinetic and pair amplitude matrices:

$$T = \begin{pmatrix} \xi_{1k} & 0 & 0 \\ 0 & \xi_{2k} & 0 \\ 0 & 0 & \dots \end{pmatrix}, \quad \Delta = \begin{pmatrix} \Delta_{11} & \Delta_{12} & 0 \\ \Delta_{21} & \Delta_{22} & 0 \\ 0 & 0 & \dots \end{pmatrix}, \tag{A.14}$$

and the matrices for the normal and anomalous Green functions

$$G_\omega = \begin{pmatrix} G_{11,\omega} & G_{12,\omega} & \dots \\ G_{21,\omega} & G_{22,\omega} & \dots \\ \dots & \dots & \dots \end{pmatrix}, \quad F_\omega = \begin{pmatrix} F_{11,\omega} & F_{12,\omega} & 0 \\ F_{21,\omega} & F_{22,\omega} & 0 \\ 0 & 0 & \dots \end{pmatrix}. \tag{A.15}$$

Using the above matrices and assuming crossband pair formation every two bands (i.e. between band 1 and 2, between band 3 and 4, and so on), we obtain the Nambu-Gorkov equations for N-band system:

$$\left(i\hbar\omega - \xi_k\right) G_\omega = 1_{N\times N} + \Delta\overline{F}_\omega, \tag{A.16}$$

$$\left(i\hbar\omega + \xi_k\right) \overline{F}_\omega = \Delta^* G_\omega \tag{A.17}$$

$$\left(i\hbar\omega + \xi_k\right) \overline{G}_\omega = 1_{N\times N} + \Delta^* F_\omega \tag{A.18}$$

$$\left(i\hbar\omega - \xi_k\right) F_\omega = \Delta\overline{G}_\omega. \tag{A.19}$$

From Eqs. (A.18) and (A.19), we obtain the anomalous Green function F_ω,

$$F_\omega = \left[\left(i\hbar\omega + \xi_k\right)\Delta^{-1}\left(i\hbar\omega - \xi_k\right) - \Delta^*\right]^{-1}, \tag{A.20}$$

after tedious but straightforward algebraic calculations we obtain F_ω:

$$F_\omega = \bar{F}_{ij\omega} \otimes \bar{F}_{kl\omega} \otimes ... \otimes \bar{F}_{pq\omega}, \tag{A.21}$$

where the number of times we make the tensorial product is the greatest integer of $N/2$. $\bar{F}_{ij\omega}$ is given by

$$\bar{F}_{ij\omega} = \begin{pmatrix} -\frac{\Delta_{ii}\left(\hbar^2\omega^2+\xi_2^2\right)+D\Delta_{jj}^*}{\left(\hbar^2\omega^2+E_+^2\right)\left(\hbar^2\omega^2+E_-^2\right)} & \frac{\left[\Delta_{ij}(i\hbar\omega+\xi_i)\left(i\hbar\omega-\xi_j\right)+D\Delta_{ij}^*\right]}{\left(\hbar^2\omega^2+E_+^2\right)\left(\hbar^2\omega^2+E_-^2\right)} \\ \frac{\left[\Delta_{ji}(i\hbar\omega-\xi_i)\left(i\hbar\omega+\xi_j\right)+D\Delta_{ji}^*\right]}{\left(\hbar^2\omega^2+E_+^2\right)\left(\hbar^2\omega^2+E_-^2\right)} & -\frac{\left[\Delta_{jj}\left(\hbar^2\omega^2+\xi_i^2\right)+D\Delta_{ii}^*\right]}{\left(\hbar^2\omega^2+E_+^2\right)\left(\hbar^2\omega^2+E_-^2\right)} \end{pmatrix}, \tag{A.22}$$

where the excitation spectra $E_\pm$ is given by

$$E_\pm = \sqrt{\frac{1}{2}\left(\varepsilon_i^2+\varepsilon_j^2+2\left|\Delta_{ij}\right|^2 \pm b\right)}, \tag{A.23}$$

$$b = \sqrt{\left(\varepsilon_i^2-\varepsilon_j^2\right)^2+4\left|\Delta_{ij}\right|^2 c}, \tag{A.24}$$

$$c = \left(\xi_i-\xi_j\right)^2+\left|\Delta_{ii}\right|^2+\left|\Delta_{jj}\right|^2+2\left|\Delta_{ii}\right|\left|\Delta_{jj}\right| cos\theta, \tag{A.25}$$

where

$\xi_i = \frac{k^2}{2m} - \mu + c_i$ spectra of a free electron

$\varepsilon_i^2 = \xi_i^2 + \left|\Delta_{ii}\right|^2$ BCS spectra without crosspairing

$\theta = 2\varphi_{ij} - \varphi_{ii} - \varphi_{jj}$ phase dependence of the excitation gaps.

The pair amplitude definition is obtained as follows,

$$\Delta_{ij} = -T\sum_{kl} g_{ij,kl} \sum_\omega e^{i\omega 0^+} \int \frac{d^3\overrightarrow{k}}{(2\pi)^3} F_{kl,\omega}\left(\overrightarrow{k}\right). \tag{A.26}$$

Finally summing (A.26) over Matsubara's frequencies we obtain the pair amplitude equations:

$$\Delta_{ij} = \sum_{kl} g_{ij,kl} I_{kl}, \tag{A.27}$$

$$I_{kl} = \int \frac{d^3\overrightarrow{k}}{(2\pi)^3}\Delta_{kl}\left[f_{kl}^+\frac{tanh\left(\frac{\beta E_+}{2}\right)}{4E_+}+f_{kl}^-\frac{tanh\left(\frac{\beta E_-}{2}\right)}{4E_-}\right]. \tag{A.28}$$

where

$f_{kk}^\pm = 1 \pm \frac{p}{b}$ with k as the index of any band

$f_{ll}^\pm = 1 \pm \frac{q}{b}$ with l as the index consecutive to k

$f_{kl}^\pm = 1 \pm \frac{r}{b}$ with kl as the index of the crosspairing

$p = \varepsilon_k^2 - \varepsilon_l^2 + 2\left|\Delta_{kl}\right|^2\left(1+\frac{|\Delta_{ll}|}{|\Delta_{kk}|}e^{i\theta}\right)$

$q = \varepsilon_l^2 - \varepsilon_k^2 + 2\left|\Delta_{kl}\right|^2\left(1+\frac{|\Delta_{kk}|}{|\Delta_{ll}|}e^{i\theta}\right)$

$r = \left(\xi_k-\xi_l\right)^2+\left|\Delta_{kk}\right|^2+\left|\Delta_{ll}\right|^2+2\left|\Delta_{kk}\right|\left|\Delta_{ll}\right|e^{-i\theta}$

If the number of bands is two, the scattering elements $\bar{g}_{ij,mn}$ is given by the following matrix:

$$\bar{g}_{ij,nm} = \begin{pmatrix} g_{11,11} & g_{11,22} & g_{11,12} \\ g_{22,11} & g_{22,22} & g_{22,12} \\ g_{12,11} & g_{12,22} & g_{12,12} \end{pmatrix}, \tag{A.29}$$

where the pair amplitudes are given by

$$\Delta_{ij} = \begin{pmatrix} \Delta_{11} & \Delta_{12} \\ \Delta_{21} & \Delta_{22} \end{pmatrix}, \tag{A.30}$$

Now under the assumption that we have crosspairing every two bands, the Gor'kov couplings scale with the tensor product $g_{ij,rs} = \bar{g}_{ij,kl} \otimes \bar{g}_{pq,rs}$. For example, for $N = 4$:

$$g_{ij,nm} = \begin{pmatrix} g_{11,11} & g_{11,22} & g_{11,12} & g_{11,33} & g_{11,44} & g_{11,34} \\ g_{22,11} & g_{22,22} & g_{22,12} & g_{22,33} & g_{22,44} & g_{22,34} \\ g_{12,11} & g_{12,22} & g_{12,12} & g_{12,33} & g_{12,44} & g_{12,34} \\ g_{33,11} & g_{33,22} & g_{33,12} & g_{33,33} & g_{33,44} & g_{33,34} \\ g_{44,11} & g_{44,22} & g_{44,12} & g_{44,33} & g_{44,44} & g_{44,34} \\ g_{34,11} & g_{34,22} & g_{34,12} & g_{34,33} & g_{34,44} & g_{34,34} \end{pmatrix}, \tag{A.31}$$

where we neglected the couplings $g_{13,13} = g_{14,14} = g_{23,23} = g_{24,24} = 0$. This implies that the pair amplitude matrix for $N = 4$ is given by diagonal blocks:

$$\Delta_{ij} = \begin{pmatrix} \Delta_{11} & \Delta_{12} & 0 & 0 \\ \Delta_{21} & \Delta_{22} & 0 & 0 \\ 0 & 0 & \Delta_{33} & \Delta_{34} \\ 0 & 0 & \Delta_{43} & \Delta_{44} \end{pmatrix}, \tag{A.32}$$

which consistently have $\Delta_{13} = \Delta_{14} = \Delta_{23} = \Delta_{24} = 0$ which is the our assumption of crosspairing every two bands.

For the case of N odd, we proceed similarly to the case with N even and add one column and one row to the Gor'kov couplings and pair amplitudes matrices.

A.2 DERIVATION OF THE NORMAL GREEN FUNCTION

Similarly to the derivation of the pair amplitude equations, we can obtained from Eqs. (A.16) and (A.17) an expression for G_ω:

$$G_\omega = [(i\hbar\omega - \xi_k) - \Delta(i\hbar\omega + \xi_k)^{-1}\Delta^*]^{-1} \tag{A.33}$$

after tedious but straightforward algebraic calculations we obtain G_ω:

$$G_\omega = \bar{G}_{ij\omega} \otimes \bar{G}_{kl\omega} \otimes ... \otimes \bar{G}_{pq\omega}, \tag{A.34}$$

where the number of times we make the tensorial product is the greatest integer of $N/2$ times. $\bar{G}_{ij\omega}$ is given by

$$\bar{G}_{ij\omega} = \frac{(i\hbar\omega + \xi_2)(i\hbar\omega + \xi_1)}{(\hbar^2\omega^2 + E_+^2)(\hbar^2\omega^2 + E_-^2)} \times \tag{A.35}$$
$$\times \begin{pmatrix} i\hbar\omega - \xi_2 - \frac{|\Delta_{12}|^2}{i\hbar\omega+\xi_1} - \frac{|\Delta_{22}|^2}{i\hbar\omega+\xi_2} & \frac{\Delta_{11}\Delta_{12}^*}{i\hbar\omega+\xi_1} + \frac{\Delta_{12}\Delta_{22}^*}{i\hbar\omega+\xi_2} \\ \frac{\Delta_{12}\Delta_{11}^*}{i\hbar\omega+\xi_1} + \frac{\Delta_{22}\Delta_{12}^*}{i\hbar\omega+\xi_2} & i\hbar\omega - \xi_1 - \frac{|\Delta_{11}|^2}{i\hbar\omega+\xi_1} - \frac{|\Delta_{12}|^2}{i\hbar\omega+\xi_2} \end{pmatrix},$$

We observe that the elements the above matrix (A.36) are symmetric under the exchange of the band index $1 \leftrightarrow 2$.

Now we calculate the spectral function $S_{ij\omega}(\vec{k})$,

$$S_{ij\omega}(\vec{k}) = -\frac{1}{\pi}\Im\bar{G}_{ij\omega}(\vec{k})(i\omega \to \omega + i\epsilon), \quad \epsilon = 0^+. \tag{A.36}$$

The denominator of the normal Green function (A.36) can be expanded as follows ($\hbar = 1$),

$$\frac{1}{(\omega^2 + E_+)(\omega^2 + E_-)} = \frac{1}{b}\Big(- \frac{1}{2E_+}\frac{1}{i\omega + E_+} - \frac{1}{2E_+}\frac{1}{i\omega + E_+} + \tag{A.37}$$
$$+ \frac{1}{2E_-}\frac{1}{i\omega + E_-} + \frac{1}{2E_-}\frac{1}{-i\omega + E_-}\Big)$$

taking the limit $i\omega \to \omega + i\epsilon$, $\epsilon = 0^+$ and using the relation

$$\frac{1}{x \pm i\epsilon} = P(\frac{1}{x \pm \epsilon}) \mp i\pi\delta(x), \tag{A.38}$$

we obtain

$$\begin{aligned} S_{11\omega}(\vec{k}) = &\left[\frac{1}{2}\left(1 - \frac{\xi_1}{E_+}\right)\frac{E_+^2 - \varepsilon_2^2}{b} - \frac{1}{2}\left(1 - \frac{\xi_2}{E_+}\right)\frac{|\Delta_{12}|^2}{b}\right]\delta(E_+ + \omega) + \\ &+ \left[\frac{1}{2}\left(1 + \frac{\xi_1}{E_+}\right)\frac{E_+^2 - \varepsilon_2^2}{b} - \frac{1}{2}\left(1 + \frac{\xi_2}{E_+}\right)\frac{|\Delta_{12}|^2}{b}\right]\delta(E_+ - \omega) + \\ &+ \left[\frac{1}{2}\left(1 - \frac{\xi_1}{E_-}\right)\frac{\varepsilon_2^2 - E_-^2}{b} + \frac{1}{2}\left(1 - \frac{\xi_2}{E_+}\right)\frac{|\Delta_{12}|^2}{b}\right]\delta(E_- + \omega) + \\ &+ \left[\frac{1}{2}\left(1 + \frac{\xi_1}{E_-}\right)\frac{\varepsilon_2^2 - E_-^2}{b} + \frac{1}{2}\left(1 + \frac{\xi_2}{E_-}\right)\frac{|\Delta_{12}|^2}{b}\right]\delta(E_- - \omega), \end{aligned}$$

where we have neglected all the principle values because they do not contribute to the imaginary part.

Analogously we can obtain the spectral wave function for $S_{12\omega}(\vec{k})$,

$$\begin{aligned}
S_{12\omega}(\vec{k}) = &\left[\frac{1}{2}\left(1-\frac{\xi_2}{E_+}\right)\frac{|\Delta_{11}||\Delta_{12}|}{b}\cos(\varphi_{11}-\varphi_{12})+\right.\\
&\left.+\frac{1}{2}\left(1-\frac{\xi_1}{E_+}\right)\frac{|\Delta_{22}||\Delta_{12}|}{b}\cos(\varphi_{12}-\varphi_{22})\right]\delta(\omega+E_+)+\\
&+\left[\frac{1}{2}\left(1+\frac{\xi_2}{E_+}\right)\frac{|\Delta_{11}||\Delta_{12}|}{b}\cos(\varphi_{11}-\varphi_{12})+\right.\\
&\left.+\frac{1}{2}\left(1+\frac{\xi_1}{E_+}\right)\frac{|\Delta_{22}||\Delta_{12}|}{b}\cos(\varphi_{12}-\varphi_{22})\right]\delta(-\omega+E_+)+\\
&-\left[\frac{1}{2}\left(1-\frac{\xi_2}{E_-}\right)\frac{|\Delta_{11}||\Delta_{12}|}{b}\cos(\varphi_{11}-\varphi_{12})+\right.\\
&\left.+\frac{1}{2}\left(1-\frac{\xi_1}{E_-}\right)\frac{|\Delta_{22}||\Delta_{12}|}{b}\cos(\varphi_{12}-\varphi_{22})\right]\delta(\omega+E_-)+\\
&-\left[\frac{1}{2}\left(1+\frac{\xi_2}{E_-}\right)\frac{|\Delta_{11}||\Delta_{12}|}{b}\cos(\varphi_{11}-\varphi_{12})+\right.\\
&\left.+\frac{1}{2}\left(1+\frac{\xi_1}{E_-}\right)\frac{|\Delta_{22}||\Delta_{12}|}{b}\cos(\varphi_{12}-\varphi_{22})\right]\delta(-\omega+E_-)
\end{aligned}$$

Now we introduce the spectral wave function coefficients for holes,

$$\begin{aligned}
u^2_{k11} &= \frac{1}{2}\left(1+\frac{\xi_1}{E_+}\right), \quad u^2_{k12} = \frac{1}{2}\left(1+\frac{\xi_2}{E_+}\right),\\
u^2_{k21} &= \frac{1}{2}\left(1+\frac{\xi_1}{E_-}\right), \quad u^2_{k22} = \frac{1}{2}\left(1+\frac{\xi_2}{E_-}\right),
\end{aligned} \tag{A.39}$$

and for electrons,

$$\begin{aligned}
v^2_{k11} &= \frac{1}{2}\left(1-\frac{\xi_1}{E_+}\right), \quad v^2_{k12} = \frac{1}{2}\left(1-\frac{\xi_2}{E_+}\right),\\
v^2_{k21} &= \frac{1}{2}\left(1-\frac{\xi_1}{E_-}\right), \quad v^2_{k22} = \frac{1}{2}\left(1-\frac{\xi_2}{E_-}\right).
\end{aligned} \tag{A.40}$$

Using the above expression for the electron and hole coefficients of the spectral wave function (A.39) and (A.40) we write the elements of the spectral wave function in a more compact form:

$$S_{11\omega}(\vec{k}) = \left(v_{k11}^2 \frac{E_+^2 - \varepsilon_2^2}{b} - v_{k12}^2 \frac{|\Delta_{12}|^2}{b}\right)\delta(E_+ + \omega) + \\ + \left(u_{k11}^2 \frac{E_+^2 - \varepsilon_2^2}{b} - u_{k12}^2 \frac{|\Delta_{12}|^2}{b}\right)\delta(E_+ - \omega) + \\ + \left(v_{k21}^2 \frac{\varepsilon_2^2 - E_-^2}{b} + v_{k22}^2 \frac{|\Delta_{12}|^2}{b}\right)\delta(E_- + \omega) + \\ + \left(u_{k21}^2 \frac{\varepsilon_2^2 - E_-^2}{b} - u_{k22}^2 \frac{|\Delta_{12}|^2}{b}\right)\delta(E_- - \omega), \tag{A.41}$$

$$S_{12\omega}(\vec{k}) = \frac{|\Delta_{12}|}{b}\Big[v_{k12}^2|\Delta_{11}|\cos(\varphi_{12} - \varphi_{11}) + \\ + v_{k11}^2|\Delta_{22}|\cos(\varphi_{12} - \varphi_{22})\Big]\delta(E_+ + \omega) + \\ + \frac{|\Delta_{12}|}{b}\Big[u_{k12}^2|\Delta_{11}|\cos(\varphi_{12} - \varphi_{11}) + u_{k11}^2|\Delta_{22}||\Delta_{12}|\cos(\varphi_{12} - \varphi_{22})\Big]\delta(E_+ - \omega) + \\ - \frac{|\Delta_{12}|}{b}\Big[v_{k22}^2|\Delta_{11}|\cos(\varphi_{12} - \varphi_{11}) + v_{k21}^2|\Delta_{22}|\cos(\varphi_{12} - \varphi_{22})\Big]\delta(E_- + \omega) + \\ - \frac{|\Delta_{12}|}{b}\Big[u_{k22}^2|\Delta_{11}|\cos(\varphi_{12} - \varphi_{11}) + u_{k21}^2|\Delta_{22}|\cos(\varphi_{12} - \varphi_{22})\Big]\delta(E_+ - \omega). \tag{A.42}$$

The sum rule of the spectral wave function requires that

$$\int_{-\infty}^{+\infty} d\omega S_{ij\omega}(\vec{k}) = 1_{2\times 2}, \tag{A.43}$$

where the right hand side of Eq. (A.43) is the 2×2 identity.

We can perform the sum rule for the spectral wave function by writing the delta of Dirac in a Lorentzian form

$$\delta(E_i \pm \omega) = \lim_{\epsilon \to 0} \frac{1}{\pi} \frac{\epsilon}{(E_i \pm \omega)^2 + \epsilon^2}. \tag{A.44}$$

If we perform the sum rule for $S_{11\omega}(\vec{k})$, we have

$$\int_{-\infty}^{+\infty} d\omega S_{11\omega}(\vec{k}) = \frac{1}{b}\Big[(v_{k11}^2 + u_{k11}^2)(E_+^2 - \varepsilon_2^2) + (v_{k21}^2 + u_{k21}^2)(\varepsilon_2^2 - E_-^2) + \\ - v_{k12}^2|\Delta_{12}|^2 - u_{k12}^2|\Delta_{12}|^2 + v_{k22}^2|\Delta_{12}|^2 + u_{k22}^2|\Delta_{12}|^2\Big]. \tag{A.45}$$

Now if we use the following identities, $u_{k11}^2 + v_{k11}^2 = 1$, $u_{k21}^2 + v_{k21}^2 = 1$, $u_{k22}^2 + v_{k22}^2 - u_{k12}^2 - v_{k12}^2 = 0$, we get

$$\int_{-\infty}^{+\infty} d\omega S_{11\omega}(\vec{k}) = \frac{1}{b}(E_+^2 - E_-^2), \tag{A.46}$$

furthermore using $E_+^2 - E_-^2 = b$,

$$\int_{-\infty}^{+\infty} d\omega S_{11\omega}(\vec{k}) = 1. \tag{A.47}$$

Complementary we calculate the sum rule for $S_{12\omega}(\vec{k})$,

$$\begin{aligned} \int_{-\infty}^{+\infty} d\omega S_{12\omega}(\vec{k}) = \frac{1}{b}\Big[&(u_{k12}^2 + v_{k12}^2)|\Delta_{11}||\Delta_{12}| + \\ + \quad &(u_{k11}^2 + v_{k11}^2)|\Delta_{22}||\Delta_{12}| - (u_{k22}^2 + v_{k22}^2)|\Delta_{11}||\Delta_{12}| + \\ - \quad &(u_{k21}^2 + v_{k12}^2)|\Delta_{22}||\Delta_{12}|\Big]. \end{aligned} \tag{A.48}$$

Similarly we use the following identities, $u_{k12}^2 + v_{k12}^2 = 1$, $u_{k11}^2 + v_{k11}^2 = 1$, $u_{k22}^2 + v_{k22}^2 = 1$, $u_{k21}^2 + v_{k21}^2 = 0$, we get

$$\int_{-\infty}^{+\infty} d\omega S_{12\omega}(\vec{k}) = 0. \tag{A.49}$$

Therefore using (A.47) and (A.49) we verify the sum rule,

$$\int_{-\infty}^{+\infty} d\omega S_{ij\omega}(\vec{k}) = \begin{pmatrix} 1 & 0 \\ 0 & 1 \end{pmatrix}. \tag{A.50}$$

Last but not least we calculate the density of states which can be obtained from the spectral wave function as follows

$$N_{ij\omega} = \int \frac{d^3k}{(2\pi)^3} S_{ij\omega}(\vec{k}). \tag{A.51}$$

If we substitute Eqs. (A.41) and (A.42) into (A.51) we obtain the expressions for the density of states to be integrated numerically.

B

GINZBURG-LANDAU IN PRESENCE OF CROSSPAIRING

To obtained the GL equation in presence of IBP and CBP we need to sum over the matrix elements $g_{ij,kl}$ and Matsubara frequencies the following integrals:

$$I_{kl}^{(A)} = \int d^3y G_{km\omega}^{(0)}(\vec{r},\vec{y})\Delta_{mn}(\vec{y})\bar{G}_{nl\omega}^{(0)}(\vec{y},\vec{r}) \tag{B.1}$$

$$I_{kl}^{(B)} = \int d^3y_1 d^3y_2 d^3y_3 G_{km\omega}^{(0)}(\vec{r},\vec{y}_1)\Delta_{mn}(\vec{y}_1)\bar{G}_{no\omega}^{(0)}(\vec{y}_1,\vec{y}_2)\times$$
$$\times\Delta_{op}^{*}(\vec{y}_2)G_{pq\omega}^{(0)}(\vec{y}_2,\vec{y}_3)\Delta_{qr}(\vec{y}_3)\bar{G}_{rl\omega}^{(0)}(\vec{y}_3,\vec{r}). \tag{B.2}$$

First based on the CPT symmetry we use the following identity:

$$\bar{G}_{ij\omega}^{(0)}(\vec{x},\vec{y}) = -G_{ij-\omega}^{(0)*}(\vec{y},\vec{x}), \tag{B.3}$$

using the above identity (B.3) in (B.1) and (B.2), we get

$$I_{kl}^{(A)} = -\int d^3y G_{km\omega}^{(0)}(\vec{r},\vec{y})\Delta_{mn}(\vec{y})G_{nl-\omega}^{(0)*}(\vec{r},\vec{y}) \tag{B.4}$$

$$I_{kl}^{(B)} = \int d^3y_1 d^3y_2 d^3y_3 G_{km\omega}^{(0)}(\vec{r},\vec{y}_1)\Delta_{mn}(\vec{y}_1)G_{no-\omega}^{(0)*}(\vec{y}_2,\vec{y}_1)\times$$
$$\times\Delta_{op}^{*}(\vec{y}_2)G_{pq\omega}^{(0)}(\vec{y}_2,\vec{y}_3)\Delta_{qr}(\vec{y}_3)G_{rl-\omega}^{(0)*}(\vec{r},\vec{y}_3). \tag{B.5}$$

Now the expression for the normal Green functions as usual transform covariantly under a local gauge transformations:

$$G_{ij\omega}^{(0)}(\vec{r},\vec{r}') = e^{\frac{i}{\hbar}\frac{e}{c}\int_{\vec{r}'}^{\vec{r}}\vec{A}.d\vec{l}}\left[G_{ij\omega}^{(0)}(\vec{r},\vec{r}')\right]\Big|_{\vec{B}=0}. \tag{B.6}$$

Furthermore, the exponential in Eq. (B.6) using the path integral formalism can be expanded around the classical trajectory which is the straight line:

$$e^{\frac{i}{\hbar}\frac{e}{c}\int_{\vec{r}'}^{\vec{r}}\vec{A}.d\vec{l}} \approx e^{\frac{i}{\hbar}\frac{e}{c}\vec{A}.(\vec{r}-\vec{r}')}. \tag{B.7}$$

The above approximation (B.7) is consistent with the Gor'kov derivation.

Before we proceed we use the Fourier representation of the normal Green functions

$$\left[G_{ij\omega}^{(0)}(\vec{r},\vec{r}')\right]\Big|_{\vec{B}=0} = \begin{pmatrix} \int \frac{d^3k}{(2\pi)^3}\frac{e^{i\vec{k}.(\vec{r}-\vec{r}')}}{i\hbar\omega-\tilde{\xi}_{1k}} & 0 \\ 0 & \int \frac{d^3k}{(2\pi)^3}\frac{e^{i\vec{k}.(\vec{r}-\vec{r}')}}{i\hbar\omega-\tilde{\xi}_{2k}} \end{pmatrix}. \tag{B.8}$$

The sum over the matrix elements $g_{ij,kl}$ and Matsubara frequencies of (B.4) is given by:

$$-\frac{1}{\beta}\sum_{kl} g_{ij,kl}\sum_{\omega} I_{kl}^{(A)} = -\frac{1}{\beta}g_{ij,11}\sum_{\omega} I_{11}^{(A)} - \frac{1}{\beta}g_{ij,22}\sum_{\omega} I_{22}^{(A)} + \\ - \frac{1}{\beta}g_{ij,12}\sum_{\omega} I_{12}^{(A)} - \frac{1}{\beta}g_{ij,21}\sum_{\omega} I_{21}^{(A)}. \quad \text{(B.9)}$$

Using (B.8), we get that the sum over Matsubara frequencies of $I_{kl}^{(A)}$ can be written as

$$\sum_{\omega} I_{kl}^{(A)} = -\sum_{\omega}\int d^3y \begin{pmatrix} G_{11\omega}^{(0)}\Delta_{11}(\vec{y})G_{11-\omega}^{(0)*} & G_{11\omega}^{(0)}\Delta_{12}(\vec{y})G_{22-\omega}^{(0)*} \\ G_{22\omega}^{(0)}\Delta_{21}(\vec{y})G_{11-\omega}^{(0)*} & G_{11\omega}^{(0)}\Delta_{22}(\vec{y})G_{22-\omega}^{(0)*} \end{pmatrix}. \quad \text{(B.10)}$$

Now we Taylor expand $\Delta_{mn}(\vec{y})$ around $\vec{r}$,

$$\Delta_{mn}(\vec{y}) = \Delta_{mn}(\vec{r}) + (\vec{z}.\vec{\nabla})\Delta_{mn}(\vec{r}) + \frac{(\vec{z}.\vec{\nabla})^2}{2}\Delta_{mn}(\vec{r}), \quad \text{(B.11)}$$

where $\vec{z} = \vec{y} - \vec{r}$ and we have only taken the terms relevant for the Gor'kov derivation. Substituting (B.11) into (B.10)

$$-\sum_{\omega}\int d^3y \begin{pmatrix} G_{11\omega}^{(0)}\hat{O}G_{11-\omega}^{(0)*}\Delta_{11}(\vec{r}) & G_{11}^{(0)}\hat{O}G_{22-\omega}^{(0)*}\Delta_{12}(\vec{r}) \\ G_{22\omega}^{(0)}\hat{O}G_{11-\omega}^{(0)*}\Delta_{21}(\vec{r}) & G_{11}^{(0)}\hat{O}G_{22-\omega}^{(0)*}\Delta_{22}(\vec{r}) \end{pmatrix}. \quad \text{(B.12)}$$

where $\hat{O} = 1 + (\vec{z}.\vec{D})^2/2$, $\vec{D} = \hbar/i\vec{\nabla} - 2e/c\vec{A}$, and we have neglected terms odd in $\vec{z}$ because its limits of integration are symmetric.

It is important to note that our system is symmetric under the exchange of indices $1 \leftrightarrow 2$. Therefore it is sufficient to calculate $\sum_\omega I_{11}^{(A)}$, $\sum_\omega I_{12}^{(A)}$, $\sum_\omega I_{11}^{(B)}$ and $\sum_\omega I_{12}^{(B)}$.

$$\sum_{\omega} I_{11}^{(A)} = -\sum_{\omega}\int d^3y \Bigg[\int \frac{d^3k_1}{(2\pi)^3}\frac{e^{i\vec{k}_1.(\vec{r}-\vec{y})}}{i\hbar\omega - \xi_{1k_1}}\int \frac{d^3k_2}{(2\pi)^3}\frac{e^{-i\vec{k}_2.(\vec{r}-\vec{y})}}{-i\hbar\omega - \xi_{1k_2}} + \\ - \int \frac{d^3k_1}{(2\pi)^3}\frac{e^{i\vec{k}_1.(\vec{r}-\vec{y})}}{i\hbar\omega - \xi_{1k_1}}\frac{(\vec{z}.\vec{\nabla})^2}{2}\int \frac{d^3k_2}{(2\pi)^3}\frac{e^{-i\vec{k}_2.(\vec{r}-\vec{y})}}{-i\hbar\omega - \xi_{1k_2}}\Bigg]\Delta_{11}(\vec{r}) \quad \text{(B.13)}$$

The above expression can be calculated following the same steps as given in Section (2.3.3) for the one band system. Then,

$$-\frac{1}{\beta}\sum_{\omega} I_{11}^{(A)} = N_{11}(0)\left[\ln\left(\frac{2e^{\gamma}\Omega}{\pi T_c}\right) + \tau + \frac{v_{F_1}^2}{6}\frac{7\zeta(3)}{8\pi^2 T_c^2}\vec{D}^2\right]\Delta_{11}(\vec{r}). \quad \text{(B.14)}$$

Analytic expressions for $\sum_\omega I_{12}^{(A)}$ are only attainable when $\xi_1 = \xi_2$. Therefore:

$$-\frac{1}{\beta}\sum_{\omega} I_{12}^{(A)} = N_{12}(0)\left[\ln\left(\frac{2e^{\gamma}\Omega}{\pi T_c}\right) + \tau + \frac{v_{F_{12}}^2}{6}\frac{7\zeta(3)}{8\pi^2 T_c^2}\vec{D}^2\right]\Delta_{12}(\vec{r}),$$

(B.15)

where one formally define $N_{12}(0)$ and $v_{F_{12}}$ as:

$$N_{12}(0) = \frac{1}{2}\left[N_{11}(0) + N_{22}(0)\right], \quad v_{F_{12}}^2 = \frac{1}{2}\left(v_{F_1}^2 + v_{F_2}^2\right). \tag{B.16}$$

Now we proceed by taking the sum over Matsubara frequencies of Eq. (B.5):

$$-\frac{1}{\beta}\sum_{\omega} I_{kl}^{(B)} = \sum_{\omega}\int d^3y_1 d^3y_2 d^3y_3 \begin{pmatrix} B_{11} & B_{12} \\ B_{21} & B_{22} \end{pmatrix} \tag{B.17}$$

with

$$\begin{aligned} B_{11} &= G_{11\omega}^{(0)}(\vec{r},\vec{y}_1)G_{11-\omega}^{(0)*}(\vec{y}_2,\vec{y}_1)G_{11\omega}^{(0)}(\vec{y}_2,\vec{y}_3)G_{11-\omega}^{(0)*}(\vec{r},\vec{y}_3)|\Delta_{11}|^2\Delta_{11} + \\ &+ G_{11\omega}^{(0)}(\vec{r},\vec{y}_1)G_{22-\omega}^{(0)*}(\vec{y}_2,\vec{y}_1)G_{11\omega}^{(0)}(\vec{y}_2,\vec{y}_3)G_{11-\omega}^{(0)*}(\vec{r},\vec{y}_3)|\Delta_{12}|^2\Delta_{11} + \\ &+ G_{11\omega}^{(0)}(\vec{r},\vec{y}_1)G_{11-\omega}^{(0)*}(\vec{y}_2,\vec{y}_1)G_{22\omega}^{(0)}(\vec{y}_2,\vec{y}_3)G_{11-\omega}^{(0)*}(\vec{r},\vec{y}_3)|\Delta_{12}|^2\Delta_{11} + \\ &+ G_{11\omega}^{(0)}(\vec{r},\vec{y}_1)G_{22-\omega}^{(0)*}(\vec{y}_2,\vec{y}_1)G_{22\omega}^{(0)}(\vec{y}_2,\vec{y}_3)G_{11-\omega}^{(0)*}(\vec{r},\vec{y}_3)\Delta_{12}^2\Delta_{22}^*. \end{aligned}$$

and

$$\begin{aligned} B_{12} &= G_{11\omega}^{(0)}(\vec{r},\vec{y}_1)G_{11-\omega}^{(0)*}(\vec{y}_2,\vec{y}_1)G_{11\omega}^{(0)}(\vec{y}_2,\vec{y}_3)G_{22-\omega}^{(0)*}(\vec{r},\vec{y}_3)|\Delta_{11}|^2\Delta_{12} + \\ &+ G_{11\omega}^{(0)}(\vec{r},\vec{y}_1)G_{22-\omega}^{(0)*}(\vec{y}_2,\vec{y}_1)G_{11\omega}^{(0)}(\vec{y}_2,\vec{y}_3)G_{22-\omega}^{(0)*}(\vec{r},\vec{y}_3)|\Delta_{12}|^2\Delta_{12} + \\ &+ G_{11\omega}^{(0)}(\vec{r},\vec{y}_1)G_{11-\omega}^{(0)*}(\vec{y}_2,\vec{y}_1)G_{22\omega}^{(0)}(\vec{y}_2,\vec{y}_3)G_{22-\omega}^{(0)*}(\vec{r},\vec{y}_3)\Delta_{11}\Delta_{12}^*\Delta_{22} + \\ &+ G_{11\omega}^{(0)}(\vec{r},\vec{y}_1)G_{22-\omega}^{(0)*}(\vec{y}_2,\vec{y}_1)G_{22\omega}^{(0)}(\vec{y}_2,\vec{y}_3)G_{22-\omega}^{(0)*}(\vec{r},\vec{y}_3)|\Delta_{22}|^2\Delta_{12}. \end{aligned}$$

The sum over the matrix elements $g_{ij,kl}$ and Matsubara frequencies of (B.5) is given by:

$$\begin{aligned} -\frac{1}{\beta}\sum_{kl} g_{ij,kl}\sum_{\omega} I_{kl}^{(B)} &= -\frac{1}{\beta}g_{ij,11}\sum_{\omega} I_{11}^{(B)} - \frac{1}{\beta}g_{ij,22}\sum_{\omega} I_{22}^{(B)} + \\ &- g_{ij,12}\sum_{\omega} I_{12}^{(B)} - \frac{1}{\beta}g_{ij,21}\sum_{\omega} I_{21}^{(B)}. \end{aligned} \tag{B.18}$$

Again here, complete analytic expressions for $\sum_\omega I_{ij}^{(B)}$ are only attainable when $\xi_1 = \xi_2$. Therefore:

$$-\frac{1}{\beta}\sum_{\omega} I_{11}^{(B)} = b_{11}|\Delta_{11}|^2\Delta_{11} + 2b_{12}|\Delta_{12}|^2\Delta_{11} + b_{12}\Delta_{12}^2\Delta_{22}^* \tag{B.19}$$

$$\begin{aligned} -\frac{1}{\beta}\sum_{\omega} I_{12}^{(B)} &= b_{12}|\Delta_{12}|^2\Delta_{12} + b_{12}|\Delta_{11}|^2\Delta_{12} + b_{12}|\Delta_{22}|^2\Delta_{12} + \\ &+ b_{12}\Delta_{11}\Delta_{22}\Delta_{12}^*, \end{aligned} \tag{B.20}$$

where

$$b_{12} = N_{12}(0)\frac{7\zeta(3)}{8(\pi T_c)^2}. \tag{B.21}$$

C

NUMERICAL METHODS

In this appendix we will present the numerical methods to solve the pair amplitude equations and the multicomponent GL equations in presence of both intraband pairing and crosspairing.

C.1 NUMERICAL METHOD TO SOLVE THE PAIR AMPLITUDE EQUATIONS

To solve the pair amplitude equations (4.7) we first change the integration variable from the momentum to band representation,

$$\int d^3\vec{k}\Delta_{ij}(\dots) \equiv N_{ij}(0)\int d\epsilon\Delta_{ij}(\dots), \tag{C.1}$$

where $N_{ij}(0)$ is the band dependent density of states. In a two-band system with overlapping bands the limits of integration for all cases is given by the interval $\langle\mu-\Omega,\mu+\Omega\rangle$.

To integrate we use the Legendre-Gaussian quadrature method. This method approximates a definite integral as discrete sum of a weighted integrands as follows:

$$\int_a^b f(x)dx = \sum_{i=1}^{\infty}\omega_i f(x_i) \approx \sum_i^n f(x_i), \tag{C.2}$$

where n is the number of roots x_i that will approximate the above integral as a sum. This approximation which is only defined for the interval $[-1,1]$ can always be taken in consideration if we perform change of variables as follows:

$$\begin{aligned}\int_a^b f(x)dx &= \frac{b-a}{2}\int_{-1}^{1} f\left(\frac{b-a}{2}x_i+\frac{b+a}{2}\right)dx \\ &\approx \frac{b-a}{2}\sum_{i=1}^{n}\omega_i f\left(\frac{b-a}{2}x_i+\frac{b-a}{2}\right).\end{aligned} \tag{C.3}$$

Assuming that f_{ij} are our integrands, then we have

$$\int_{\mu-\Omega}^{\mu+\Omega} d\epsilon f_{ij}(\Delta_{ij}) \approx \Omega\sum_{i=1}^{n}\omega_i f\left(\Omega x_i+\Omega\right), \tag{C.4}$$

once we have this expression we perform the integration by taking from any subroutine or table the weights ω_i and roots x_i. Usually four

hundred roots and weights ($n = 400$) is good enough for getting a smooth solution.

Once we have implemented the integration method we proceed to solve the system of equations (4.7) using the Newton-Raphson method. Newton-Raphson is an iterative method where the wanted root is approximated by using the derivative of the function in consideration. For example, if we want to solve the equation $g(x) = 0$, then we can approximate the root of this equation by

$$x_{n+1} = x_n - \frac{g(x_n)}{g'(x_n)}, \quad g'(x_n) = \left.\frac{\partial g(x)}{\partial x}\right|_{x=x_n}. \tag{C.5}$$

One can write formally the pair amplitude equations as $g_{ij}(\Delta_{ij}) = 0$, then we approximate the solutions as follows

$$\Delta_{ij}^{n+1} = \Delta_{ij}^{n} - \frac{g_{ij}(\Delta_{ij})}{J}, \tag{C.6}$$

where J is the Jacobian given by

$$J = \begin{pmatrix} \frac{\partial g_{11}}{\partial \Delta_{11}} & \frac{\partial g_{11}}{\partial \Delta_{22}} & \frac{\partial g_{11}}{\partial \Delta_{12}} \\ \frac{\partial g_{22}}{\partial \Delta_{11}} & \frac{\partial g_{22}}{\partial \Delta_{22}} & \frac{\partial g_{22}}{\partial \Delta_{12}} \\ \frac{\partial g_{12}}{\partial \Delta_{11}} & \frac{\partial g_{12}}{\partial \Delta_{22}} & \frac{\partial g_{12}}{\partial \Delta_{12}} \end{pmatrix}. \tag{C.7}$$

The Newthon-Raphson method is computationally expensive due to the Jacobian calculation and its inversion. Nonetheless has second order of convergence which implies that one will approach the solution after few interations (three or four depending on the desired accuracy of the solution). Finally to calculate the derivatives for each matrix element of the Jacobian we use the central difference of the finite difference method:

$$\frac{\partial g_{ij}}{\partial \Delta_{ij}} = \frac{g_{ij}(\Delta_{ij} + \delta) - g_{ij}(\Delta_{ij} - \delta)}{2\delta}. \tag{C.8}$$

C.2 NUMERICAL METHOD TO SOLVE THE GINZBURG-LANDAU EQUATIONS

We solve the GL equations (5.44-5.46) in a two-dimensional grid with periodic boundary conditions. Therefore each point of the grid has four neighbors as shown in Fig. C.1. Furthermore, the 2D discretization breaks the gauge symmetry of the system. To restore this symmetry we introduce the link variables for the phase of the GL components as follows:

$$U_i^{x_i, x_i+\delta} = \exp\left[-i \int_{x_i}^{x_i+\delta} A_i(\vec{r}).dx_i\right], \tag{C.9}$$

with $i = x, y$ are the index of the lattice and δ is the distance between two grid points, see Fig. C.1. To observe the variation of the GL components on the grid one has to take $\delta \leq 0.3\xi$ with ξ being the average coherence length of the system.

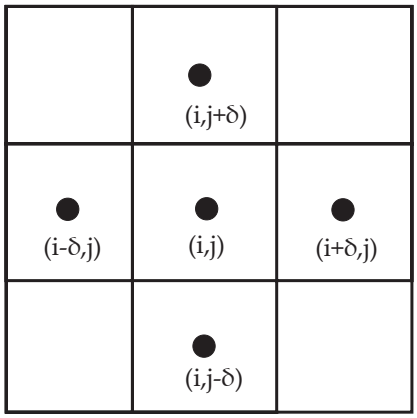

Figure C.1: Representation of the 2D discretization. When one has periodic boundary condition each point of the grid has four neighbors. Each point of the grid is spaced by a distance δ.

The kinetic term on the lattice point (i, j) can be rewritten using the link variables as follows

$$\left(\frac{\nabla_i}{i} - A_i\right)^2 \psi_j = \frac{1}{U_i^j} \nabla_i (\nabla_i (U_i^j \psi_j)). \tag{C.10}$$

Now analogously to the single-component GL equation we introduce a time-derivative term to each equation of our system (5.44-5.46). Then we get

$$\left[r_a^2 \bar{L}_{11} - 2 r_a r_c |\Delta_{12}|^2 - \sqrt{r_a r_b} r_c \frac{\Delta_{12}^2 \Delta_{22}^*}{\Delta_{11}}\right] \Delta_{11} = \frac{\partial \Delta_{11}}{\partial t},$$
$$\left[r_b^2 \bar{L}_{22} - 2 r_b r_c |\Delta_{12}|^2 - \sqrt{r_a r_b} r_c \frac{\Delta_{12}^2 \Delta_{11}^*}{\Delta_{22}}\right] \Delta_{22} = \frac{\partial \Delta_{22}}{\partial t},$$
$$\left[r_c^2 \bar{L}_{12} - r_c (r_a |\Delta_{11}|^2 + r_b |\Delta_{22}|^2) - \sqrt{r_a r_b} r_c \frac{\Delta_{11} \Delta_{22} \Delta_{12}^*}{\Delta_{12}}\right] \Delta_{12} = \frac{\partial \Delta_{12}}{\partial t}.$$

The introduction of the time derivative can be seen as artificial, however can just simply interpret it as an iterative equation where the consecutive approximation of the solution is scaled by a time-step dt.

$$dt\left[r_a^2\bar{L}_{11}^0 - 2r_a r_c|\Delta_{12}^0|^2 - \sqrt{r_a r_b}r_c\frac{\Delta_{12}^{02}\Delta_{22}^{0*}}{\Delta_{11}^0}\right]\Delta_{11}^0 + \Delta_{11}^0 = \Delta_{11},$$

$$dt\left[r_b^2\bar{L}_{22}^0 - 2r_b r_c|\Delta_{12}^0|^2 - \sqrt{r_a r_b}r_c\frac{\Delta_{12}^{02}\Delta_{11}^{0*}}{\Delta_{22}^0}\right]\Delta_{22}^0 + \Delta_{22}^0 = \Delta_{22},$$

$$dt\left[r_c^2\bar{L}_{12}^0 - r_c(r_a|\Delta_{11}^0|^2 + r_b|\Delta_{22}^0|^2) - \sqrt{r_a r_b}r_c\frac{\Delta_{11}^0\Delta_{22}^0\Delta_{12}^{0*}}{\Delta_{12}^0}\right]\Delta_{12}^0 + \Delta_{12}^0 = \Delta_{12},$$

When one runs the code we usually start with a larger time-step ($dt \approx 1$) and then whenever the solutions for the components Δ_{ij} diverges we restart the values of Δ_{ij} and reduce in 20% the value of the time-step until we obtain a convergent solution. In this thesis we assumed that one has reached a stable or steady solution if after two consecutive iterations $\max(||\Delta_{ij}| - |\Delta_{ij}^0||) < \varepsilon$, with $\varepsilon = 10^{-7}$.

BIBLIOGRAPHY

[1] A. A. Abrikosov. "Nobel Lecture: Type-II superconductors and the vortex lattice." In: *Rev. Mod. Phys.* 76 (3 2004), pp. 975–979. DOI: 10.1103/RevModPhys.76.975. URL: https://link.aps.org/doi/10.1103/RevModPhys.76.975.

[2] A. A. Abrikosov and L. P. Gor'kov. "On the Theory of Superconducting Alloys." In: *JETP, 1959, Vol. 8, No. 6, p. 1090* 8 (3 1959), pp. 1090–1098. URL: http://www.jetp.ac.ru/cgi-bin/dn/e_008_06_1090.pdf.

[3] F. Altomare and A. M. Chang. *One-Dimensional Superconductivity in Nanowires*. 1st ed. The address: Wiley-VCH, 2013. ISBN: 9783527649044.

[4] P.W. Anderson. "Theory of dirty superconductors." In: *Journal of Physics and Chemistry of Solids* 11.1 (1959), pp. 26 –30. ISSN: 0022-3697. DOI: https://doi.org/10.1016/0022-3697(59)90036-8. URL: http://www.sciencedirect.com/science/article/pii/0022369759900368.

[5] A. Aperis, P. Maldonado, and P. M. Oppeneer. "Ab initio theory of magnetic-field-induced odd-frequency two-band superconductivity in MgB_2." In: *Phys. Rev. B* 92 (5 2015), p. 054516. DOI: 10.1103/PhysRevB.92.054516. URL: https://link.aps.org/doi/10.1103/PhysRevB.92.054516.

[6] E. Babaev, J. Carlström, M. Silaev, and J.M. Speight. "Type-1.5 superconductivity in multicomponent systems." In: *Physica C: Superconductivity and its Applications* 533 (2017). Ninth international conference on Vortex Matter in nanostructured Superdonductors, pp. 20 –35. ISSN: 0921-4534. DOI: https://doi.org/10.1016/j.physc.2016.08.003. URL: http://www.sciencedirect.com/science/article/pii/S0921453416301198.

[7] Egor Babaev and Martin Speight. "Semi-Meissner state and neither type-I nor type-II superconductivity in multicomponent superconductors." In: *Phys. Rev. B* 72 (18 2005), p. 180502. DOI: 10.1103/PhysRevB.72.180502. URL: https://link.aps.org/doi/10.1103/PhysRevB.72.180502.

[8] J. Bardeen, L. N. Cooper, and J. R. Schrieffer. "Theory of Superconductivity." In: *Phys. Rev.* 108 (5 1957), pp. 1175–1204. DOI: 10.1103/PhysRev.108.1175. URL: https://link.aps.org/doi/10.1103/PhysRev.108.1175.

[9] John Bardeen and David Pines. "Electron-Phonon Interaction in Metals." In: *Phys. Rev.* 99 (4 1955), pp. 1140–1150. DOI: 10.1103/PhysRev.99.1140. URL: https://link.aps.org/doi/10.1103/PhysRev.99.1140.

[10] J. Bekaert, A. Aperis, B. Partoens, P. M. Oppeneer, and M. V. Milošević. "Evolution of multigap superconductivity in the atomically thin limit: Strain-enhanced three-gap superconductivity in monolayer MgB_2." In: *Phys. Rev. B* 96 (9 2017), p. 094510. DOI: 10.1103/PhysRevB.96.094510. URL: https://link.aps.org/doi/10.1103/PhysRevB.96.094510.

[11] J. Bekaert et al. "Free surfaces recast superconductivity in few-monolayer MgB_2: Combined first-principles and ARPES demonstration." In: *Scientific Reports* 7.1 (2017), p. 14458. ISSN: 2045-2322. DOI: 10.1038/s41598-017-13913-z. URL: https://doi.org/10.1038/s41598-017-13913-z.

[12] M Bendele et al. "Spectromicroscopy of electronic phase separation in $K_xFe_{2-y}Se_2$ superconductor." In: *Scientific Reports* 4 (2014), p. 5592. URL: https://doi.org/10.1038/srep05592http://10.0.4.14/srep05592.

[13] A. Bianconi, A. Valletta, A. Perali, and N.L. Saini. "High Tc superconductivity in a superlattice of quantum stripes." In: *Solid State Communications* 102.5 (1997), pp. 369 –374. ISSN: 0038-1098. DOI: https://doi.org/10.1016/S0038-1098(97)00011-2. URL: http://www.sciencedirect.com/science/article/pii/S0038109897000112.

[14] Antonio Bianconi. "Shape resonances in superstripes." In: *Nature Physics* 9 (2013), p. 536. URL: https://doi.org/10.1038/nphys2738http://10.0.4.14/nphys2738.

[15] Antonio Bianconi, Antonio Valletta, Andrea Perali, and Naurang L Saini. "Superconductivity of a striped phase at the atomic limit." In: *Physica C: Superconductivity* 296.3 (1998), pp. 269 –280. ISSN: 0921-4534. DOI: https://doi.org/10.1016/S0921-4534(97)01825-X. URL: http://www.sciencedirect.com/science/article/pii/S092145349701825X.

[16] A. M. Black-Schaffer and A. V. Balatsky. "Odd-frequency superconducting pairing in multiband superconductors." In: *Phys. Rev. B* 88 (10 2013), p. 104514. DOI: 10.1103/PhysRevB.88.104514. URL: https://link.aps.org/doi/10.1103/PhysRevB.88.104514.

[17] John M. Blatt. "Electron Pairs in the Theory of Superconductivity:" in: *Progress of Theoretical Physics* 23.3 (Mar. 1960), pp. 447–450. ISSN: 0033-068X. DOI: 10.1143/PTP.23.447. eprint: http://oup.prod.sis.lan/ptp/article-pdf/23/3/447/5206014/23-3-447.pdf. URL: https://dx.doi.org/10.1143/PTP.23.447.

[18] John M. Blatt and Colin J. Thompson. "Shape Resonances in Superconducting Thin Films." In: *Phys. Rev. Lett.* 10 (8 1963), pp. 332–334. DOI: 10.1103/PhysRevLett.10.332. URL: https://link.aps.org/doi/10.1103/PhysRevLett.10.332.

[19] Sangita Bose, Antonio M García-García, Miguel M Ugeda, Juan D Urbina, Christian H Michaelis, Ivan Brihuega, and Klaus Kern. "Observation of shell effects in superconducting nanoparticles of Sn." In: *Nature Materials* 9 (2010), p. 550. URL: https://doi.org/10.1038/nmat2768http://10.0.4.14/nmat2768https://www.nature.com/articles/nmat2768{\#}supplementary-information.

[20] J. W. Brendan and P. D. Mukunda. "Time-reversal-symmetry-broken state in the BCS formalism for a multi-band superconductor." In: *J. Phys. Condens. Matter* 25.42 (2013), p. 425702. DOI: 10.1088/0953-8984/25/42/425702. URL: https://doi.org/10.1088%2F0953-8984%2F25%2F42%2F425702.

[21] Jens Bruér, Ivan Maggio-Aprile, Nathan Jenkins, Zoran Ristić, Andreas Erb, Christophe Berthod, Oystein Fischer, and Christoph Renner. "Revisiting the vortex-core tunnelling spectroscopy in $YBa_2Cu_3O_{7-\delta}$." In: *Nature Communications* 7 (2016), p. 11139. URL: https://doi.org/10.1038/ncomms11139http://10.0.4.14/ncomms11139https://www.nature.com/articles/ncomms11139{\#}supplementary-information.

[22] Marco Cariglia, Alfredo Vargas-Paredes, Mauro M. Doria, Antonio Bianconi, Milorad V. Milošević, and Andrea Perali. "Shape-Resonant Superconductivity in Nanofilms: from Weak to Strong Coupling." In: *Journal of Superconductivity and Novel Magnetism* 29.12 (2016), pp. 3081–3086. ISSN: 1557-1947. DOI: 10.1007/s10948-016-3673-1. URL: https://doi.org/10.1007/s10948-016-3673-1.

[23] Yajiang Chen, A A Shanenko, A Perali, and F M Peeters. "Superconducting nanofilms: molecule-like pairing induced by quantum confinement." In: *Journal of Physics: Condensed Matter* 24.18 (2012), p. 185701. DOI: 10.1088/0953-8984/24/18/185701. URL: https://doi.org/10.1088%2F0953-8984%2F24%2F18%2F185701.

[24] H. J. Choi, D. Roundy, H. Sun, M. L. Cohen, and S. G. Louie. "First-principles calculation of the superconducting transition in MgB_2 within the anisotropic Eliashberg formalism." In: *Phys. Rev. B* 66 (2 2002), p. 020513. DOI: 10.1103/PhysRevB.66.020513. URL: https://link.aps.org/doi/10.1103/PhysRevB.66.020513.

[25] A. Continenza and G. Profeta. "Chemical doping in pnictides superconductors: The case of $Ca(Fe_{1-x}X_x)_2As_2$, X = Co, Ni, Pt." In: *Journal of Magnetism and Magnetic Materials* 452 (2018), pp. 179 –183. ISSN: 0304-8853. DOI: https://doi.org/10.1016/j.jmmm.2017.12.060. URL: http://www.sciencedirect.com/science/article/pii/S0304885317331888.

[26] D. Costanzo, S. Jo, H. Berger, and A. F. Morpurgo. "Gate-induced superconductivity in atomically thin MoS2 crystals." In: *Nature Nanotechnology* 11 (2016), p. 339. URL: https://doi.org/10.1038/nnano.2015.314http://10.0.4.14/nnano.2015.314https://www.nature.com/articles/nnano.2015.314{\#}supplementary-information.

[27] P. J. Curran, W. M. Desoky, M. V. Milošević, A. Chaves, J.-B. Laloë, J. S. Moodera, and S. J. Bending. "Spontaneous symmetry breaking in vortex systems with two repulsive lengthscales." In: *Scientific Reports* 5 (2015), p. 15569. URL: https://doi.org/10.1038/srep15569http://10.0.4.14/srep15569.

[28] D. van Delft and P. Kes. *The discovery of superconductivity*. Physics Today, 2010. URL: https://physicstoday.scitation.org/doi/10.1063/1.3490499.

[29] C. Di Giorgio, F. Bobba, A. M. Cucolo, A. Scarfato, S. A. Moore, G. Karapetrov, D. D'Agostino, V. Novosad, V. Yefremenko, and M. Iavarone. "Observation of superconducting vortex clusters in S/F hybrids." In: *Scientific Reports* 6 (2016). Article, 38557 EP –. URL: https://doi.org/10.1038/srep38557.

[30] H . Ding et al. "Electronic structure of optimally doped pnictide $Ba_{0.6}K_{0.4}Fe_2As_2$: a comprehensive angle-resolved photoemission spectroscopy investigation." In: *Journal of Physics: Condensed Matter* 23.13 (2011), p. 135701. DOI: 10.1088/0953-8984/23/13/135701. URL: https://doi.org/10.1088%2F0953-8984%2F23%2F13%2F135701.

[31] H. Ding et al. "Observation of Fermi-surface–dependent nodeless superconducting gaps in $Ba_{0.6}K_{0.4}Fe_2As_2$." In: *EPL* 83.4 (2008), p. 47001. DOI: 10.1209/0295-5075/83/47001. URL: https://doi.org/10.1209%2F0295-5075%2F83%2F47001.

[32] O.V. Dolgov, E.P. Fetisov, and D.I. Khomskii. "Superconductivity of heavy fermions in a two-band model." In: *Physics Letters A* 125.5 (1987), pp. 267 –270. ISSN: 0375-9601. DOI: https://doi.org/10.1016/0375-9601(87)90207-6. URL: http://www.sciencedirect.com/science/article/pii/0375960187902076.

[33] Mauro M. Doria, Marco Cariglia, and Andrea Perali. "Multigap superconductivity and barrier-driven resonances in superconducting nanofilms with an inner potential barrier." In: *Phys. Rev. B* 94 (22 2016), p. 224513. DOI: 10.1103/PhysRevB.94.224513.

URL: https://link.aps.org/doi/10.1103/PhysRevB.94.224513.

[34] Mauro M. Doria, Marco Cariglia, and Andrea Perali. "Multigap superconductivity and barrier-driven resonances in superconducting nanofilms with an inner potential barrier." In: *Phys. Rev. B* 94 (22 2016), p. 224513. DOI: 10.1103/PhysRevB.94.224513. URL: https://link.aps.org/doi/10.1103/PhysRevB.94.224513.

[35] D. V. Efremov, M. M. Korshunov, O. V. Dolgov, A. A. Golubov, and P. J. Hirschfeld. "Disorder-induced transition between $s_{\pm}$ and s_{++} states in two-band superconductors." In: *Phys. Rev. B* 84 (18 2011), p. 180512. DOI: 10.1103/PhysRevB.84.180512. URL: https://link.aps.org/doi/10.1103/PhysRevB.84.180512.

[36] Daejin Eom, S. Qin, M.-Y. Chou, and C. K. Shih. "Persistent Superconductivity in Ultrathin Pb Films: A Scanning Tunneling Spectroscopy Study." In: *Phys. Rev. Lett.* 96 (2 2006), p. 027005. DOI: 10.1103/PhysRevLett.96.027005. URL: https://link.aps.org/doi/10.1103/PhysRevLett.96.027005.

[37] A. Floris, A. Sanna, S. Massidda, and E. K. U. Gross. "Two-band superconductivity in Pb from ab initio calculations." In: *Phys. Rev. B* 75 (5 2007), p. 054508. DOI: 10.1103/PhysRevB.75.054508. URL: https://link.aps.org/doi/10.1103/PhysRevB.75.054508.

[38] M. Fretto, E. Enrico, N. De Leo, L. Boarino, R. Rocci, and V. Lacquaniti. "Nano SNIS Junctions Fabricated by 3D FIB Sculpting for Application to Digital Electronics." In: *IEEE Transactions on Applied Superconductivity* 23.3 (2013), pp. 1101104–1101104. ISSN: 1051-8223. DOI: 10.1109/TASC.2013.2240759.

[39] A M Gabovich, A I Voitenko, J F Annett, and M Ausloos. "Charge- and spin-density-wave superconductors." In: *Superconductor Science and Technology* 14.4 (2001), R1–R27. DOI: 10.1088/0953-2048/14/4/201. URL: https://doi.org/10.1088%2F0953-2048%2F14%2F4%2F201.

[40] J. Garaud, J. Carlström, and E. Babaev. "Topological Solitons in Three-Band Superconductors with Broken Time Reversal Symmetry." In: *Phys. Rev. Lett.* 107 (19 2011), p. 197001. DOI: 10.1103/PhysRevLett.107.197001. URL: https://link.aps.org/doi/10.1103/PhysRevLett.107.197001.

[41] J. Garaud, J. Carlström, E. Babaev, and M. Speight. "Chiral $\mathbb{C}P^2$ skyrmions in three-band superconductors." In: *Phys. Rev. B* 87 (1 2013), p. 014507. DOI: 10.1103/PhysRevB.87.014507. URL: https://link.aps.org/doi/10.1103/PhysRevB.87.014507.

[42] Antonio M. García-García, Juan Diego Urbina, Emil A. Yuzbashyan, Klaus Richter, and Boris L. Altshuler. "Bardeen-Cooper-Schrieffer Theory of Finite-Size Superconducting Metallic Grains." In: *Phys. Rev. Lett.* 100 (18 2008), p. 187001. DOI: 10.1103/PhysRevLett.100.187001. URL: https://link.aps.org/doi/10.1103/PhysRevLett.100.187001.

[43] Jian-Feng Ge, Zhi-Long Liu, Canhua Liu, Chun-Lei Gao, Dong Qian, Qi-Kun Xue, Ying Liu, and Jin-Feng Jia. "Superconductivity above 100 K in single-layer FeSe films on doped $SrTiO_3$." In: *Nature Materials* 14 (2014), p. 285. URL: https://doi.org/10.1038/nmat4153http://10.0.4.14/nmat4153https://www.nature.com/articles/nmat4153{\#}supplementary-information.

[44] J. Geyer, R. M. Fernandes, V. G. Kogan, and J. Schmalian. "Interface energy of two-band superconductors." In: *Phys. Rev. B* 82 (10 2010), p. 104521. DOI: 10.1103/PhysRevB.82.104521. URL: https://link.aps.org/doi/10.1103/PhysRevB.82.104521.

[45] G. Ghigo, D. Torsello, G. A. Ummarino, L. Gozzelino, M. A. Tanatar, R. Prozorov, and P. C. Canfield. "Disorder-Driven Transition from $s_{\pm}$ to s_{++} Superconducting Order Parameter in Proton Irradiated $Ba(Fe_{1-x}Rh_x)_2As_2$ Single Crystals." In: *Phys. Rev. Lett.* 121 (10 2018), p. 107001. DOI: 10.1103/PhysRevLett.121.107001. URL: https://link.aps.org/doi/10.1103/PhysRevLett.121.107001.

[46] V. L. Ginzburg and L. D. Landau. "On the Theory of superconductivity." In: *Zh. Eksp. Teor. Fiz.* 20 (1950), pp. 1064–1082.

[47] V. L. Ginzburg and L. D. Landau. "On the Theory of superconductivity." In: *Collected Papers of L.D. Landau* (1965), pp. 546–568.

[48] F. Giorgianni, T. Cea, C. Vicario, C. P. Hauri, W. K. Withanage, X. Xi, and L. Benfatto. "Leggett mode controlled by light pulses." In: *Nature Physics* 15.4 (2019), pp. 341–346. ISSN: 1745-2481. DOI: 10.1038/s41567-018-0385-4. URL: https://doi.org/10.1038/s41567-018-0385-4.

[49] F. Giubileo, D. Roditchev, W. Sacks, R. Lamy, D. X. Thanh, J. Klein, S. Miraglia, D. Fruchart, J. Marcus, and Ph. Monod. "Two-Gap State Density in MgB_2: A True Bulk Property Or A Proximity Effect?" In: *Phys. Rev. Lett.* 87 (17 2001), p. 177008. DOI: 10.1103/PhysRevLett.87.177008. URL: https://link.aps.org/doi/10.1103/PhysRevLett.87.177008.

[50] F. Giubileo, F. Bobba, A. Scarfato, A. M. Cucolo, A. Kohen, D. Roditchev, N. D. Zhigadlo, and J. Karpinski. "Local tunneling study of three-dimensional order parameter in the π band of

Al-doped MgB_2 single crystals." In: *Phys. Rev. B* 76 (2 2007), p. 024507. DOI: 10.1103/PhysRevB.76.024507. URL: https://link.aps.org/doi/10.1103/PhysRevB.76.024507.

[51] R. S. Gonnelli et al. "Effect of Magnetic Impurities in a Two-Band Superconductor: A Point-Contact Study of Mn-Substituted MgB_2 Single Crystals." In: *Phys. Rev. Lett.* 97 (3 2006), p. 037001. DOI: 10.1103/PhysRevLett.97.037001. URL: https://link.aps.org/doi/10.1103/PhysRevLett.97.037001.

[52] L. P. Gor'kov. "On the Energy Spectrum of Superconductors." In: *JETP, 1958, Vol. 7, No. 3, p. 505* 7 (3 1958), pp. 505–508. URL: http://www.jetp.ac.ru/cgi-bin/dn/e_007_03_0505.pdf.

[53] L. P. Gor'kov. "Microscopy derivation of the Ginzburg-Landau equations in the theory of superconductivity." In: *Zh. Eksp. Teor. Fiz.* 36 (1959), pp. 1364–1367.

[54] L. P. Gor'kov. "The Properties of a Superconductor in an Arbitrary Magnetic Field Near the Critical Temperature." In: *Methods of quantum field theory in statistical physics*. New York, NY: Dovers, 1975. Chap. 7, pp. 319–324.

[55] M A Griffith, T O Puel, M A Continentino, and G B Martins. "Multiband superconductivity in BiS_2-based layered compounds." In: *Journal of Physics: Condensed Matter* 29.30 (2017), p. 305601. DOI: 10.1088/1361-648x/aa76ac. URL: https://doi.org/10.1088%2F1361-648x%2Faa76ac.

[56] E. Gubankova, W. V. Liu, and F. Wilczek. "Breached Pairing Superfluidity: Possible Realization in QCD." In: *Phys. Rev. Lett.* 91 (3 2003), p. 032001. DOI: 10.1103/PhysRevLett.91.032001. URL: https://link.aps.org/doi/10.1103/PhysRevLett.91.032001.

[57] Andrea Guidini and Andrea Perali. "Band-edge BCS–BEC crossover in a two-band superconductor: physical properties and detection parameters." In: *Superconductor Science and Technology* 27.12 (2014), p. 124002. DOI: 10.1088/0953-2048/27/12/124002. URL: https://doi.org/10.1088%2F0953-2048%2F27%2F12%2F124002.

[58] Andrea Guidini, Luca Flammia, Milorad V. Milošević, and Andrea Perali. "BCS-BEC Crossover in Quantum Confined Superconductors." In: *Journal of Superconductivity and Novel Magnetism* 29.3 (2016), pp. 711–715. ISSN: 1557-1947. DOI: 10.1007/s10948-015-3308-y. URL: https://doi.org/10.1007/s10948-015-3308-y.

[59] Yang Guo et al. "Superconductivity Modulated by Quantum Size Effects." In: *Science* 306.5703 (2004), pp. 1915–1917. ISSN: 0036-8075. DOI: 10.1126/science.1105130. eprint: https://science.sciencemag.org/content/306/5703/1915.full.pdf.

URL: https://science.sciencemag.org/content/306/5703/1915.

[60] T. Hanaguri, S. Kasahara, J. Böker, I. Eremin, T. Shibauchi, and Y. Matsuda. "Quantum Vortex Core and Missing Pseudogap in the Multiband BCS-BEC Crossover Superconductor FeSe." In: *Phys. Rev. Lett.* 122 (7 2019), p. 077001. DOI: 10.1103/PhysRevLett.122.077001. URL: https://link.aps.org/doi/10.1103/PhysRevLett.122.077001.

[61] J. Herbrych, N. Kaushal, A. Nocera, G. Alvarez, A. Moreo, and E. Dagotto. "Spin dynamics of the block orbital-selective Mott phase." In: *Nature Communications* 9.1 (2018), p. 3736. ISSN: 2041-1723. DOI: 10.1038/s41467-018-06181-6. URL: https://doi.org/10.1038/s41467-018-06181-6.

[62] R. E. Hetzel, A. Sudbø, and D. A. Huse. "First-order melting transition of an Abrikosov vortex lattice." In: *Phys. Rev. Lett.* 69 (3 1992), pp. 518–521. DOI: 10.1103/PhysRevLett.69.518. URL: https://link.aps.org/doi/10.1103/PhysRevLett.69.518.

[63] Davide Innocenti, Nicola Poccia, Alessandro Ricci, Antonio Valletta, Sergio Caprara, Andrea Perali, and Antonio Bianconi. "Resonant and crossover phenomena in a multiband superconductor: Tuning the chemical potential near a band edge." In: *Phys. Rev. B* 82 (18 2010), p. 184528. DOI: 10.1103/PhysRevB.82.184528. URL: https://link.aps.org/doi/10.1103/PhysRevB.82.184528.

[64] Robert Joynt and Louis Taillefer. "The superconducting phases of UPt_3." In: *Rev. Mod. Phys.* 74 (1 2002), pp. 235–294. DOI: 10.1103/RevModPhys.74.235. URL: https://link.aps.org/doi/10.1103/RevModPhys.74.235.

[65] Shigeru Kasahara et al. "Field-induced superconducting phase of FeSe in the BCS-BEC cross-over." In: *Proceedings of the National Academy of Sciences* 111.46 (2014), pp. 16309–16313. ISSN: 0027-8424. DOI: 10.1073/pnas.1413477111. eprint: https://www.pnas.org/content/111/46/16309.full.pdf. URL: https://www.pnas.org/content/111/46/16309.

[66] A. F. Kemper, M. A. Sentef, B. Moritz, J. K. Freericks, and T. P. Devereaux. "Direct observation of Higgs mode oscillations in the pump-probe photoemission spectra of electron-phonon mediated superconductors." In: *Phys. Rev. B* 92 (22 2015), p. 224517. DOI: 10.1103/PhysRevB.92.224517. URL: https://link.aps.org/doi/10.1103/PhysRevB.92.224517.

[67] V. G. Kogan and J. Schmalian. "Ginzburg-Landau theory of two-band superconductors: Absence of type-1.5 superconductivity." In: *Phys. Rev. B* 83 (5 2011), p. 054515. DOI: 10.1103/

PhysRevB.83.054515. URL: https://link.aps.org/doi/10.1103/PhysRevB.83.054515.

[68] F. G. Korchorbé and M. E. Palistrant. "Superconductivity in a two-band system with low carrier density." In: *Zh. Eksp. Teor. Fiz.* 104 (1993), pp. 442–451.

[69] H. Krull, N. Bittner, G. S. Uhrig, D. Manske, and A. P. Schnyder. "Coupling of Higgs and Leggett modes in non-equilibrium superconductors." In: *Nature Communications* 7 (2016). Article, 11921 EP –. URL: https://doi.org/10.1038/ncomms11921.

[70] S. A. Kuzmichev, T. E. Kuzmicheva, and S. N. Tchesnokov. "Determination of the electron-phonon coupling constants from the experimental temperature dependences of superconducting gaps in MgB_2." In: *JETP Letters* 99 (May 2014), pp. 295–302. DOI: 10.1134/S0021364014050129.

[71] A. J. Leggett. "Number-Phase Fluctuations in Two-Band Superconductors." In: *Progress of Theoretical Physics* 36.5 (Nov. 1966), pp. 901–930. ISSN: 0033-068X. DOI: 10.1143/PTP.36.901. eprint: http://oup.prod.sis.lan/ptp/article-pdf/36/5/901/5256693/36-5-901.pdf. URL: https://doi.org/10.1143/PTP.36.901.

[72] L. J. Li, T. Nishio, Z. A. Xu, and V. V. Moshchalkov. "Low-field vortex patterns in the multiband $BaFe_{2-x}Ni_xAs_2$ superconductor ($x = 0.1, 0.16$)." In: *Phys. Rev. B* 83 (22 2011), p. 224522. DOI: 10.1103/PhysRevB.83.224522. URL: https://link.aps.org/doi/10.1103/PhysRevB.83.224522.

[73] W.X. Li, R. Zeng, L. Lu, and S.X. Dou. "Dependence of superconducting properties on lattice strain in MgB_2." In: *Physica C: Superconductivity and its Applications* 470 (2010). Proceedings of the 9th International Conference on Materials and Mechanisms of Superconductivity, S629 –S630. ISSN: 0921-4534. DOI: https://doi.org/10.1016/j.physc.2009.11.053. URL: http://www.sciencedirect.com/science/article/pii/S0921453409007709.

[74] Y. Li et al. "Pressure-induced superconductivity in topological semimetal NbAs2." In: *npj Quantum Materials* 3.1 (2018), p. 58. ISSN: 2397-4648. DOI: 10.1038/s41535-018-0132-1. URL: https://doi.org/10.1038/s41535-018-0132-1.

[75] W. V. Liu and F. Wilczek. "Interior Gap Superfluidity." In: *Phys. Rev. Lett.* 90 (4 2003), p. 047002. DOI: 10.1103/PhysRevLett.90.047002. URL: https://link.aps.org/doi/10.1103/PhysRevLett.90.047002.

[76] F. London and H. London. "The Electromagnetic Equations of the Supraconductor." In: *Proceedings of the Royal Society of London. Series A - Mathematical and Physical Sciences* 149.866 (Mar. 1935), pp. 71–88. ISSN: 1471-2946. DOI: 10.1098/rspa.1935.0048. URL: http://dx.doi.org/10.1098/rspa.1935.0048.

[77] Xiaoli Lu, Chen Fang, Wei-Feng Tsai, Yongjin Jiang, and Jiangping Hu. "s-wave superconductivity with orbital-dependent sign change in checkerboard models of iron-based superconductors." In: *Phys. Rev. B* 85 (5 2012), p. 054505. DOI: 10.1103/PhysRevB.85.054505. URL: https://link.aps.org/doi/10.1103/PhysRevB.85.054505.

[78] Y Lubashevsky, E Lahoud, K Chashka, D Podolsky, and A Kanigel. "Shallow pockets and very strong coupling superconductivity in $FeSe_xTe_{1-x}$." In: *Nature Physics* 8 (2012), p. 309. URL: https://doi.org/10.1038/nphys2216http://10.0.4.14/nphys2216https://www.nature.com/articles/nphys2216{\#}supplementary-information.

[79] F. Marsiglio, P. Pieri, A. Perali, F. Palestini, and G. C. Strinati. "Pairing effects in the normal phase of a two-dimensional Fermi gas." In: *Phys. Rev. B* 91 (5 2015), p. 054509. DOI: 10.1103/PhysRevB.91.054509. URL: https://link.aps.org/doi/10.1103/PhysRevB.91.054509.

[80] Jean Matricon and Georges Waysand. *The cold wars: a history of superconductivity*. Piscataway, NJ: Rutgers University Press, 1994. URL: http://cds.cern.ch/record/1558599.

[81] C. E. Matt et al. "Direct observation of orbital hybridisation in a cuprate superconductor." In: *Nature Communications* 9.1 (2018), p. 972. ISSN: 2041-1723. DOI: 10.1038/s41467-018-03266-0. URL: https://doi.org/10.1038/s41467-018-03266-0.

[82] J. Mayoh and A. M. García-García. "Strong enhancement of bulk superconductivity by engineered nanogranularity." In: *Phys. Rev. B* 90 (13 2014), p. 134513. DOI: 10.1103/PhysRevB.90.134513. URL: https://link.aps.org/doi/10.1103/PhysRevB.90.134513.

[83] James Mayoh and Antonio M. García-García. "Number theory, periodic orbits, and superconductivity in nanocubes." In: *Phys. Rev. B* 90 (1 2014), p. 014509. DOI: 10.1103/PhysRevB.90.014509. URL: https://link.aps.org/doi/10.1103/PhysRevB.90.014509.

[84] I. I. Mazin, D. J. Singh, M. D. Johannes, and M. H. Du. "Unconventional Superconductivity with a Sign Reversal in the Order Parameter of $LaFeAsO_{1-x}F_x$." In: *Phys. Rev. Lett.* 101 (5 2008), p. 057003. DOI: 10.1103/PhysRevLett.101.057003. URL: https://link.aps.org/doi/10.1103/PhysRevLett.101.057003.

[85] W. Meissner and R. Ochsenfeld. "Ein neuer Effekt bei Eintritt der Supraleitfähigkeit." In: *Naturwissenschaften* 21.44 (1933), pp. 787–788. ISSN: 1432-1904. DOI: 10.1007/BF01504252. URL: https://doi.org/10.1007/BF01504252.

[86] M. V. Milošević and A. Perali. "Emergent phenomena in multicomponent superconductivity: an introduction to the focus issue." In: *Superconductor Science and Technology* 28.6 (2015), p. 060201. DOI: 10.1088/0953-2048/28/6/060201. URL: https://doi.org/10.1088%2F0953-2048%2F28%2F6%2F060201.

[87] M.V. Milošević and R. Geurts. "The Ginzburg–Landau theory in application." In: *Physica C: Superconductivity* 470.19 (2010). Vortex Matter in Nanostructured Superconductors, pp. 791 – 795. ISSN: 0921-4534. DOI: https://doi.org/10.1016/j.physc.2010.02.056. URL: http://www.sciencedirect.com/science/article/pii/S0921453410001632.

[88] N. Mohanta and A. Taraphder. "Multiband theory of superconductivity at the $LaAlO_3/SrTiO_3$ interface." In: *Phys. Rev. B* 92 (17 2015), p. 174531. DOI: 10.1103/PhysRevB.92.174531. URL: https://link.aps.org/doi/10.1103/PhysRevB.92.174531.

[89] A. Moreo, M. Daghofer, A. Nicholson, and E. Dagotto. "Interband pairing in multiorbital systems." In: *Phys. Rev. B* 80 (10 2009), p. 104507. DOI: 10.1103/PhysRevB.80.104507. URL: http://link.aps.org/doi/10.1103/PhysRevB.80.104507.

[90] A. Moreo, M. Daghofer, J. A. Riera, and E. Dagotto. "Properties of a two-orbital model for oxypnictide superconductors: Magnetic order, B_{2g} spin-singlet pairing channel, and its nodal structure." In: *Phys. Rev. B* 79 (13 2009), p. 134502. DOI: 10.1103/PhysRevB.79.134502. URL: https://link.aps.org/doi/10.1103/PhysRevB.79.134502.

[91] A. Moreo, M. Daghofer, J. A. Riera, and E. Dagotto. "Properties of a two-orbital model for oxypnictide superconductors: Magnetic order, B_{2g} spin-singlet pairing channel, and its nodal structure." In: *Phys. Rev. B* 79 (13 2009), p. 134502. DOI: 10.1103/PhysRevB.79.134502. URL: https://link.aps.org/doi/10.1103/PhysRevB.79.134502.

[92] J. Nagamatsu, N. Nagakawa, T. Muranaka, Y. Zenitani, and J. Akimitsu. "Superconductivity at 39 K in magnesium diboride." In: *Nature* 410 (2001), p. 63. URL: https://doi.org/10.1038/nature01619http://10.0.4.14/nature01619.

[93] Tai-Kai Ng. "Ginzburg-Landau Theory of Dirty Two Band $s_{\pm}$ Superconductors." In: *Phys. Rev. Lett.* 103 (23 2009), p. 236402. DOI: 10.1103/PhysRevLett.103.236402. URL: https://link.aps.org/doi/10.1103/PhysRevLett.103.236402.

[94] K Okazaki et al. "Superconductivity in an electron band just above the Fermi level: possible route to BCS-BEC superconductivity." In: *Scientific Reports* 4 (2014), p. 4109. URL: https://doi.org/10.1038/srep04109http://10.0.4.14/srep04109https://www.nature.com/articles/srep04109{\#}supplementary-information.

[95] N. V. Orlova, P. Kuopanportti, and M. V. Milosevic. "Skyrmionic vortex lattices in coherently coupled three-component Bose-Einstein condensates." In: *Phys. Rev. A* 94 (2 2016), p. 023617. DOI: 10.1103/PhysRevA.94.023617. URL: https://link.aps.org/doi/10.1103/PhysRevA.94.023617.

[96] N. V. Orlova, A. A. Shanenko, M. V. Milosevic, F. M. Peeters, A. V. Vagov, and V. M. Axt. "Ginzburg-Landau theory for multiband superconductors: Microscopic derivation." In: *Phys. Rev. B* 87 (13 2013), p. 134510. DOI: 10.1103/PhysRevB.87.134510. URL: https://link.aps.org/doi/10.1103/PhysRevB.87.134510.

[97] N. V. Orlova, A. A. Shanenko, M. V. Milosevic, F. M. Peeters, A. V. Vagov, and V. M. Axt. "Ginzburg-Landau theory for multiband superconductors: Microscopic derivation." In: *Phys. Rev. B* 87 (13 2013), p. 134510. DOI: 10.1103/PhysRevB.87.134510. URL: https://link.aps.org/doi/10.1103/PhysRevB.87.134510.

[98] F. Palestini, A. Perali, P. Pieri, and G. C. Strinati. "Dispersions, weights, and widths of the single-particle spectral function in the normal phase of a Fermi gas." In: *Phys. Rev. B* 85 (2 2012), p. 024517. DOI: 10.1103/PhysRevB.85.024517. URL: https://link.aps.org/doi/10.1103/PhysRevB.85.024517.

[99] A. Perali, P. Pieri, and G. C. Strinati. "Extracting the Condensate Density from Projection Experiments with Fermi Gases." In: *Phys. Rev. Lett.* 95 (1 2005), p. 010407. DOI: 10.1103/PhysRevLett.95.010407. URL: https://link.aps.org/doi/10.1103/PhysRevLett.95.010407.

[100] A. Perali, A. Bianconi, A. Lanzara, and N.L. Saini. "The gap amplification at a shape resonance in a superlattice of quantum stripes: A mechanism for high Tc." In: *Solid State Communications* 100.3 (1996), pp. 181 –186. ISSN: 0038-1098. DOI: https://doi.org/10.1016/0038-1098(96)00373-0. URL: http://www.sciencedirect.com/science/article/pii/0038109896003730.

[101] A. Perali, C. Castellani, C. Di Castro, M. Grilli, E. Piegari, and A. A. Varlamov. "Two-gap model for underdoped cuprate superconductors." In: *Phys. Rev. B* 62 (14 2000), R9295–R9298. DOI: 10.1103/PhysRevB.62.R9295. URL: https://link.aps.org/doi/10.1103/PhysRevB.62.R9295.

[102] Andrea Perali, Davide Innocenti, Antonio Valletta, and Antonio Bianconi. "Anomalous isotope effect near a 2.5 Lifshitz transition in a multi-band multi-condensate superconductor made of a superlattice of stripes." In: *Superconductor Science and Technology* 25.12 (2012), p. 124002. DOI: 10.1088/0953-2048/25/12/124002. URL: https://doi.org/10.1088%2F0953-2048%2F25%2F12%2F124002.

[103] S. Poncé, E.R. Margine, C. Verdi, and F. Giustino. "EPW: Electron–phonon coupling, transport and superconducting properties using maximally localized Wannier functions." In: *Computer Physics Communications* 209 (2016), pp. 116 –133. ISSN: 0010-4655. DOI: https://doi.org/10.1016/j.cpc.2016.07.028. URL: http://www.sciencedirect.com/science/article/pii/S0010465516302260.

[104] S. Porta, L. Privitera, N. Traverso Ziani, M. Sassetti, F. Cavaliere, and B. Trauzettel. "Feasible model for photo-induced interband pairing." In: *arXiv e-prints*, arXiv:1903.12396 (2019), arXiv:1903.12396. arXiv: 1903.12396 [cond-mat.mes-hall].

[105] Shengyong Qin, Jungdae Kim, Qian Niu, and Chih-Kang Shih. "Superconductivity at the Two-Dimensional Limit." In: *Science* 324.5932 (2009), pp. 1314–1317. ISSN: 0036-8075. DOI: 10.1126/science.1170775. eprint: https://science.sciencemag.org/content/324/5932/1314.full.pdf. URL: https://science.sciencemag.org/content/324/5932/1314.

[106] I Razado-Colambo, J Avila, J.-P. Nys, C Chen, X Wallart, M.-C. Asensio, and D Vignaud. "NanoARPES of twisted bilayer graphene on SiC: absence of velocity renormalization for small angles." In: *Scientific Reports* 6 (2016), p. 27261. URL: https://doi.org/10.1038/srep27261http://10.0.4.14/srep27261https://www.nature.com/articles/srep27261{\#}supplementary-information.

[107] Christopher Reeg, Jelena Klinovaja, and Daniel Loss. "Destructive interference of direct and crossed Andreev pairing in a system of two nanowires coupled via an *s*-wave superconductor." In: *Phys. Rev. B* 96 (8 2017), p. 081301. DOI: 10.1103/PhysRevB.96.081301. URL: https://link.aps.org/doi/10.1103/PhysRevB.96.081301.

[108] N. W. Salovich et al. "Effect of heavy-ion irradiation on superconductivity in $Ba_{0.6}K_{0.4}Fe_2As_2$." In: *Phys. Rev. B* 87 (18 2013), p. 180502. DOI: 10.1103/PhysRevB.87.180502. URL: https://link.aps.org/doi/10.1103/PhysRevB.87.180502.

[109] M. R. Schafroth. "Theory of Superconductivity." In: *Phys. Rev.* 96 (5 1954), pp. 1442–1442. DOI: 10.1103/PhysRev.96.1442. URL: https://link.aps.org/doi/10.1103/PhysRev.96.1442.

[110] A Schilling, R A Fisher, N E Phillips, U Welp, D Dasgupta, W K Kwok, and G W Crabtree. "Calorimetric measurement of the latent heat of vortex-lattice melting in untwinned $YBa_2Cu_3O_{7-\delta}$, url = https://doi.org/10.1038/382791a0, volume = 382, year = 1996." In: *Nature* 6594 (), pp. 791–793. ISSN: 1476-4687. DOI: 10.1038/382791a0.

[111] A. Schilling, R. A. Fisher, N. E. Phillips, U. Welp, W. K. Kwok, and G. W. Crabtree. "Anisotropic Latent Heat of Vortex-Lattice Melting in Untwinned $YBa_2Cu_3O_{7-\delta}$." In: *Phys. Rev. Lett.* 78 (25 1997), pp. 4833–4836. DOI: 10.1103/PhysRevLett.78.4833. URL: https://link.aps.org/doi/10.1103/PhysRevLett.78.4833.

[112] M. B. Schilling et al. "Tracing the $s_{\pm}$ symmetry in iron pnictides by controlled disorder." In: *Phys. Rev. B* 93 (17 2016), p. 174515. DOI: 10.1103/PhysRevB.93.174515. URL: https://link.aps.org/doi/10.1103/PhysRevB.93.174515.

[113] A. A. Shanenko, M. D. Croitoru, M. Zgirski, F. M. Peeters, and K. Arutyunov. "Size-dependent enhancement of superconductivity in Al and Sn nanowires: Shape-resonance effect." In: *Phys. Rev. B* 74 (5 2006), p. 052502. DOI: 10.1103/PhysRevB.74.052502. URL: https://link.aps.org/doi/10.1103/PhysRevB.74.052502.

[114] A. A. Shanenko, M. V. Milosevic, F. M. Peeters, and A. V. Vagov. "Extended Ginzburg-Landau Formalism for Two-Band Superconductors." In: *Physical Review Letters* 106.4 (2011), p. 047005. DOI: 10.1103/PhysRevLett.106.047005. URL: https://link.aps.org/doi/10.1103/PhysRevLett.106.047005.

[115] A. A. Shanenko, M. D. Croitoru, A. V. Vagov, V. M. Axt, A. Perali, and F. M. Peeters. "Atypical BCS-BEC crossover induced by quantum-size effects." In: *Phys. Rev. A* 86 (3 2012), p. 033612. DOI: 10.1103/PhysRevA.86.033612. URL: https://link.aps.org/doi/10.1103/PhysRevA.86.033612.

[116] A. A. Shanenko, J. Albino Aguiar, A. Vagov, M. D. Croitoru, and M. V. Milošević. "Atomically flat superconducting nanofilms: multiband properties and mean-field theory." In: *Superconductor Science and Technology* 28.5 (2015), p. 054001. DOI: 10.1088/0953-2048/28/5/054001. URL: https://doi.org/10.1088%2F0953-2048%2F28%2F5%2F054001.

[117] A.A. Shanenko, M.D. Croitoru, and F.M. Peeters. "Nanoscale superconductivity: Nanowires and nanofilms." In: *Physica C: Superconductivity and its Applications* 468.7 (2008). Proceedings of the Fifth International Conference on Vortex Matter in Nanostructured Superconductors, pp. 593 –598. ISSN: 0921-4534. DOI: https://doi.org/10.1016/j.physc.2007.11.053. URL: http://www.sciencedirect.com/science/article/pii/S0921453408000646.

[118] X Shi et al. "Enhanced superconductivity accompanying a Lifshitz transition in electron-doped FeSe monolayer." In: *Nature Communications* 8 (2017), p. 14988. URL: https://doi.org/10.1038/ncomms14988http://10.0.4.14/ncomms14988https://www.nature.com/articles/ncomms14988{\#}supplementary-information.

[119] S. Souma et al. "The origin of multiple superconducting gaps in MgB_2." In: *Nature* 423 (2003), p. 65. URL: https://doi.org/10.1038/nature01619http://10.0.4.14/nature01619.

[120] V. G. Stanev and A. E. Koshelev. "Anomalous proximity effects at the interface of s and $s_{\pm}$ superconductors." In: *Phys. Rev. B* 86 (17 2012), p. 174515. DOI: 10.1103/PhysRevB.86.174515. URL: https://link.aps.org/doi/10.1103/PhysRevB.86.174515.

[121] Vasily S. Stolyarov et al. "Domain Meissner state and spontaneous vortex-antivortex generation in the ferromagnetic superconductor EuFe2(As0.79P0.21)2." In: *Science Advances* 4.7 (2018). DOI: 10.1126/sciadv.aat1061. eprint: https://advances.sciencemag.org/content/4/7/eaat1061.full.pdf. URL: https://advances.sciencemag.org/content/4/7/eaat1061.

[122] H. Suhl, B. T. Matthias, and L. R. Walker. "Bardeen-Cooper-Schrieffer Theory of Superconductivity in the Case of Overlapping Bands." In: *Phys. Rev. Lett.* 3 (12 1959), pp. 552–554. DOI: 10.1103/PhysRevLett.3.552. URL: http://link.aps.org/doi/10.1103/PhysRevLett.3.552.

[123] J. Tahir-Kheli. "Interband pairing theory of superconductivity." In: *Phys. Rev. B* 58 (18 1998), pp. 12307–12322. DOI: 10.1103/PhysRevB.58.12307. URL: https://link.aps.org/doi/10.1103/PhysRevB.58.12307.

[124] K. Tanaka and F. Marsiglio. "Anderson prescription for surfaces and impurities." In: *Phys. Rev. B* 62 (9 2000), pp. 5345–5348. DOI: 10.1103/PhysRevB.62.5345. URL: https://link.aps.org/doi/10.1103/PhysRevB.62.5345.

[125] C.J. Thompson and J.M. Blatt. "Shape resonances in superconductors - II simplified theory." In: *Physics Letters* 5.1 (1963), pp. 6–9. ISSN: 0031-9163. DOI: https://doi.org/10.1016/S0375-9601(63)80003-1. URL: http://www.sciencedirect.com/science/article/pii/S0375960163800031.

[126] D. R. Tilley. "The Ginzburg-Landau equations for pure two band superconductors." In: *Proceedings of the Physical Society* 84.4 (1964), pp. 573–584. DOI: 10.1088/0370-1328/84/4/313. URL: https://doi.org/10.1088%2F0370-1328%2F84%2F4%2F313.

[127] T. V. Trevisan, M. Schütt, and R. M. Fernandes. "Impact of disorder on the superconducting transition temperature near a Lifshitz transition." In: *Phys. Rev. B* 98 (9 2018), p. 094514. DOI: 10.1103/PhysRevB.98.094514. URL: https://link.aps.org/doi/10.1103/PhysRevB.98.094514.

[128] T. V. Trevisan, M. Schütt, and R. M. Fernandes. "Unconventional Multiband Superconductivity in Bulk $SrTiO_3$ and $LaAlO_3$ and $SrTiO_3$ Interfaces." In: *Phys. Rev. Lett.* 121 (12 2018), p. 127002. DOI: 10.1103/PhysRevLett.121.127002. URL: https://link.aps.org/doi/10.1103/PhysRevLett.121.127002.

[129] T. V. Trevisan, M. Schütt, and R. M. Fernandes. "Unconventional Multiband Superconductivity in Bulk $SrTiO_3$ and $LaAlO_3/SrTiO_3$ Interfaces." In: *Phys. Rev. Lett.* 121 (12 2018), p. 127002. DOI: 10.1103/PhysRevLett.121.127002. URL: https://link.aps.org/doi/10.1103/PhysRevLett.121.127002.

[130] A. V. Vagov, A. A. Shanenko, M. V. Milosevic, V. M. Axt, and F. M. Peeters. "Extended Ginzburg-Landau formalism: Systematic expansion in small deviation from the critical temperature." In: *Physical Review B* 85.1 (2012), p. 014502. DOI: 10.1103/PhysRevB.85.014502. URL: https://link.aps.org/doi/10.1103/PhysRevB.85.014502.

[131] A. Vagov, A. A. Shanenko, M. V. Milosevic, V. M. Axt, and F. M. Peeters. "Two-band superconductors: Extended Ginzburg-Landau formalism by a systematic expansion in small deviation from the critical temperature." In: *Physical Review B* 86.14 (2012), p. 144514. DOI: 10.1103/PhysRevB.86.144514. URL: https://link.aps.org/doi/10.1103/PhysRevB.86.144514.

[132] D. Valentinis, D. van der Marel, and C. Berthod. "BCS superconductivity near the band edge: Exact results for one and several bands." In: *Phys. Rev. B* 94 (2 2016), p. 024511. DOI: 10.1103/PhysRevB.94.024511. URL: https://link.aps.org/doi/10.1103/PhysRevB.94.024511.

[133] D. Valentinis, D. van der Marel, and C. Berthod. "Rise and fall of shape resonances in thin films of BCS superconductors." In: *Phys. Rev. B* 94 (5 2016), p. 054516. DOI: 10.1103/PhysRevB.94.054516. URL: https://link.aps.org/doi/10.1103/PhysRevB.94.054516.

[134] D. Valentinis, S. Gariglio, A. Fête, J.-M. Triscone, C. Berthod, and D. van der Marel. "Modulation of the superconducting critical temperature due to quantum confinement at the $LaAlO_3/SrTiO_3$ interface." In: *Phys. Rev. B* 96 (9 2017), p. 094518. DOI: 10.1103/PhysRevB.96.094518. URL: https://link.aps.org/doi/10.1103/PhysRevB.96.094518.

[135] D. Wang et al. "Evidence for Majorana bound states in an iron-based superconductor." In: *Science* 362.6412 (2018), pp. 333–335. ISSN: 0036-8075. DOI: 10.1126/science.aao1797. URL: http://science.sciencemag.org/content/362/6412/333.

[136] Mianqi Xue, Genfu Chen, Huaixin Yang, Yuanhua Zhu, Duming Wang, Junbao He, and Tingbing Cao. "Superconductivity in Potassium-Doped Few-Layer Graphene." In: *Journal of the American Chemical Society* 134.15 (2012), pp. 6536–6539. ISSN: 0002-7863. DOI: 10.1021/ja3003217. URL: https://doi.org/10.1021/ja3003217.

[137] J-X. Yin et al. "Observation of a robust zero-energy bound state in iron-based superconductor Fe(Te,Se)." In: *Nature Physics* 11 (2015), p. 543. URL: https://doi.org/10.1038/nphys3371http://10.0.4.14/nphys3371https://www.nature.com/articles/nphys3371{\#}supplementary-information.

[138] Z P Yin, K Haule, and G Kotliar. "Spin dynamics and orbital-antiphase pairing symmetry in iron-based superconductors." In: *Nature Physics* 10 (2014), p. 845. URL: https://doi.org/10.1038/nphys3116http://10.0.4.14/nphys3116https://www.nature.com/articles/nphys3116{\#}supplementary-information.

[139] R. Yu, J. Zhu, and Q. Si. "Orbital Selectivity Enhanced by Nematic Order in FeSe." In: *Phys. Rev. Lett.* 121 (22 2018), p. 227003. DOI: 10.1103/PhysRevLett.121.227003. URL: https://link.aps.org/doi/10.1103/PhysRevLett.121.227003.

[140] E Zeldov, D Majer, M Konczykowski, V B Geshkenbein, V M Vinokur, and H Shtrikman. "Thermodynamic observation of first-order vortex-lattice melting transition in $Bi_2Sr_2CaCu_2O_8$." In: *Nature* 375.6530 (1995), pp. 373–376. ISSN: 1476-4687. DOI: 10.1038/375373a0. URL: https://doi.org/10.1038/375373a0.

[141] P. Zhang et al. "Observation of Momentum-Confined In-Gap Impurity State in $Ba_{0.6}K_{0.4}Fe_2As_2$: Evidence for Antiphase $s_{\pm}$ Pairing." In: *Phys. Rev. X* 4 (3 2014), p. 031001. DOI: 10.1103/PhysRevX.4.031001. URL: https://link.aps.org/doi/10.1103/PhysRevX.4.031001.

[142] X. Zhang, Y. Zhou, B. Cui, M. Zhao, and F. Liu. "Theoretical Discovery of a Superconducting Two-Dimensional Metal–Organic Framework." In: *Nano Letters* 17.10 (2017), pp. 6166–6170. ISSN: 1530-6984. DOI: 10.1021/acs.nanolett.7b02795. URL: https://doi.org/10.1021/acs.nanolett.7b02795.

[143] H. J. Zhao, V. R. Misko, J. Tempere, and F. Nori. "Pattern formation in vortex matter with pinning and frustrated inter-vortex interactions." In: *Phys. Rev. B* 95 (10 2017), p. 104519. DOI:

10.1103/PhysRevB.95.104519. URL: https://link.aps.org/doi/10.1103/PhysRevB.95.104519.